

AD-A257 099



2

NAVAL POSTGRADUATE SCHOOL
Monterey, California



DTIC
ELECTE
NOV 10 1992
S A D

THESIS

EXPERIMENTAL DEVELOPMENT OF TUBESIDE
HEAT TRANSFER CORRELATIONS FOR LAMINAR
FLOW WITH AND WITHOUT INSERTS

by

Joseph D. Guido

September 1992

Co-Advisor:
Co-Advisor:

Paul J. Marto
Stephen B. Memory

Approved for public release; distribution is unlimited.



92-29265

UNCLASSIFIED

SECURITY CLASSIFICATION OF THIS PAGE

REPORT DOCUMENTATION PAGE				Form Approved OMB No. 0704-0188	
1a. REPORT SECURITY CLASSIFICATION UNCLASSIFIED			1b. RESTRICTIVE MARKINGS		
2a. SECURITY CLASSIFICATION AUTHORITY			3. DISTRIBUTION/AVAILABILITY OF REPORT Approved for public release; distribution is unlimited.		
2b. DECLASSIFICATION/DOWNGRADING SCHEDULE			5. MONITORING ORGANIZATION REPORT NUMBER(S)		
4. PERFORMING ORGANIZATION REPORT NUMBER(S)			7a. NAME OF MONITORING ORGANIZATION Naval Postgraduate School		
6a. NAME OF PERFORMING ORGANIZATION Naval Postgraduate School		6b. OFFICE SYMBOL (If applicable) 34		7b. ADDRESS (City, State, and ZIP Code) Monterey, California 93943-5000	
6c. ADDRESS (City, State, and ZIP Code) Monterey, California 93943-5000			9. PROCUREMENT INSTRUMENT IDENTIFICATION NUMBER		
8a. NAME OF FUNDING/SPONSORING ORGANIZATION		8b. OFFICE SYMBOL (If applicable)		10. SOURCE OF FUNDING NUMBERS	
8c. ADDRESS (City, State, and ZIP Code)			PROGRAM ELEMENT NO.	PROJECT NO.	TASK NO. WORK UNIT ACCESSION NO.
11. TITLE (Include Security Classification) EXPERIMENTAL DEVELOPMENT OF TUBESIDE HEAT TRANSFER CORRELATIONS FOR LAMINAR FLOW WITH AND WITHOUT INSERTS					
12. PERSONAL AUTHOR(S) Guido, Joseph D.					
13a. TYPE OF REPORT Master's Thesis		13b. TIME COVERED FROM ____ TO ____		14. DATE OF REPORT (Yr., Mo., Day) 1992, June 17	
15. PAGE COUNT 177					
16. SUPPLEMENTARY NOTATION: The views expressed in this thesis are those of the author and do not reflect the official policy or position of the Department of Defense or the U.S. Government.					
17. COSATI CODES			18. SUBJECT TERMS (Continue on reverse if necessary and identify by block number)		
FIELD	GROUP	SUB-GROUP	Laminar Flow, Tubeside Heat Transfer, Twisted Tape and HEATEX Inserts		
19. ABSTRACT (Continue on reverse if necessary and identify by block number) An experimental study of laminar flow heat transfer of an ethylene glycol/water mixture in an electrically heated horizontal tube using wire mesh (HEATEX) and twisted tape inserts was investigated. Twelve thermocouples, inserted in the tube wall at four longitudinal locations, enabled a mean inside experimental heat-transfer coefficient to be accurately measured. A constant wall heat flux boundary condition was placed on the wall by wrapping six 200 W flexible heater tapes tightly around the tube. The ethylene glycol/water mixture provided a coolant Reynolds number between 200-5000 and a Prandtl number between 30-140. Two smooth inside diameters and a roped tube profile were tested with and without the inserts. Heat-transfer correlations for tubes without inserts were developed and compared with theory for both thermally and hydrodynamically developing flow. Correlations were also developed for the two types of inserts. Nusselt numbers for fully developed flow were found to be a function of Reynolds and Prandtl numbers for the wire mesh insert and a function of tape twist ratio, Reynolds and Prandtl numbers for the twisted tape insert. Heat transfer enhancements of over 7 for the wire mesh insert and over 4 for the twisted tape insert at high Reynolds numbers were obtained over the empty tube. By using these correlations in conjunction with earlier obtained refrigerant condensation data (using the same tubes, inserts, and coolant), more accurate values of the outside condensation heat-transfer coefficients were obtained.					
20. DISTRIBUTION/AVAILABILITY OF ABSTRACT [XX] UNCLASSIFIED/UNLIMITED [] SAME AS RPT. [] DTIC USERS			21. ABSTRACT SECURITY CLASSIFICATION Unclassified		
22a. NAME OF RESPONSIBLE INDIVIDUAL Professor P.J. Marto			22b. TELEPHONE (Include Area Code) (408) 646-3382		22c. OFFICE SYMBOL MX

Approved for public release; distribution is unlimited.

**EXPERIMENTAL DEVELOPMENT OF TUBESIDE HEAT TRANSFER
CORRELATIONS FOR LAMINAR FLOW WITH AND WITHOUT INSERTS**

by

Joseph D. Guido
Lieutenant Commander, United States Navy
B.S.N.E., University of Florida, 1981

**Submitted in partial fulfillment of the
requirements for the degree of**

MASTER OF SCIENCE MECHANICAL ENGINEERING

from the

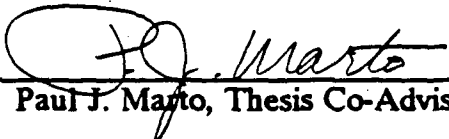
NAVAL POSTGRADUATE SCHOOL

September 1992

Author:


Joseph D. Guido

Approved by:


Paul J. Marto, Thesis Co-Advisor


Stephen B. Memory, Thesis Co-Advisor


Anthony J. Healey, Chairman
Department of Mechanical Engineering

Accession For	
NTIS CRA&I	<input checked="checked" type="checkbox"/>
DTIC TAB	<input type="checkbox"/>
Unannounced	<input type="checkbox"/>
Justification	
By	
Distribution /	
Availability Codes	
Dist	Availability or Special
A-1	

ABSTRACT

An experimental study of laminar flow heat transfer of an ethylene glycol/water mixture in an electrically heated horizontal tube using wire mesh (HEATEX) and twisted tape inserts was investigated. Twelve thermocouples, inserted in the tube wall at four longitudinal locations, enabled a mean inside experimental heat-transfer coefficient to be accurately measured. A constant wall heat flux boundary condition was placed on the wall by wrapping six 200 W flexible heater tapes tightly around the tube. The ethylene glycol/water mixture provided a coolant Reynolds number between 200-5000 and a Prandtl number between 30-140. Two smooth inside diameters and a roped tube profile were tested with and without the inserts. Heat-transfer correlations for tubes without inserts were developed and compared with theory for both thermally and hydrodynamically developing flow. Correlations were also developed for the two types of inserts. Nusselt numbers for fully developed flow were found to be a function of Reynolds and Prandtl numbers for the wire mesh insert and a function of tape twist ratio, Reynolds and Prandtl numbers for the twisted tape insert. Heat transfer enhancements of over 7 for the wire mesh insert and over 4 for the twisted tape insert at high Reynolds numbers were obtained over the empty tube. By using these correlations in conjunction with earlier obtained refrigerant condensation data (using the same tubes, inserts, and coolant), more accurate values of the outside condensation heat-transfer coefficients were obtained.

TABLE OF CONTENTS

I. INTRODUCTION	1
A. BACKGROUND	1
B. REFRIGERANT CONDENSATION RESEARCH AT NPS	2
C. OBJECTIVES	7
II. LITERATURE SURVEY	8
A. INTRODUCTION	8
B. LAMINAR FLOW IN CIRCULAR DUCTS	9
1. Boundary Layers and Entrance Lengths	9
a. Hydrodynamic Boundary Layer	9
b. Thermal Boundary Layer	10
2. Fully Developed Flow	12
3. Entry Length Problem	14
a. Thermal Entry Region - Uniform Wall Temperature ...	15
b. Thermal Entry Region - Constant Wall Heat Flux	17
c. Combined Entry Length	17

C.	AUGMENTATION TECHNIQUES TO ENHANCE TUBESIDE HEAT TRANSFER	19
1.	General Introduction	19
2.	Heat Transfer Enhancement with Twisted Tape Elements ...	20
3.	Heat Transfer Enhancement with Wire Mesh (HEATEX) Elements	22
III.	EXPERIMENTAL APPARATUS	25
A.	SYSTEM OVERVIEW	25
B.	TUBES AND INSERTS TESTED	28
1.	Tubes Tested	28
2.	Insert Elements Tested	29
C.	COOLANT SYSTEM	31
1.	Primary Coolant System	31
2.	Secondary Coolant System	31
D.	INSTRUMENTATION AND TEST SECTION	32
1.	Instrumentation	32
2.	Thermocouple Attachment Method	34
3.	Test Section	36
E.	DATA ACQUISITION AND CONTROL SYSTEM	37
IV.	EXPERIMENTAL PROCEDURES	39
A.	CALIBRATION EXPERIMENTS	39

B.	PROCEDURES FOR DETERMINATION OF INSIDE HEAT TRANSFER RATE	40
1.	General Procedures	40
2.	Specific Experiments	42
a.	Copper Smooth Tube	42
b.	Cu/Ni Externally Finned Tube	43
c.	Cu/Ni Korodense Tube	44
V.	DATA REDUCTION	45
A.	AVERAGE INSIDE HEAT TRANSFER COEFFICIENT	45
B.	ADDITIONAL TUBE LENGTHS	53
C.	LOCAL NUSSELT NUMBERS	55
VI.	RESULTS AND DISCUSSION	56
A.	GENERAL	56
B.	SMOOTH TUBE	58
1.	Smooth Tube - No Insert	58
2.	Smooth Tube - Twisted Tape	61
3.	Smooth Tube - HEATEX Insert	61
C.	CU/NI EXTERNALLY FINNED TUBE	72
1.	Cu/Ni Finned Tube - No Insert	72
2.	Cu/Ni Finned Tube - Twisted Tape Insert	73

3. Cu/Ni Finned Tube - HEATEX Insert	73
D. KORODENSE TUBE	84
1. Korodense Tube - No Insert	84
2. Korodense Tube - Twisted Tape Insert	85
3. Korodense Tube - HEATEX Insert	86
E. INSERT COMPARISON BETWEEN TUBES	96
F. LAMINAR FLOW ENHANCEMENT RATIO	101
G. REPROCESSED REFRIGERANT CONDENSATION DATA	107
 VII. CONCLUSIONS	 110
A. GENERAL	110
B. SPECIFIC	110
 VIII. RECOMMENDATIONS	 112
APPENDIX A. FLOW METER CALIBRATION	113
APPENDIX B. HEAT LOSS TO AMBIENT EXPERIMENT	116
APPENDIX C. FRICTIONAL/HEAT LEAKAGE EXPERIMENT	120
APPENDIX D. POWER CALIBRATION	122
APPENDIX E. TUBE AND INSERT SPECIFICATIONS	125
APPENDIX F. UNCERTAINTY ANALYSIS FOR THE INSIDE HEAT TRANSFER COEFFICIENT	127
APPENDIX G. PROGRAM LISTING	141

LIST OF REFERENCES	156
INITIAL DISTRIBUTION LIST	159

LIST OF TABLES

TABLE 3.1 DATA ACQUISITION UNIT CHANNEL ASSIGNMENTS . .	38
TABLE 4.1 DATA FILE NAMES	41
TABLE 6.1 SUMMARY OF CORRELATIONS	57
TABLE 6.2 SUMMARY OF LAMINAR FLOW ENHANCEMENT RATIOS	102
TABLE A.1. MASS FLOW RATE (KG/S) AT -15, 0 AND 24°C	114
TABLE A-2. FLOWMETER CALIBRATION REGRESSION RESULTS	114
TABLE B.1 EQUILIBRIUM AVERAGE WALL TEMPERATURE RESULTS	117
TABLE C.1 HEAT LEAKAGE RESULTS	121
TABLE D.1 POWER CALIBRATION RESULTS	124
TABLE E.1 TUBE CHARACTERISTICS/SPECIFICATIONS	125
TABLE E.2 INSERT CHARACTERISTICS/SPECIFICATIONS	126
TABLE F.1 SUMMARY OF RESULTS FOR SAMPLE UNCERTAINTY ANALYSIS	140

LIST OF FIGURES

Figure 1.1 NPS Evaporator/Condenser Refrigeration Apparatus.	4
Figure 2.1 Laminar Hydrodynamic Boundary Layer Development in a Circular Tube (Courtesy [Ref. 10])	10
Figure 2.2 Thermal Boundary Layer Development in a Heated Circular Tube (Courtesy of [Ref. 10])	11
Figure 2.3 Local Nusselt Number Obtained from Entry Length Solutions for Laminar Flow in a Circular Tube (Courtesy [Ref. 10])	15
Figure 3.1 Primary and Secondary Coolant Systems.	26
Figure 3.2 Data Acquisition and Control Systems.	27
Figure 3.3 Wolverine Korodense Tube (Courtesy [Ref. 21])	29
Figure 3.4 Twisted Tape and HEATEX Inserts	30
Figure 3.5 Instrumented Tube.	33
Figure 4.1 Heat Balance.	40
Figure 5.1 Temperature Rise Corrections.	48
Figure 5.2 Cu/Ni Finned Tube Temperature Rise Corrections.	51
Figure 5.3 Additional Tube Lengths.	54
Figure 6.1 Smooth tube - No insert (Nu_m vs. Re) results.	63
Figure 6.2 Smooth tube - No insert (Nu_m vs. Re) laminar flow results.	64
Figure 6.3 Smooth tube - No insert (Nu_m vs. Re) transitional flow results. ...	65
Figure 6.4 Smooth tube - No insert (Nu_m vs. x^*) results.	66

Figure 6.5 Smooth tube - No insert laminar flow correlation results.	67
Figure 6.6 Smooth tube - Twisted tape (Nu_m vs. Re) results.	68
Figure 6.7 Smooth tube - Twisted tape correlation results.	69
Figure 6.8 Smooth tube - HEATEX (Nu_m vs. Re) results.	70
Figure 6.9 Smooth tube - HEATEX correlation results.	71
Figure 6.10 Cu/Ni externally finned tube - No insert (Nu_m vs. Re) results. . .	75
Figure 6.11 Cu/Ni externally finned tube - No insert (Nu_m vs. Re) laminar flow results.	76
Figure 6.12 Cu/Ni externally finned tube - No insert (Nu_m vs. Re) transitional flow results.	77
Figure 6.13 Cu/Ni externally finned tube - No insert (Nu_m vs. x^*) results. . .	78
Figure 6.14 Cu/Ni externally finned tube - No insert laminar flow correlation results.	79
Figure 6.15 Cu/Ni externally finned tube - Twisted tape (Nu_m vs. Re) results.	80
Figure 6.16 Cu/Ni externally finned tube - Twisted tape correlation results. .	81
Figure 6.17 Cu/Ni externally finned tube - HEATEX (Nu_m vs. Re) results. .	82
Figure 6.18 Cu/Ni externally finned tube - HEATEX correlation results. . .	83
Figure 6.19 Korodense tube - No insert (Nu_m vs. Re) results.	87
Figure 6.20 Korodense tube - No insert (Nu_m vs. Re) laminar flow results. .	88
Figure 6.21 Korodense tube - No insert (Nu_m vs. Re) transitional flow results.	89
Figure 6.22 Korodense tube - No insert (Nu_m vs. x^*) results.	90
Figure 6.23 Korodense tube - No insert laminar flow correlation results. . .	91

Figure 6.24 Korodense tube - Twisted tape (Nu_m vs. Re) results.	92
Figure 6.25 Korodense tube - Twisted tape correlation results.	93
Figure 6.26 Korodense tube - HEATEX (Nu_m vs. Re) results.	94
Figure 6.27 Korodense tube - HEATEX correlation results.	95
Figure 6.28 No insert comparison under laminar flow for all three tubes. ...	97
Figure 6.29 Twisted tape insert comparison under laminar flow for all three tubes.	99
Figure 6.30 HEATEX insert comparisons under laminar flow for all three tubes.	100
Figure 6.31 Insert condition comparison for laminar flow in a smooth tube.	104
Figure 6.32 Insert condition comparison for laminar flow in a Cu/Ni externally finned tube.	105
Figure 6.33 Insert condition comparison for laminar flow in a Korodense tube.	106
Figure 6.34 Reprocessed refrigerant condensation data using new correlations.	109
Figure A.1 Flowmeter Calibration.	115
Figure B.1 Heat loss to ambient; Average wall temperature versus time for 1W and 7W.	118
Figure B.2 Heat loss to ambient; Average wall temperature versus heat input.	119
Figure D.1 Electrical schematic of power calibration experiment.	124

NOMENCLATURE

A	area, m^2
c_p	specific heat, J/kg K
D	diameter, m
Gz	Graetz number
h	heat transfer coefficient, W/m^2K
H	pitch for 180° rotation of tape
I	current, amps
k	thermal conductivity, $W/m K$
L	length, m
LMTD	log mean temperature difference
\dot{m}	mass flow rate, kg/s
Nu	Nusselt number
P	perimeter, m or Power, W
Pr	Prandtl number
\dot{q}	heat transfer rate, W
q''	heat flux, W/m^2
r	radius, m
R	electrical resistance, ohms
R_w	wall resistance, K/W

Re	Reynolds number
Re_s	Reynolds number for swirl flow
T	Temperature, K
t	fin thickness, m
U	overall heat transfer coefficient, $W/m^2 K$
u	velocity component in x direction, m/s
v	velocity component in y direction, m/s
V	velocity, m/s or Voltage, volts
x[*]	dimensionless axial coordinate, $(x/D)/(Re Pr)$
y	twist ratio, H/D

Greek Symbols

δ	tape thickness, m or boundary layer thickness
ϵ	heat transfer enhancement ratio
μ	dynamic viscosity, kg/m s
ν	kinematic viscosity, m^2/s
ρ	density, kg/m^3

Subscripts

c	coolant or cross section
D	tube diameter
fd	fully developed
f	fin
h	hydrodynamically

HL	heated length
i	inside or inlet
lam	laminar
m	mean
o	outside or outlet
s	surface
sat	saturation
t	thermally
t/c	thermocouple
x	local
w	wall

I. INTRODUCTION

A. BACKGROUND

With the increasing complexity of shipboard weapons and combat systems used aboard United States Naval vessels, the need for more energy efficient, lightweight, and high capacity refrigeration, air conditioning, and chilled water systems has grown tremendously. One way to meet this need is to redesign the refrigeration condenser. In redesigning these condensers, changes in condenser tube material can be combined with various heat transfer enhancement methods to achieve a lighter weight, more efficient condenser tube.

Emphasis on refrigerant condensation research reached a much higher level of importance due to the pressing environmental issues of ozone depletion and global warming. In September 1987, an international conference was held in Montreal, Canada, in which 24 nations representing the United Nation's Environment Program (UNEP), signed the Montreal Protocol on Substances that Deplete the Ozone Layer. This agreement called for a near term freeze on the production and consumption of chlorofluorocarbons (CFCs), the major contributor to ozone depletion [Ref. 1]. In August 1988, the Environmental Protection Agency (EPA) adopted the regulations of the Montreal Protocol under the Clean Air Act [Ref. 2]. These regulations required a freeze in both production and consumption of CFC-11,

12, 113, 114 and 115 at 1986 levels. The U.S. Navy currently uses CFC-12 and CFC-114 in its shipboard air conditioning and refrigeration systems. In June 1990 at a progress meeting held in London, England, UNEP delegates agreed to even larger reductions, calling for a 50% reduction by 1995, 85% reduction by 1997, and for CFCs to be totally phased out by the year 2000 [Ref. 3]. In the spring of 1992, President Bush moved up the CFC phase out deadline to 1995.

Because of the Navy's commitment to the CFC phase out policy and the increasing need for lighter weight, more efficient refrigeration systems, refrigerant condensation research has surfaced to the forefront of Naval Research.

B. REFRIGERANT CONDENSATION RESEARCH AT NPS

In order to examine heat transfer characteristics of various condenser tube designs and alternative refrigerants, a condenser/evaporator test platform was constructed at the Naval Postgraduate School. Construction was begun by Zebrowski [Ref. 4] and completed by Mabrey [Ref. 5] in 1988. The test platform, shown in Figure 1.1, consisted of an evaporator and a condenser section with an associated ethylene glycol/water mixture coolant system.

The evaporator section was designed so that in addition to supplying the refrigerant vapor to the condenser, it could also be utilized to conduct bundle boiling experiments. The condenser section consisted mainly of four instrumented condenser tubes and a series of auxiliary condenser coils used to control pressure in the apparatus. Details of design, construction and operation of the condenser/evaporator

test platform are provided by Zebrowski [Ref. 4], Mabrey [Ref. 5] and Mazzone [Ref. 6].

Unlike a typical vapor compression refrigeration system used aboard ships, the test platform at NPS lacked a compressor between the evaporator and the condenser. This compressor is normally required to increase the pressure (and hence temperature) of the refrigerant vapor sufficiently enough so that it can give up its latent heat to the ambient sea water, the primary coolant. Because there was no compressor in the NPS test platform, the condenser must operate at the saturation conditions of the evaporator. Therefore, a much colder coolant, a refrigerated ethylene glycol/water mixture, was needed to condense the vapor, leading to laminar flow conditions within the condenser tubes. This in turn leads to poor heat transfer due to a large inside thermal resistance.

The primary objective of the condensation experiments of Mabrey [Ref. 5] and Mazzone [Ref. 6] was to accurately determine outside heat transfer coefficients. Briefly, this was accomplished by first determining the heat transfer rate to the coolant by:

$$\dot{q} = \dot{m} c_p \Delta T \quad (1.1)$$

where \dot{m} is the coolant mass flow rate and ΔT the coolant temperature rise.

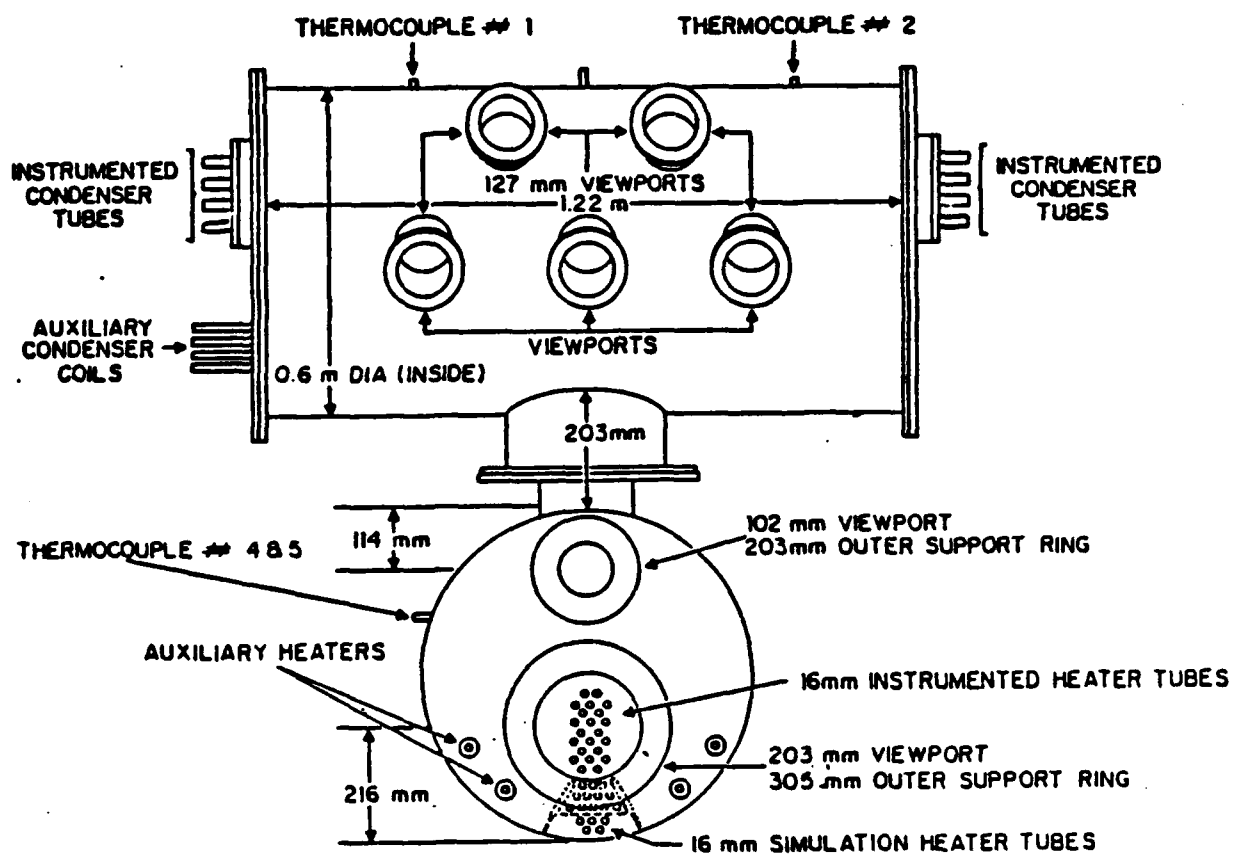


Figure 1.1 NPS Evaporator/Condenser Refrigeration Apparatus.

The overall heat transfer coefficient, U_o , could then be determined by:

$$U_o = \frac{\dot{q}}{A_o LMTD} \quad (1.2)$$

where A_o is the outside surface area of the tube and LMTD is the log mean temperature difference, defined as:

$$LMTD = \frac{\Delta T}{\ln \left[\frac{T_{sat} - T_{in}}{T_{sat} - T_{out}} \right]} \quad (1.3)$$

The overall heat transfer coefficient can also be thought of in terms of a sum of thermal resistances. The overall thermal resistance is given by:

$$\frac{1}{U_o A_o} = \frac{1}{h_o A_o} + R_w + \frac{1}{h_i A_i} \quad (1.4)$$

The overall thermal resistance can be measured experimentally; the wall resistance, R_w , is known, and the inside resistance can be determined from a chosen correlation. Therefore, the outside heat transfer coefficient, h_o , can be calculated by:

$$h_o = \frac{1}{\frac{1}{U_o} - R_w A_o - \frac{1}{h_i} \left(\frac{A_o}{A_i} \right)} \quad (1.5)$$

There is one major drawback to this method. As mentioned earlier, when laminar flow heat transfer conditions exist within the condenser tube, it leads to poor heat transfer performance and therefore represents the dominant thermal resistance within the condenser. This inside resistance then becomes the controlling factor in

the determination of the outside heat transfer coefficient. Indeed, if the inside resistance is a large proportion of the overall resistance, then the accuracy of the calculated outside heat transfer coefficient becomes uncertain. Therefore, the accuracy of the outside heat transfer coefficient relies heavily on an accurate correlation to determine h_i .

An alternative is to reduce the inside controlling resistance by augmenting the inside heat-transfer coefficient. Augmentation techniques for lowering the inside thermal resistance primarily focus on repeatedly bringing fresh fluid from the coolant bulk stream to the heated inside surface. This results in breaking up the thermal boundary layer and thereby reducing the thermal resistance. The technique utilized in the NPS condensation experiments to break up this thermal boundary layer made use of two types of inserts, a twisted tape insert and a wire mesh (HEATEX) insert. These inserts and their use will be discussed in more detail in later chapters.

The results of condensation experiments conducted by Mazzone [Ref. 6] show signs of inaccuracies related to the choice and accuracy of the inside heat transfer coefficient correlation. For example, in attempting to determine the outside heat transfer coefficient for a smooth tube with no insert, Mazzone found that the correlation used to determine the inside resistance yielded values that were greater than the actual measured overall resistance! Obviously, no sensible values of h_o could be determined. Similar problems existed (but to a lesser extent, due to the greatly reduced inside thermal resistance) when using various types of inserts. Mazzone concluded that "... laminar flow correlations for twisted tape, HEATEX, and no

insert conditions must be developed which have better accuracy than those used ... allowing for more accurate determination of outside heat transfer coefficients." Therefore, the determination of accurate inside heat transfer coefficients is paramount in the final outcome of the refrigeration condensation project.

C. OBJECTIVES

The main focus of this thesis was therefore to accurately determine inside heat transfer coefficients in support of refrigerant condensation experiments being conducted at NPS.

The specific objectives of this study were to:

1. Design and build a test apparatus to accurately determine inside heat transfer coefficients for the same tubes and inserts used in the condensation experiments.
2. Develop correlations for inside heat transfer coefficients under laminar flow conditions both with and without inserts.
3. Using the correlations mentioned above, reprocess existing condensation data to determine more accurate values of the outside heat transfer coefficients.

II. LITERATURE SURVEY

A. INTRODUCTION

Laminar fully developed and developing forced convection flows have been analyzed in great detail for various boundary conditions. The study of heat transfer in laminar flow through a closed duct was first made by Graetz [Ref. 7] in 1883 and later by Nusselt [Ref. 8] in 1910. An excellent and thorough study of the theoretical development (with both analytical and experimental solutions) for various laminar forced convection internal flow boundary conditions is given by Shah and London [Ref. 9].

This survey will be concerned with laminar flow heat transfer in fully developed and developing flows subjected to both a constant wall temperature and constant heat flux boundary condition. It will also summarize some of the augmentation techniques used to enhance tubeside laminar flow heat transfer and discuss the details involved when using twisted tape and wire mesh inserts to enhance inside heat transfer.

B. LAMINAR FLOW IN CIRCULAR DUCTS

1. Boundary Layers and Entrance Lengths

a. *Hydrodynamic Boundary Layer*

For laminar flow in a circular tube, fluid enters the tube with a uniform velocity as shown in Figure 2.1; but when the fluid particles make contact with the tube wall, viscous effects cause them to assume a zero velocity. These viscous effects, associated with shear stresses acting in planes parallel to the tube wall, tend to retard the motion of particles in adjoining fluid layers, causing a momentum boundary layer to develop. The momentum boundary layer thickness, δ , increases until its growth is stopped by symmetry at the tube centerline. The viscous effects then extend over the entire cross section of the tube. The flow is then said to be hydrodynamically fully developed. At this point, the fluid velocity distribution at a given cross section is independent of the axial distance, x (i.e., $\partial u/\partial x=0$) [Refs. 9, 10, 11, 12].

The hydrodynamic entry length for laminar flow ($Re_D \leq 2300$) is defined as that region where the hydrodynamic boundary layer is developing and may be obtained from the approximation [Ref. 10]:

$$\left(\frac{X_{fd,h}}{D} \right)_{lam} \approx 0.05 Re_D \quad (2.1)$$

This expression shows that for $Re_D=2300$, the entrance length is 115 times the tube diameter, a considerable length for most experimental facilities.

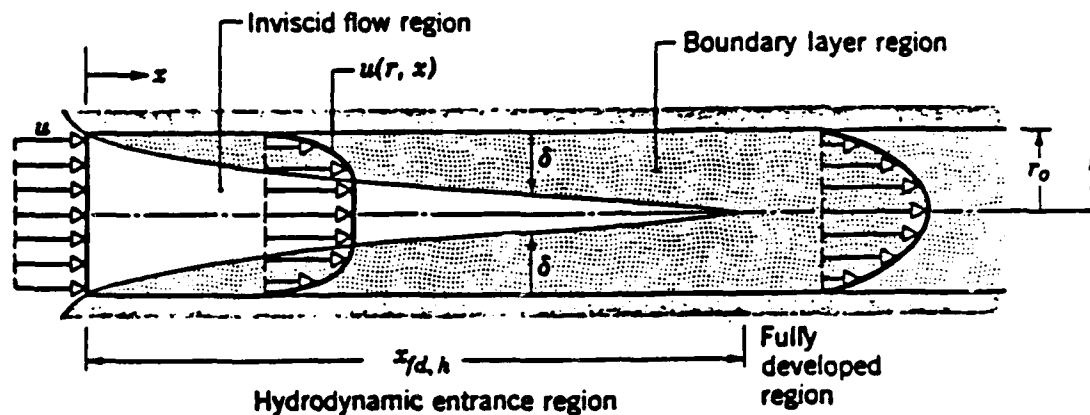


Figure 2.1 Laminar Hydrodynamic Boundary Layer Development in a Circular Tube (Courtesy [Ref. 10])

b. Thermal Boundary Layer

When a fluid with a uniform temperature distribution enters a circular duct with a wall temperature that is greater than the uniform fluid temperature, temperature gradients in the fluid develop and convective heat transfer occurs, as shown in Figure 2.2. The region of fluid where these temperature gradients exist is called the thermal boundary layer. The thermal boundary layer thickness, δ_t , grows until a dimensionless fluid temperature distribution is independent of x . The thermal boundary layer is then considered fully developed. This point is usually expressed in

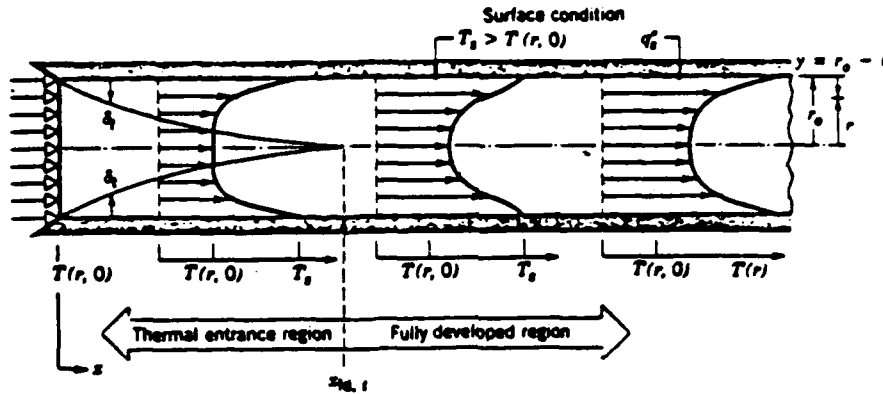


Figure 2.2 Thermal Boundary Layer Development in a Heated Circular Tube (Courtesy of [Ref. 10])

terms of a non-dimensional temperature profile given by [Ref. 11]:

$$\frac{\partial}{\partial x} \left[\frac{T_s(x) - T(r, x)}{T_s(x) - T_m(x)} \right] = 0 \quad (2.2)$$

where T_s is the tube surface temperature, T is the local fluid temperature, and T_m is the mean temperature of the fluid over the cross section of the tube. The exact shape of the fully developed temperature profile is dependent upon the boundary conditions imposed, either a uniform surface temperature or constant heat flux.

For laminar flow, the thermal entry length may be expressed as the following [Ref. 10]:

$$\left(\frac{X_{fd}}{D} \right) \approx 0.05 Re_D Pr \quad (2.3)$$

It should be noted that the rate of development of the velocity and temperature profiles in the entry region depend upon the fluid Prandtl number. For

$Pr = 1$, both velocity and temperature profiles develop at the same rate. However, for $Pr > 1$, the hydrodynamic boundary layer develops more rapidly than the thermal boundary layer ($X_{fd,h} < X_{fd,t}$). For very large Prandtl number ($Pr > 100$), $X_{fd,h}$ is so much smaller than $X_{fd,t}$, that it is reasonable to assume that a fully developed velocity profile exists throughout the thermal entry region. [Refs. 9, 10, 11, 12]

2. Fully Developed Flow

Fully developed laminar flow of an incompressible fluid through a circular duct exists when both the thermal and velocity profiles are fully developed. Two boundary conditions must now be addressed, that of a uniform wall temperature and constant wall heat flux.

For these conditions, the general form of the energy equation in cylindrical coordinates for an incompressible fluid having constant properties (with no heat generation and neglecting body forces, pressure gradients and viscous dissipation), is given by [Ref. 11]:

$$u \frac{\partial T}{\partial x} + v \frac{\partial T}{\partial r} = \frac{\alpha}{r} \frac{\partial}{\partial r} \left(r \frac{\partial T}{\partial r} \right) \quad (2.4)$$

It can be shown that for these two cases, the energy equation reduces to the following differential equations,

$$\text{Constant Wall Heat Flux: } \frac{1}{r} \frac{\partial}{\partial r} \left(r \frac{\partial T}{\partial r} \right) = \frac{u}{\alpha} \left(\frac{dT_m}{dx} \right) \quad (2.5)$$

Uniform Wall Temperature:
$$\frac{1}{r} \frac{\partial}{\partial r} \left(r \frac{\partial T}{\partial r} \right) = \frac{u}{\alpha} \left(\frac{T_s - T}{T_s - T_m} \right) \left(\frac{dT_m}{dx} \right) \quad (2.6)$$

For the constant wall heat flux boundary condition, Kays [Ref. 11] solves the differential equation (equation 2.5) for a fully developed velocity and temperature profile and expresses the Nusselt number as:

$$Nu = \frac{hD}{k} = 4.364 \quad (2.7)$$

Note that for this specified case, the heat transfer coefficient, h , depends only on the thermal conductivity, k , and the tube diameter, D .

A solution to the uniform wall temperature case is more complex, and involves evaluating the infinite series solution to the differential equation (equation 2.6) for the hydrodynamically developed, thermally developing flow situation. In evaluating the series solution, the resulting asymptotic Nusselt number is given by [Ref. 11]:

$$Nu = 3.657 \quad (2.8)$$

This result is 16% less than the solution for the constant wall heat flux boundary condition. The asymptotic values in equations 2.7 and 2.8 are shown in Figure 2.3. Note that the inverse of the Graetz number is equivalent to the dimensionless axial distance x^* .

3. Entry Length Problem

The solution to the energy equation for the entry region is far more difficult to obtain because velocity and temperature vary both axially and radially. There are two entry length problems to be considered, a combined entry length, where both temperature and velocity profiles develop simultaneously, and the thermal entry length problem, where the thermal conditions develop in the presence of a fully developed velocity profile. This latter case would exist if the place at which heat transfer begins is preceded by an unheated starting length, a situation that exists in most experimental facilities. It should be noted that for $Pr \ll 1$ (i.e., liquid metals), the thermal boundary layer would develop faster than the hydrodynamic boundary layer. However, this case has little practical application and is therefore rarely considered in the literature.

Solutions have been obtained for both entry length conditions mentioned above [Refs. 9, 10, 11, 12] and these results are also presented in Figure 2.3. The Nusselt number is plotted against a dimensionless axial coordinate x^* (the inverse of the Graetz number) given by:

$$x^* = \frac{x/D}{Re_D Pr} \quad (2.9)$$

Fully developed conditions are reached at $x^* \approx 0.05$ where the solutions for the thermal entry length converge with those for the combined entry length. For $x^* > 0.05$, the two types of entry length asymptotically reach the fully developed solutions

of 4.36 and 3.66 for the constant wall heat flux and uniform wall temperature boundary conditions respectively.

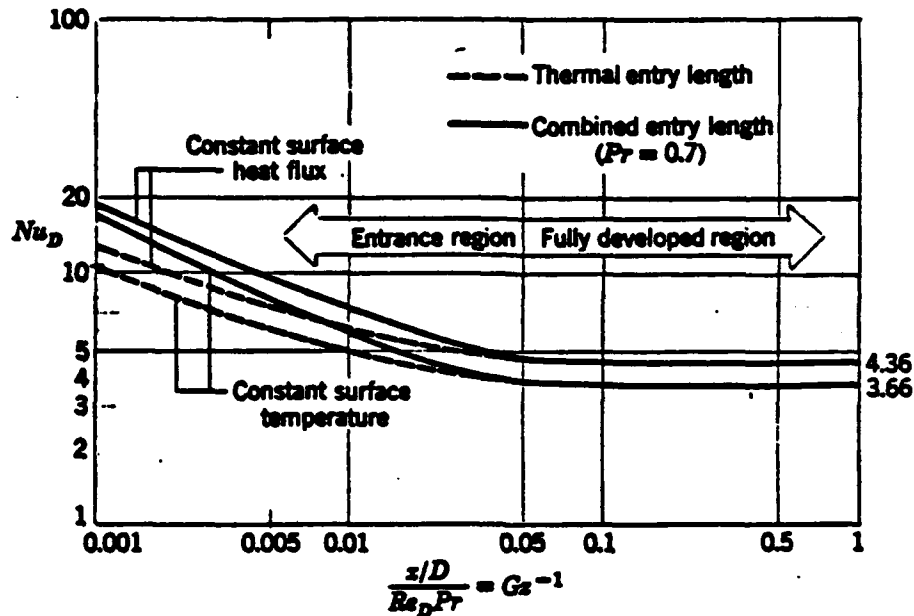


Figure 2.3 Local Nusselt Number Obtained from Entry Length Solutions for Laminar Flow in a Circular Tube (Courtesy [Ref. 10])

a. Thermal Entry Region - Uniform Wall Temperature

The thermal entry length problem, first studied by Graetz in 1883 and later by Nusselt in 1910, is more commonly known as the *Graetz Problem*. They considered an incompressible fluid with constant properties flowing through a circular tube having a fully developed laminar velocity profile and a developing laminar temperature profile subjected to a uniform wall temperature. Shah and London [Ref. 9] present a numerically derived infinite series solution to the *Graetz Problem*.

A more useful correlation presented by Incropera and Dewitt [Ref. 10] for the uniform wall temperature thermal entry length problem was developed by Hausen and is of the form:

$$Nu_m = 3.66 + \frac{0.0668(D/L)Re_D Pr}{1 + 0.04[(D/L)Re_D Pr]^{2/3}} \quad (2.10)$$

This correlation was used by Mazzone [Ref. 6] in his refrigerant condensation experiments to predict the average inside heat transfer coefficient for a smooth tube without any type of insert.

Shah and London [Ref. 9] present a more complete set of correlations derived from experimental data for heat exchanger tubes in laminar flow for local (Nu_x) and mean (Nu_m) Nusselt numbers based on various x^* ranges. The correlations for local Nusselt number are given by:

$$\begin{aligned} Nu_x &= 1.077(x^*)^{-1/3} - 0.7 & \text{for } x^* \leq 0.01 \\ Nu_x &= 3.657 + 6.874(10^3 x^*)^{-0.488} e^{-57.2x^*} & \text{for } x^* > 0.01 \end{aligned} \quad (2.11)$$

and for mean Nusselt numbers by:

$$\begin{aligned} Nu_m &= 1.615(x^*)^{-1/3} - 0.7 & \text{for } x^* \leq 0.005 \\ Nu_m &= 1.615(x^*)^{-1/3} - 0.2 & \text{for } 0.005 < x^* < 0.03 \\ Nu_m &= 3.657 + \frac{0.0499}{x^*} & \text{for } x^* \geq 0.03 \end{aligned} \quad (2.12)$$

The reader is reminded that both the Hausen correlation and the Shah and London correlations presented above are for a thermally developing flow with a fully developed velocity profile subjected to a uniform wall temperature.

b. Thermal Entry Region - Constant Wall Heat Flux

For the thermal entry length problem under a constant wall heat flux boundary condition, Shah and London [Ref. 9] present several numerical solutions but recommend the following approximate equations for the local Nusselt number:

$$\begin{aligned} Nu_x &= 1.302(x^*)^{-1/3} - 1 & \text{for } x^* \leq 5 \times 10^{-5} \\ Nu_x &= 1.302(x^*)^{-1/3} - 0.5 & \text{for } 5 \times 10^{-5} \leq x^* \leq 1.5 \times 10^{-3} \\ Nu_x &= 4.364 + 8.68(10^3 x^*)^{-0.506} e^{-41x^*} & \text{for } x^* \geq 1.5 \times 10^{-3} \end{aligned} \quad (2.13)$$

Shah and London also recommend the following approximate equations for the mean Nusselt number:

$$\begin{aligned} Nu_m &= 1.953(x^*)^{-1/3} & \text{for } x^* \leq 0.03 \\ Nu_m &= 4.364 + \frac{0.0722}{x^*} & \text{for } x^* > 0.03 \end{aligned} \quad (2.14)$$

The above two sets of equations are for a thermally developing, hydrodynamically developed flow subjected to a constant wall heat flux.

c. Combined Entry Length

As discussed earlier, the rate at which the temperature and velocity profiles develop is dependent upon the Prandtl number. At medium to high Prandtl numbers ($Pr > 100$), the velocity profile develops much more rapidly than the temperature profile and a fully developed velocity profile assumption is valid; for such conditions the equations given above should be used.

For $1 < Pr < 100$, however, a fully developed velocity profile is no longer a valid assumption and a combined entry length solution must be developed.

Again, Shah and London [Ref. 9] present a comprehensive study of various solutions to the combined entry length problem, including two solutions for local Nusselt numbers developed by Churchill and Ozoe [Ref 13], the first, for a uniform wall temperature:

$$\begin{aligned} & \frac{Nu_x + 1.7}{5.357(1 + [(388/\pi)x^*]^{-8/9})^{3/8}} \\ & = \left[1 + \left(\frac{\pi/(284x^*)}{(1 + (Pr/0.0468)^{2/3})^{1/2} (1 + [(388/\pi)x^*]^{-8/9})^{3/4}} \right)^{4/3} \right]^{3/8} \end{aligned} \quad (2.15)$$

and the second, for a constant wall heat flux:

$$\begin{aligned} & \frac{Nu_x + 1}{5.364(1 + [(220/\pi)x^*]^{-10/9})^{3/10}} \\ & = \left[1 + \left(\frac{\pi/(115.2x^*)}{(1 + (Pr/0.0207)^{2/3})^{1/2} (1 + [(220/\pi)x^*]^{-10/9})^{3/5}} \right)^{5/3} \right]^{3/10} \end{aligned} \quad (2.16)$$

From the preceding paragraphs, it can be seen that the subject of laminar flow forced convection in circular ducts has been studied in great detail yielding both analytical and experimental results. The reader is referred to Shah and London [Ref. 9] and Kays and Crawford [Ref. 11] for a more complete and thorough review of this subject.

C. AUGMENTATION TECHNIQUES TO ENHANCE TUBESIDE HEAT TRANSFER

1. General Introduction

As discussed earlier, when laminar flow heat transfer occurs within tubes, it usually represents the dominant thermal resistance in a heat exchanger. These large resistances result in low inside heat transfer coefficients. In recent years, the requirement for more efficient heat exchangers has stimulated considerable interest in techniques to augment or enhance tubeside heat transfer.

The various methods to enhance tubeside heat transfer can be classified into two categories, passive and active techniques. Passive techniques involve no external energy (except increased pump work) to produce the necessary enhancement. Passive techniques are divided into the following methods:

1. Internally finned tubes (longitudinal or spiral fins) designed to increase the inside heat transfer surface area.
2. Surface roughness techniques aimed at agitating flow rather than increasing heat transfer surface area.
3. Swirl flow techniques which involve the use of inlet vortex generators, periodically spread propellers or twisted tape inserts designed to cause enhancement by creating a rotating and/or secondary flow.
4. Displaced promoters which alter the fluid flow near the surface by the use of inserts such as wire mesh, static mixer elements, rings or disks.
5. Coolant additives designed to increase the conductivity of the coolant.
6. Compound techniques that involve more than one of the above mentioned methods.

Active techniques utilize an external energy source to promote the required augmentation. These techniques include: (1) mechanical aids, (2) heated surface vibration, (3) fluid pulsation, (4) electrostatic fields, and (5) suction or injection.

All of the above techniques are aimed at creating turbulence in the relatively slow moving or stagnant boundary layer fluid by displacing this fluid from the heated surface and mixing it with the bulk fluid. Essential in all of these techniques is a balance between increased heat transfer rate and increased pumping power requirements/costs. Bergles and Joshi [Ref. 14] present an excellent review of augmentation techniques and compare heat transfer data taken at low Reynolds number flow subjected to both uniform wall temperature and constant wall heat flux.

Of particular interest to this thesis are two passive techniques, the swirl flow technique using twisted tape inserts and the displaced promoter technique using wire mesh inserts. These two methods of enhancement of tubeside heat transfer are discussed in more detail in the following sections.

2. Heat Transfer Enhancement with Twisted Tape Elements

Among the most common swirl flow augmentation techniques is the use of twisted tape inserts. The tapes usually consist of a thin stainless steel, brass or copper strip which is the width of the inside diameter of the tube. The tapes are twisted by clamping one end to an overhead, attaching weights to the other end and then twisting to the desired specifications [Ref. 15]. Enhancement occurs not only

due to the increased path length of flow, but also due to secondary flow effects and fin effects caused by tape contact with the inside tube wall.

Analytical studies of twisted tape inserts by Date and Singham [Ref. 16] suggest that swirl flows improve heat transfer by as much as a factor of 70; however, no experimental data have confirmed their unrealistically large predictions. The first experimental work of swirl flow using twisted tapes was conducted by Hong and Bergles [Ref. 15]. Their primary objective was to develop experimentally based correlations for predicting heat transfer coefficients for laminar flow of water and ethylene glycol in an electrically heated tube (heated length of 1.22 m, inside diameter of 10.2 mm) with two sizes of twisted tape inserts. They showed that the Nusselt number was independent of axial location, suggesting that fully developed conditions existed. Therefore, the mean Nusselt number should take the form:

$$Nu_m = f(Re_s, Pr, y). \quad (2.17)$$

Re_s is the Reynolds number for the swirl flow given by:

$$Re_s = \frac{4\dot{m}}{\pi\mu(D_i - 4\delta)} \quad (2.18)$$

and δ is the tape thickness. The twist ratio, y , is defined as:

$$y = \frac{H}{D_i} \quad (2.19)$$

where H is the pitch for a 180° twist of the tape. Hong and Bergles then combined Re , and y as a single parameter and came up with the following correlation for values of $Re/y > 10$:

$$Nu_m = 0.383 Pr^{0.35} (Re/y)^{0.622} \quad (2.20)$$

For values of $Re/y < 10$, the following correlation was obtained:

$$Nu_m = 5.172 \{1 + 5.484 \times 10^{-3} Pr^{0.7} (Re/y)^{1.25}\}^{0.5} \quad (2.21)$$

It should be noted that all fluid properties in equations 2.20 and 2.21 should be evaluated at the bulk fluid temperature. One additional important observation was made by Hong and Bergles regarding tube wall temperature. They found a significant variation of temperature at one axial location with two different tape orientations at that position of 90° and 120° , suggesting that the temperature profile was related to the tape orientation. Hong and Bergles concluded that for a fully developed flow, inside heat transfer coefficients depend on twist ratio and could be improved by a factor of two or three over an empty tube. These conclusions were confirmed by later studies of Saha et. al. [Ref. 17] and Marner and Bergles [Ref. 18].

3. Heat Transfer Enhancement with Wire Mesh (HEATEX) Elements

The use of wire mesh inserts to promote inside heat transfer falls into the displaced promoter technique mentioned earlier. One such wire mesh insert was commercially developed by CAL-GAVIN Limited (UK) and called "HEATEX."

This HEATEX insert consists of a central wire core on which a series of wire loops or petals are attached. The petals are attached to the core at an inclined angle that face the oncoming fluid flow. Ideally, each petal makes contact with the tube wall in the form of an arc, thereby maximizing disturbance of fluid along the tube wall. In addition to the boundary layer disturbance, radial mixing occurs caused by repeated redistribution and mixing of fluid through the mesh of loops near the tube axis [Ref. 19]. Various wire loop densities and nominal diameters are available, depending on the application.

Initial studies by Gough et. al. [Ref. 19] with HEATEX inserts suggest enhancements of a factor greater than ten times that of a similar tube with no insert. Additional experiments were conducted by Oliver and Aldington [Ref. 20] in which a correlation was determined:

$$Nu = 0.232 Re^{0.54} Pr^{0.46} \quad (2.22)$$

It must be remembered, however, that this correlation is for a specific loop density and nominal diameter HEATEX element.

The two types of HEATEX mixing elements supplied by CAL-GAVIN (nominal diameters of 13.26 and 10.16 mm) did not match the loop densities of previous studies; therefore new correlations needed to be developed. Mazzone [Ref. 6] developed correlations for these inserts from limited data supplied by CAL-GAVIN. For the 13.26 mm and 10.16 mm elements, these correlations were respectively:

$$Nu = 0.226 Re^{0.65} Pr^{0.46} \quad (13.26mm) \quad (2.23)$$

and

$$Nu = 0.063 Re^{0.76} Pr^{0.46} \quad (10.16mm) \quad (2.24)$$

Since these correlations were developed from a very limited amount of data taken under conditions that did not exactly match that of Mazzone's condensation experiments, they were always subject to inaccuracy. Therefore, the need for more accurate correlations under the exact conditions used in the condensation experiments are required.

III. EXPERIMENTAL APPARATUS

A. SYSTEM OVERVIEW

The test apparatus utilized is shown in Figures 3.1 and 3.2. The apparatus is a closed loop, low pressure system utilizing an ethylene glycol/water mixture as the coolant. The coolant is circulated by a centrifugal pump from a supply tank, through a reducing manifold and flowmeter into the test section. Coolant is then returned to the supply tank via a return header.

The test section consisted of an inlet and outlet thermocouple well/mixing chamber to measure inlet and outlet coolant temperatures and the test tube itself. The tube was instrumented with twelve thermocouples (embedded in the tube wall) to determine inside wall temperatures. A constant heat flux boundary condition was achieved using a series of flexible electrical heating elements wrapped around the tube. Monitoring the system as well as data acquisition and data processing were provided by a Hewlett-Packard microcomputer and Data Acquisition System.

EXPERIMENTAL APPARATUS PRIMARY AND SECONDARY COOLANT SYSTEMS

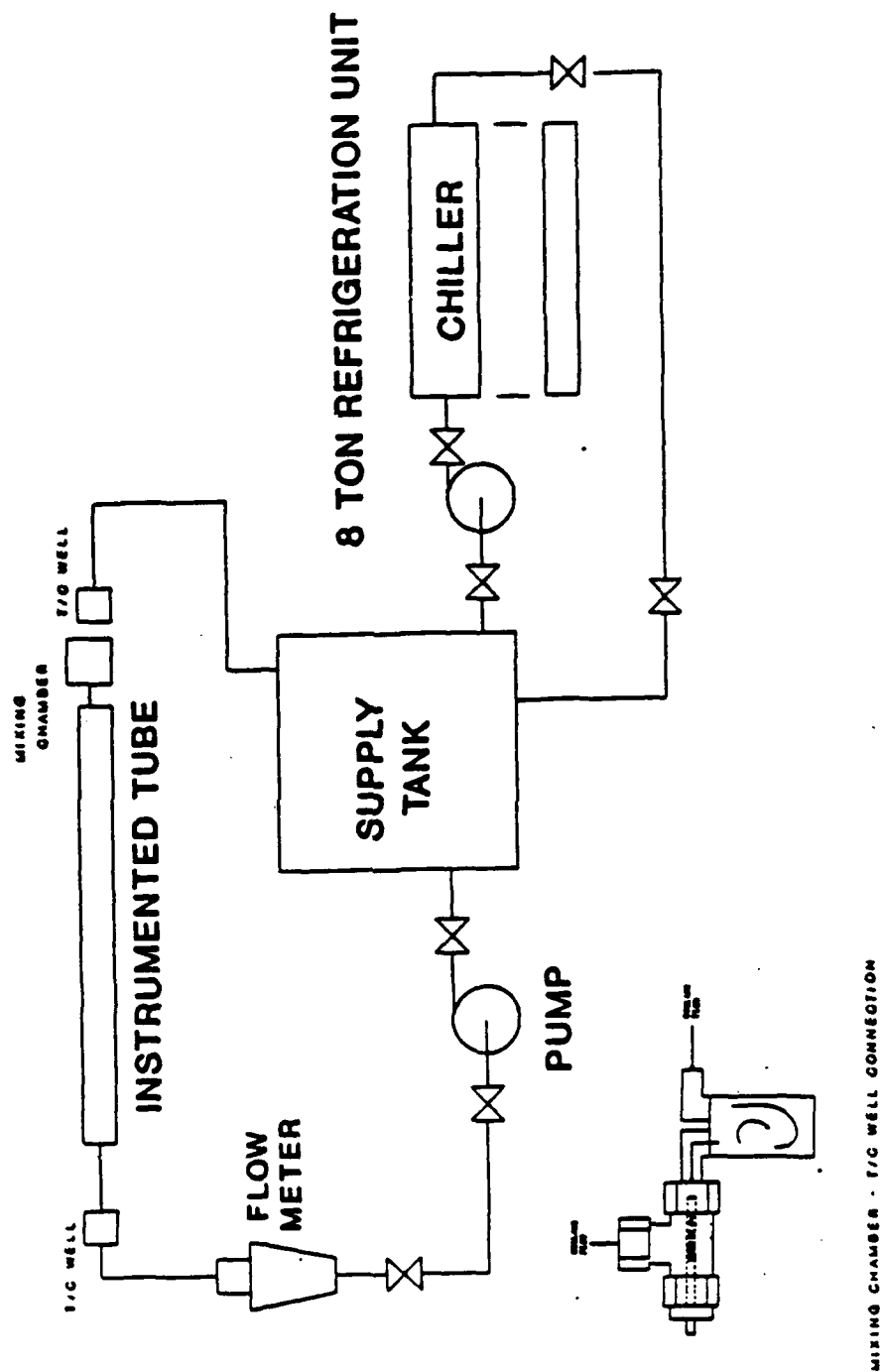


Figure 3.1 Primary and Secondary Coolant Systems.

DATA ACQUISITION & CONTROL SYSTEM

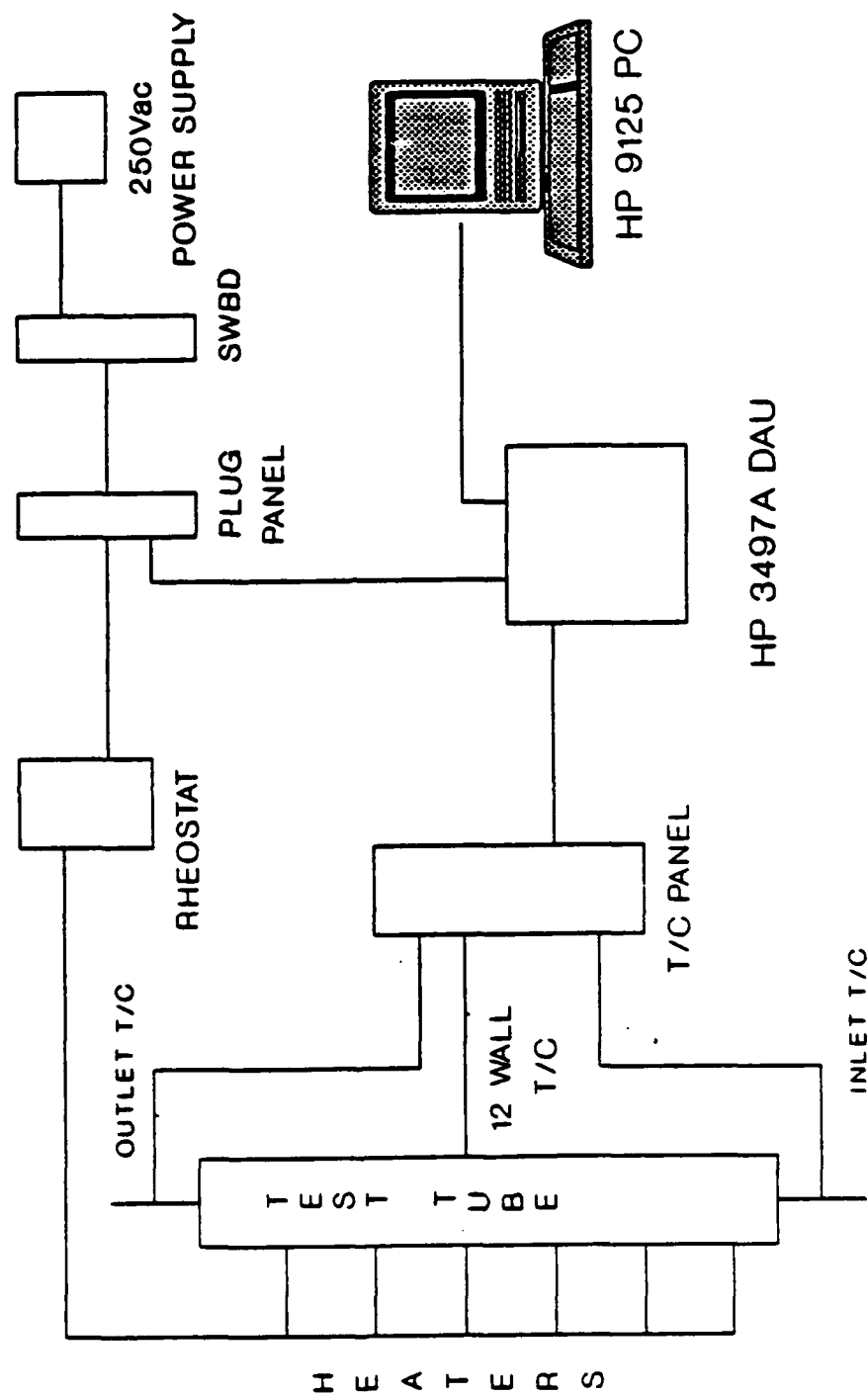


Figure 3.2 Data Acquisition and Control Systems.

B. TUBES AND INSERTS TESTED

1. Tubes Tested

Three types of tubes were utilized in the experiments, a copper smooth tube, a copper/nickel externally finned tube, and a copper/nickel corrugated or roped tube. These tubes correspond to the tubes utilized in the refrigerant condensation experiments of Mabrey [Ref. 5] and Mazzone [Ref. 6].

The smooth copper tube provided a baseline set of experimental data which were then compared with previous experimental and theoretical work for the inside heat transfer coefficient conducted by Shah and London [Ref. 9] for no insert, Oliver and Aldington [Ref. 20] for the HEATEX insert, and Hong and Bergles [Ref. 15] for the twisted tape insert.

The Cu/Ni finned tube provided a smaller inside diameter to be used in these comparisons. Note that the fins play little part in the experiments. The wall thermocouples were buried in the tube wall and were used to measure the inside wall temperature, which had a smooth bore. Consequently, for the purposes of these experiments, the tube behaved like a smooth copper tube with a different internal diameter.

The final tube tested was a Cu/Ni corrugated (or roped) tube, commercially referred to as a "Korodense" tube. The tube was manufactured and provided by Wolverine Tube Company of Decatur, Al. All tube dimensions and specifications were taken from the Wolverine Technical Bulletin No. 4020 [Ref.

21]. Figure 3.3 is a schematic of the Korodense tube. Tube specifications for all three tubes are listed in Table E.1 of Appendix E.

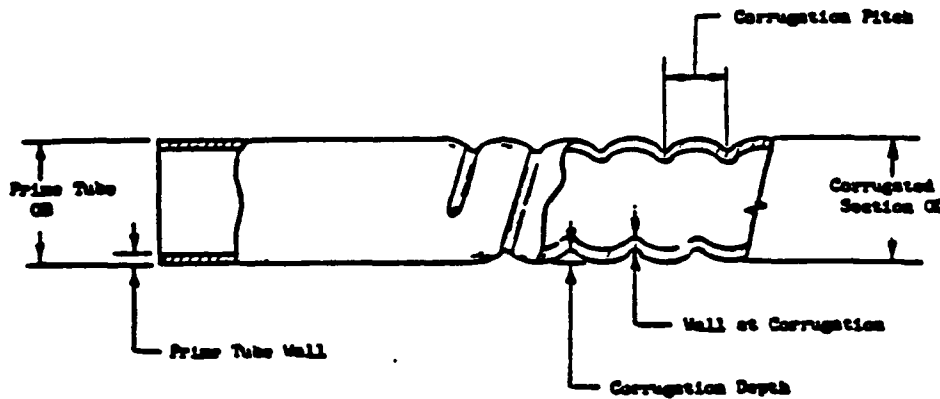


Figure 3.3 Wolverine Korodense Tube (Courtesy [Ref. 21])

2. Insert Elements Tested

Two types of insert mixing elements were utilized in this investigation, a twisted tape insert and a wire mesh insert commercially referred to as a "HEATEX" tube insert. In both cases, two sizes were required due to the two different tube inside diameters used.

The twisted tape inserts were made of a strip of brass 0.559 mm thick and either 10.16 mm or 13.26 mm wide. The tapes were manufactured in the NPS Mechanical Engineering machine shop by clamping them to the overhead, attaching a weight to the opposite end, and twisting them to the desired twist ratio. A twist ratio of 3 and 4 corresponding to the two respective tube inside diameters were manufactured. Once installed in the tube, the edges of the tape should ideally have been in contact with the tube wall.

The second type of insert used was a commercially available product referred to as HEATEX radial mixing elements. These elements were supplied by Cal Gavin of Birmingham, U.K. They are manufactured from stainless steel and consist of a central wire core onto which a series of wire loops or petals are attached. Each petal was inclined at an angle facing the oncoming flow. The outside diameter of the elements were slightly oversized for the tube, ensuring that close contact with the tube wall in the form of an arc, rather than a point, was achieved. As with the twisted tape elements, different diameter HEATEX elements were needed, 13.26 mm used in the smooth and Korodense tubes and the other 10.15 mm for the Cu/Ni finned tube. Figure 3.4 shows both the twisted tape and HEATEX inserts.

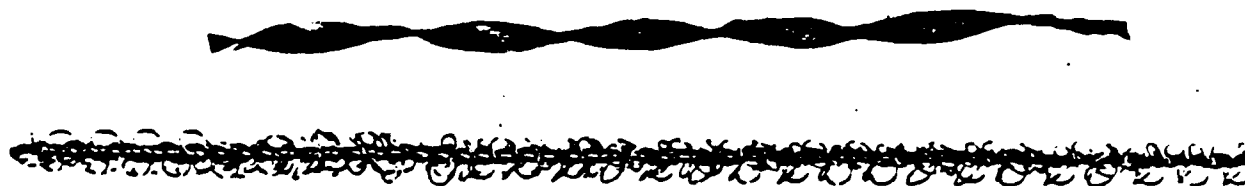


Figure 3.4 Twisted Tape and HEATEX Inserts

C. COOLANT SYSTEM

1. Primary Coolant System

An ethylene glycol/water mixture (54/46% by weight) was stored in a 1.5 m³ insulated supply tank. The mixture was circulated through the primary system by a 1½ hp, constant speed, centrifugal pump. The coolant was discharged from the pump via a 76 mm diameter PVC pipe to a manifold where it was reduced to a 15.9 mm diameter Tygon flexible tube. A rotameter type flowmeter with a ball valve at its entrance was used to control the flow rate through the system. Flowmeter calibration results are discussed in Appendix A.

Flow entered the test section through a 90° bend which housed the thermocouple well and exited through a mixing chamber/thermocouple well combination (see Figure 3.1). Prior to entering the exit mixing chamber, the coolant passed through a 10 cm length of flexible tubing containing a high density wire mesh. This wire mesh, in conjunction with the mixing chamber, served to minimize radial temperature variations and provide a uniform outlet coolant temperature. The flow then exited the test section through more flexible tubing to a manifold and return PVC header, suspended above the apparatus, and back to the coolant supply tank.

2. Secondary Coolant System

In order to achieve a wide range of Reynolds number, coolant inlet temperatures were varied from -10°C to +20°C. This was accomplished by a secondary coolant system comprised of a 28 kW (8 ton) external refrigeration system.

A 30 gpm, .75 hp centrifugal pump continuously circulated coolant between the supply tank and a chiller barrel where it was cooled to the desired temperature. Temperature was maintained by a thermostatically controlled solenoid valve at the discharge side of the chiller barrel. This system allowed for a range of coolant temperatures between -20°C and ambient to be selected while maintaining the coolant inlet temperature approximately constant ($\pm 2^{\circ}\text{C}$) during each run.

D. INSTRUMENTATION AND TEST SECTION

1. Instrumentation

All temperature measurements were made using copper/constantan type-T teflon coated thermocouples and were previously calibrated by Mabrey [Ref. 5]. The inlet coolant temperature was measured by a single thermocouple while the outlet coolant temperature was measured by two thermocouples located immediately after the mixing chamber.

Each test tube was fitted with twelve wall thermocouples to determine the average inside wall temperature. Thermocouples were placed at four different longitudinal positions along the axis of the tube. Three thermocouples at each location were spread evenly around the tube at 120°C intervals. Figure 3.5 shows a typical tube with the exact longitudinal and nodal thermocouple locations. Actual longitudinal locations varied slightly for each tube and are given in Table E.1 as x/D_i where x is the length from the start of the heated length to the thermocouple location and D_i is the inside diameter of the tube. The two extreme longitudinal

locations of the thermocouples corresponded to the beginning and end of the "effective" condensing length of the tubes being used in the condensation experiments of Mabrey [Ref. 5] and Mazzone [Ref. 6].

INSTRUMENTED TUBE

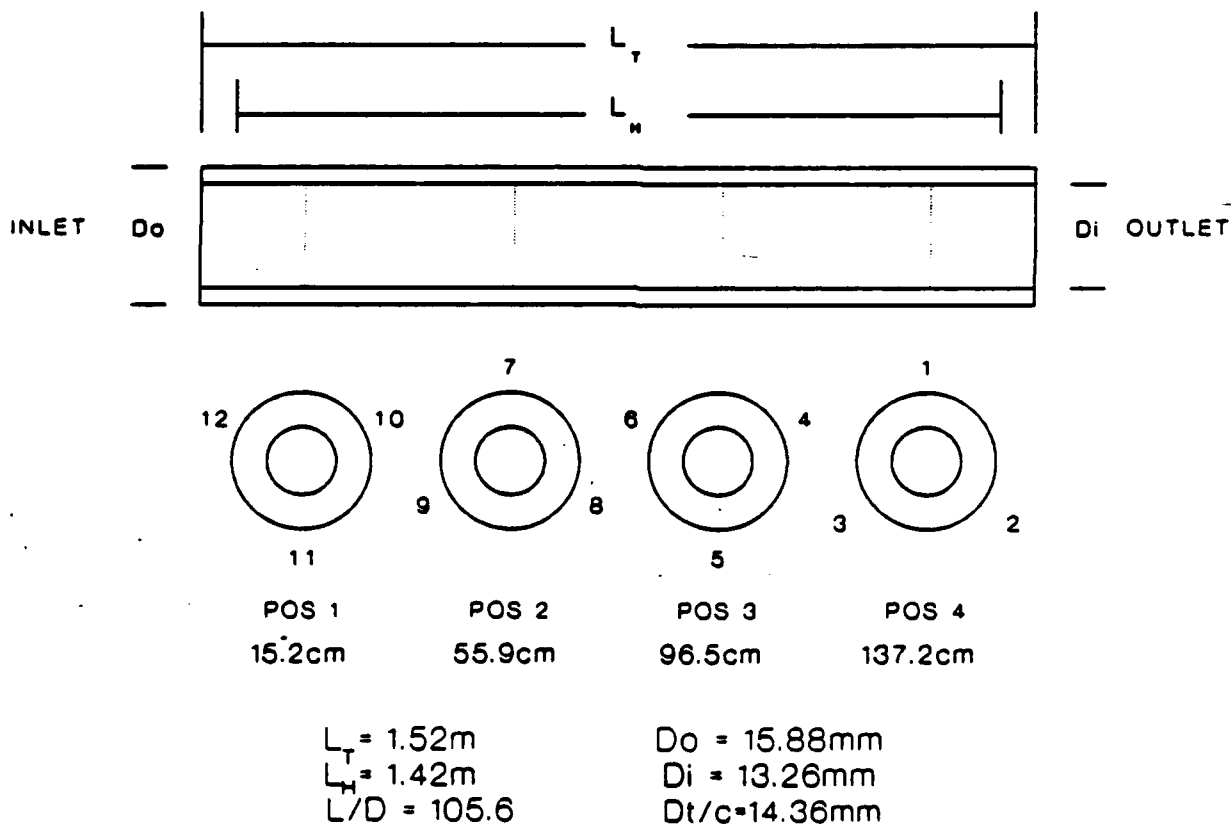


Figure 3.5 Instrumented Tube

2. Thermocouple Attachment Method

In order to attach the thermocouples to the wall of the tube, short longitudinal grooves were cut at each location. These longitudinal grooves were cut to a depth of $\frac{1}{2}$ the tube wall thickness. It was decided that a thermocouple embedded within the tube wall vice being attached to the surface would lead to a more accurate tube wall temperature and minimize the effect of direct contact heating from the heating elements. Thermocouples were then placed in these grooves and either soldered in place or tack welded and covered with a liquid metal epoxy. Different methods for attaching and covering the thermocouples were used for each tube based on the tube material and configuration (discussed below).

In the case of the smooth copper tube, the thermocouples were silver soldered in place and the remainder of the groove then covered with silver solder. Since the tubes were copper, this was relatively easy to accomplish. Care was taken to ensure that the thermocouple remained in contact with the tube wall and that no air pockets were created (which would cause an additional large resistance to heat flow). Also, great care was taken to prevent any melting of the teflon insulation past the thermocouple joint. This condition could have caused an electrical contact between the two wires of the thermocouple prior to the tube wall, leading to an unrealistically high observed wall temperature.

A different method was required to attach the thermocouples to the copper/nickel finned tube due not only to the external fins but also the 10% nickel content. Initially, a small diameter hole was machined into the tube to minimize fin

damage (rather than cutting a longitudinal groove). Since the thermocouple was to be embedded half way into the tube wall, this hole proved to be relatively deep. Also, because of the nickel content of these tubes, the preheat temperature required to ensure that the silver solder would adhere to the tube wall was much higher. These higher required temperatures and the hole depth caused a significant amount of the thermocouple teflon insulation to be melted, allowing for potential contact between the thermocouple wires at some point other than the tube wall. This technique was therefore abandoned in favor of the longitudinal groove method. However, thermocouple insulation was again being destroyed due to the higher required preheat temperatures. An alternative solder, soft solder, with lower preheat and melting temperatures, was therefore used. The final combination of longitudinal grooves and soft solder was successful.

For the copper/nickel Korodense tube, the groove and soft solder method was again tried. Initial tests in the apparatus showed wall temperatures at one longitudinal position varying by as much as 15°C. On closer examination of the thermocouple connections (using a magnifying glass), it was revealed that insulation damage was evident on over half of the thermocouples. Several more attempts at the groove and soft solder method were tried, all leading to the same results.

A third method utilizing a tack welding machine (acquired and adapted for our use) was tried. Thermocouples were tack welded into the bottom of the groove resulting in no damage to the insulation and a liquid steel epoxy was used to fill the remainder of the groove, providing additional strength and protection to the

connection. This final method proved to be the most successful and is recommended for use in any follow-up experiments.

3. Test Section

In order to achieve a constant heat flux, each tube was tightly wrapped with six silicone rubber flexible electrical heating elements rated at 240 V, 200 W each. Each strip was 2.5 cm wide and 50.6 cm long. The heating elements were connected in parallel to a 240 Vac power supply via a plug panel and power switchboard. Power to the six heaters was controlled by a STACO, 240 Vac, 23.5 kVa rheostat (see Figure 3.2).

To minimize heat loss from the heater to ambient, the tube was wrapped in a 20 mm thick neoprene type insulation. This type of insulation proved to be extremely effective giving a negligible heat loss. It also provided insulation against heat influx from ambient at the colder coolant inlet temperatures. Actual heat loss and heat influx experiments and their results are discussed in more detail in Appendices B and C. All other tubing and PVC piping was wrapped in similar type insulation.

The whole test section was then placed in a restraining stand which minimized outside vibration effects and ensured that each tube remained horizontal and in the same relative position (to the remainder of the apparatus) for each experiment.

E. DATA ACQUISITION AND CONTROL SYSTEM

A Hewlett-Packard 9125 microcomputer (MC) was used to control a Hewlett-Packard 3497A Automatic Data Acquisition Unit (DAU) (see Figure 3.2). The DAU read the output from the twelve tube wall thermocouples and three coolant thermocouples (one inlet and two outlet). Additional channels were assigned to sense heater input voltage and current at the plug panel. The voltage was converted to heater power using the heater resistance and the calibration discussed in Appendix D.

Thermocouple readings were made in microvolts which were converted to temperatures (along with the heat flux calculations) using the data reduction program. The data reduction program, DRPSING, will be discussed in more detail in a later chapter. All temperatures, power, and heat flux measurements were monitored using the MC and DAU. DAU channel assignments are listed in Table 3.1.

TABLE 3.1 DATA ACQUISITION UNIT CHANNEL ASSIGNMENTS

CHANNEL NO.	MEASURED QUANTITY
1	Thermocouple Pos 1
2	Thermocouple Pos 2
3	Thermocouple Pos 3
4	Thermocouple Pos 4
5	Thermocouple Pos 5
6	Thermocouple Pos 6
7	Thermocouple Pos 7
8	Thermocouple Pos 8
9	Thermocouple Pos 9
10	Thermocouple Pos 10
11	Thermocouple Pos 11
12	Thermocouple Pos 12
13	Tube Inlet
14, 15	Tube Outlet
25	Input Current
29	Input Voltage

IV. EXPERIMENTAL PROCEDURES

A. CALIBRATION EXPERIMENTS

Several calibration experiments were required prior to performing the main experiments. Figure 4.1 depicts a typical tube being tested. The primary heat source is from the heating elements (\dot{q}_{tape}). However, to complete the heat balance on the system, several other heat sources and heat sinks needed to be accounted for. The first experiment conducted was to determine the amount of heat being lost from the heating elements to the atmosphere vice going to the coolant. Heat loss experiments are discussed in Appendix B.

The second experiment was to account for two additional potential heat sources: heat leakage into the coolant from ambient (\dot{q}_{leak}) and frictional temperature rise (\dot{q}_{fric}). Approximately 8 cm at either end of the tube, along with the flexible tubing section prior to the thermocouple wells, were not covered by the heating elements. Since coolant inlet temperatures were primarily below ambient temperature, a potential for heat leakage to the coolant from ambient existed. Also, because of these cold inlet temperatures, frictional heating could exist, especially when using the various inserts. Heat leakage into the system and frictional effects were considered together as one heat influx. These experiments were conducted with the heater tapes turned off; any temperature rise was then monitored using the inlet

and outlet thermocouples. Appendix C discusses the experiments conducted to determine this part of the heat balance equation. As mentioned earlier, the test section and all other tubing were insulated to minimize these effects.

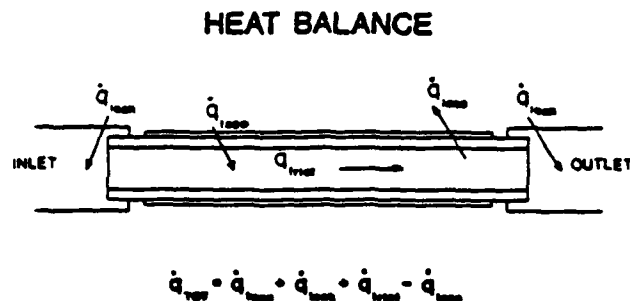


Figure 4.1 Heat Balance.

B. PROCEDURES FOR DETERMINATION OF INSIDE HEAT TRANSFER RATE

1. General Procedures

Each tube utilized in this study was tested with no insert and the appropriate twisted tape and HEATEX inserts corresponding to the tube inside diameter. For each insert condition, four nominal coolant inlet temperatures, -10°C , 0°C , $+10^{\circ}\text{C}$ and $+20^{\circ}\text{C}$ were chosen to increase the range of experimental Reynolds and Prandtl numbers that could be attained. To check that heat flux variations did not affect the results, data were taken at heat fluxes of 10 kW/m^2 and 15 kW/m^2 for each inlet temperature. For each insert, coolant inlet temperature and heat flux setting, coolant velocity was varied between 0.2 m/s and 1.4 m/s . Since the inside diameter of the Cu/Ni finned tube was smaller than the other two tubes, higher

coolant velocities of up to 2.4 m/s could be attained. A matrix of the individual data runs and data file names is shown in Table 4.1.

With the tube installed and all calibration experiments completed, the experiments to determine the inside heat transfer coefficient were conducted. Since flowmeter settings for specific coolant velocities were based upon the inlet coolant temperature, the system was initially operated at a 100% flowmeter setting with no power to the heating elements for 15 minutes. This allowed the inlet thermocouple well to stabilize. Once the desired inlet coolant temperature was reached and maintained, power to the heating elements was set to the predetermined heat flux setting for that data run (10 or 15 kW/m²). The flowmeter was then adjusted to achieve the desired coolant velocity based upon flowmeter calibration results (discussed in Appendix A). Flow was maintained for approximately 10 minutes to ensure steady state equilibrium conditions prior to taking data.

TABLE 4.1 DATA FILE NAMES

TEMP(C)/ q" (kw/m ²)	Cu Smooth Tube			Cu/Ni Finned Tube			Cu/Ni Korodense Tube		
	No Insert	Twisted Tape	HEATEX	No Insert	Twisted Tape	HEATEX	No Insert	Twisted Tape	HEATEX
20/10	SMNI04	-	SMHX04	CFNI04 (+15)	CFT01 (+15)	CFHX01 (+15)	KDNI01	KDTT01	KDHX01
20/15	SMNI04	-	SMHX04	CFNI04 (+15)	CFTT01 (+15)	CFHX01 (+15)	KDNI01	KDTT01	KDHX01
10/10	SMNI03	SMTT01	SMHX01	CFNI01	CFTT02	CFHX02	KDNI02	KDTT02	KDHX02
10/15	SMNI03	SMTT01	SMHX01	-	CFTT02	CFHX02	KDNI02	KDTT02	KDHX02
0/10	SMNI02	SMTT02	SMHX02	CFNI03	CFTT03	CFHX03	KDNI03	KDTT03	KDHX03
0/15	SMNI02	SMTT02	SMHX02	CFNI03	CFTT03	CFHX03	KDNI03	KDTT03	KDHX03
-10/10	SMNI01	SMTT03	SMHX03	CFNI02	CFTT04	CFHX04	KDNI04	KDTT04	KDHX04
-10/15	SMNI01	SMTT03	SMHX03	CFNI02	CFTT04	CFHX04	KDNI04	KDTT04	KDHX04

Velocities were increased from 0.2 m/s to 1.4 m/s in steps of 0.2 m/s and then decreased from 1.3 m/s to 0.3 m/s in similar steps. This method of increasing on even values and decreasing on odd values was done not only to determine if any hysteresis effects existed (i.e., a difference in the increasing and decreasing data), but also to ultimately increase the number of data points acquired. Also, since data were immediately plotted (as Nu_m versus Re), the method allowed for an easy determination as to whether a data point had reached a steady state condition.

Inlet and outlet coolant temperatures, tube wall temperatures, heat flux and heating element power settings were all continuously monitored using the computer program DRPSING in conjunction with the Data Acquisition System discussed earlier (DRPSING is listed in Appendix G). Individual data runs for each tube and insert condition were conducted in a similar manner.

2. Specific Experiments

a. *Copper Smooth Tube*

The first tube tested was the copper smooth tube. This tube was chosen to provide a baseline set of data needed for validation of system performance and for comparison with data acquired using other tubes. It should also be noted that two complete independent sets of data covering all insert conditions and inlet temperatures were taken over a period of two weeks. Data from both sets were compared and found to be in very good agreement ($\pm 2\%$); this validated the repeatability of data obtained from the system under the same conditions.

The initial intention for all tubes was to start with a given insert at the highest coolant inlet temperature, take data at each of the heat flux settings and then proceed to the next coolant temperature. Once one insert was completed, the system could then be shut down and the insert changed. This procedure would then be repeated for all three insert conditions. However, the coolant supply tank and coolant system were used concurrently for other experiments which required the coolant temperature to be -20°C . Since it took approximately 36-48 hours for the coolant temperature to increase from -10°C to $+20^{\circ}\text{C}$ (the sump was not fitted with a heater), only the copper smooth tube was done in this way. The method for the other two tubes is discussed below.

b. Cu/Ni Externally Finned Tube

The second tube tested was the Cu/Ni finned tube. For a given inlet temperature and tube insert, the same procedure as with the copper smooth tube was used. However, rather than decreasing coolant temperature with the same insert, the coolant temperature was maintained and the insert changed until all three of the insert conditions were completed for a given inlet temperature. Once all the data for a given inlet temperature had been taken, the supply tank temperature was decreased to the next inlet temperature condition. It took only about one hour for the secondary coolant system to decrease the temperature by 10°C . Since it was a relatively short task to change inserts, the 36 to 48 hour waiting period required to raise coolant temperatures back to $+20^{\circ}\text{C}$ between insert changes was eliminated.

It should be noted that for the Cu/Ni finned tube, the highest nominal inlet temperature attained was only +15°C vice +20°C. Colder than normal ambient temperatures existed preventing supply tank temperatures from reaching +20°C. Also, due to the smaller inside diameter, coolant velocities could be varied between 0.3 m/s and 2.4 m/s.

c. Cu/Ni Korodense Tube

The same procedure used with the finned tube was also used with the Korodense tube. In addition, another test was conducted with this tube. It was noted that larger than normal wall temperature variations existed at one longitudinal location when using the two inserts. It was suspected that the point of contact between the insert and tube wall was directly below a thermocouple position causing a higher wall temperature at that point. To verify this, the system was shut down by securing the coolant pump and the heating elements so that the flowmeter and power settings remained exactly the same. The outlet end of the tube was opened and the insert moved downstream by approximately 2 cm. The system was then closed and the coolant flow and power to the heating elements restored. Wall temperature variations still existed but were significantly less. This procedure was repeated several times with similar results.

V. DATA REDUCTION

A. AVERAGE INSIDE HEAT TRANSFER COEFFICIENT

The main objective of the data reduction scheme was to determine the average inside heat transfer coefficient (\bar{h}_i). This in turn was used to determine a mean Nusselt number (for the whole heated length of the tube) to be used as the basis for establishing the desired correlations.

To accomplish this task, the Data Acquisition Unit discussed in Chapter III made use of the computer program DRPSING. A listing of the program is given in Appendix E. The program allowed the user to monitor information from the instrumentation attached to the apparatus, acquire and then process the data to determine the desired output. In doing this, the user would select the tube and insert condition as well as the nominal coolant inlet temperature for that particular data run. The desired coolant velocity was then selected. Based on the actual measured coolant inlet temperature, coolant mixture properties and flowmeter calibration results (see Appendix A), the appropriate flowmeter setting (as a %) was calculated and set on the flowmeter.

The program then monitored coolant inlet and outlet temperatures, the twelve wall thermocouple temperatures and the actual measured heat flux and power settings. Once all readings reached a steady state condition (approximately 10 min.),

the user could terminate the display session and acquire data for that coolant velocity setting.

The DAU measures emf from the thermocouples and then converts these values to temperatures using the temperature calibration equation developed by Mabrey [Ref. 5]. Heater power was determined by measuring the voltage at the plug panel and calculating the power based on heater resistance and the power calibration contained in Appendix D.

The twelve wall thermocouples (placed axially and radially) were used to minimize the uncertainty in determining the average inside wall temperature. These twelve wall temperatures were averaged and corrected (to account for the depth of burial using a simple conduction calculation) to determine the average inside wall temperature, \bar{T}_{wi} .

The physical and thermodynamic properties of the ethylene glycol/water mixture (density, dynamic viscosity, thermal conductivity, heat capacity) were determined using equations and figures from Cragoe [Ref. 22] and Gallant [Ref. 23] and correlated by Mabrey [Ref. 5]. From these quantities, the coolant mass flow rate was calculated by:

$$\dot{m} = V_c \rho_c A_i \quad (5.1)$$

where A_i is the inside cross sectional area of the tube and V_c is the set coolant velocity. The coolant Reynolds number, Re_D was calculated by:

$$Re_D = \frac{V_c D_i \rho_c}{\mu_c} \quad (5.2)$$

where D_i is the inside diameter of the tube. The dimensionless distance (x^*) in the flow direction is calculated as:

$$x^* = \frac{x/D_i}{Re_D Pr} \quad (5.3)$$

where x is the axial distance from the beginning of the heated length.

To determine the heat transfer rate to the coolant, several factors were considered. The basic equation to determine the heat transfer rate is given by:

$$\dot{q} = \dot{m} c_p \Delta T \quad (5.4)$$

where ΔT is the measured coolant temperature rise along the tube. The temperature rise required is that for the actual heated length of the tube that is subjected to the constant heat flux condition, ΔT_{HL} . To determine ΔT_{HL} from ΔT , corrections have to be made to account for heat loss, heat leakage and heat transferred to the unheated ends. Figure 5.1 depicts a typical tube and the correction terms considered in the heat balance.

The overall ΔT is first corrected for heat loss to the ambient, (\dot{q}_{loss}) and heat leakage into the system, (\dot{q}_{leak}). The heat leakage term consisted of any temperature rise due to the influx of heat from ambient as well as that caused by frictional effects. Appendix D discusses the experiments conducted to determine both this heat loss and heat leakage correction.

TEMPERATURE RISE CORRECTIONS

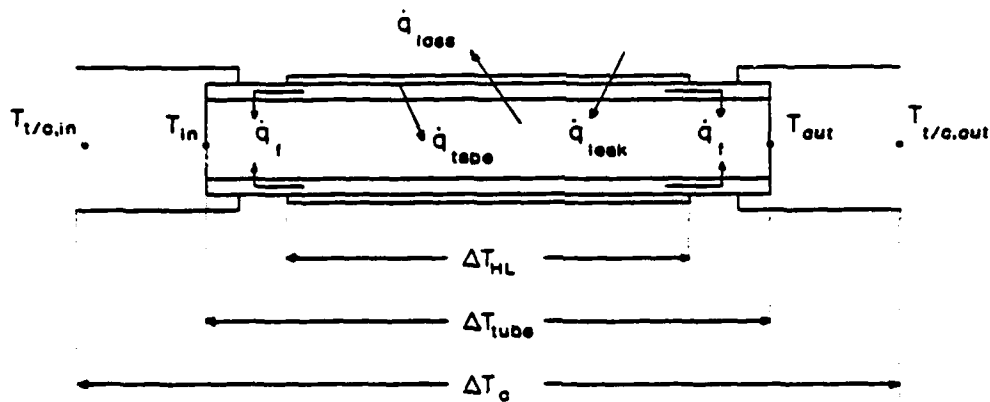


Figure 5.1 Temperature Rise Corrections.

To take account of the heat transferred to the coolant from the unheated ends, the heat transfer rate to the coolant over the entire length of the tube (heated and unheated) is first calculated. The average heat transfer coefficient can then be determined by:

$$\bar{h}_i = \frac{\dot{q}_{HL}}{A_i LMTD} \quad (5.5)$$

where A_i is the inside surface area based on the heated length (L_H) and LMTD is the log mean temperature difference defined as:

At this point in the calculation, however, the heat transfer rate to the coolant from the heated length alone (\dot{q}_{HL}) is not known. Since the heating elements did not

$$LMTD = \frac{T_{out} - T_{in}}{\ln \left[\frac{T_{wi} - T_{in}}{T_{wi} - T_{out}} \right]} \quad (5.6)$$

cover the entire length of the tube, account must be taken of heat added to the coolant from the unheated lengths at the inlet and outlet of the tube. This was accomplished by considering these ends as annular fins. An adiabatic fin tip and outer wall boundary condition was applied and the heat transfer from the fins, \dot{q}_f (as given by Incopera and Dewitt [Ref. 10]), determined from:

$$\dot{q}_f = \sqrt{h_f P k A_c} \theta_b \tanh m L_f$$

where L_f = fin length

P = fin perimeter = πD_i

A_c = fin cross sectional area

$$= \frac{\pi}{4} (D_o^2 - D_i^2)$$

$\theta_b = \bar{T}_{wi} - T_{in}$ (for inlet fin)

$= \bar{T}_{wi} - T_{out}$ (for outlet fin)

$$m = \left[\frac{h_f P}{k A_c} \right]^{0.5}$$

The fin calculation requires a known average inside heat transfer coefficient (\bar{h}_i).

Therefore, an initial estimate of \bar{h}_i is calculated by:

$$\bar{h}_i = \frac{\dot{q}_{tube}}{A_i LMTD} \quad (5.8)$$

where \dot{q}_{tube} is known. The amount of heat that passes through the unheated ends is then calculated using the fin correction above. The heat transfer rate to the coolant from the heated length (\dot{q}_{HL}) is then calculated by:

$$\dot{q}_{HL} = \dot{q}_{tube} - \dot{q}_f \quad (5.9)$$

A new average inside heat transfer coefficient (\bar{h}_i) can then be calculated using equation 5.5 and an iteration process carried out until convergence to a final average inside heat transfer coefficient is reached.

An additional correction for the Cu/Ni finned tube is needed to account for the change in inside diameter of the smooth ends (needed to fit through the tube sheet in the condenser). The heat transfer coefficient based on the smaller inside diameter corresponding to the finned portion of the tube is what ultimately is desired. As shown in Figure 5.2, the heated length extended beyond the smaller diameter section. To correct for this, the annular fin correction discussed earlier was applied to determine the temperatures at the inlet and outlet of the heated length. The coolant temperature rise along the heated length was assumed to be linear, and therefore the temperature rise along the smooth larger inside diameter lengths (L_1 and L_2) could be determined by the simple ratio:

$$\Delta T_1 = \frac{L_1 \Delta T_{HL}}{L_{HL}} \text{ and } \Delta T_2 = \frac{L_2 \Delta T_{HL}}{L_{HL}} \quad (5.10)$$

where L_{HL} is the heated length of the tube and ΔT_{HL} , the temperature rise along the heated length. These corrections were then added or subtracted from the corrected finned inlet and outlet temperatures.

Cu/Ni EXTERNALLY FINNED TUBE TEMPERATURE RISE CORRECTIONS

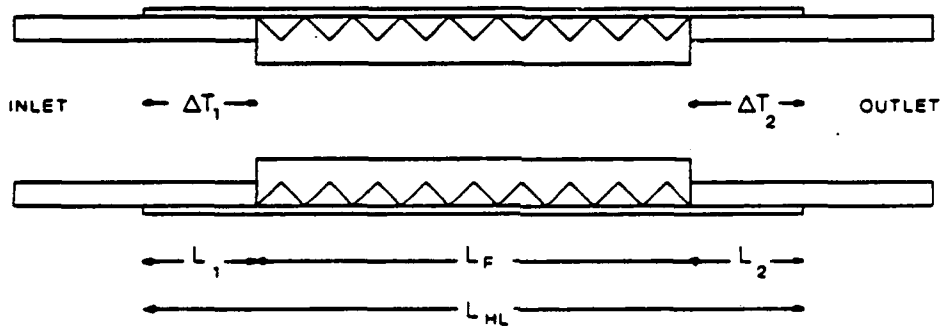


Figure 5.2 Cu/Ni Finned Tube Temperature Rise Corrections.

With the average inside heat transfer coefficient known, the mean Nusselt number can be determined by:

$$Nu_m = \frac{\bar{h}_i D_i}{k} \quad (5.11)$$

where k is the thermal conductivity of the ethylene glycol/water mixture.

The experimentally determined mean Nusselt number was then compared to various theoretical and experimental correlations, based on the insert condition. These correlations were discussed earlier but are briefly mentioned here.

For the no insert condition, the data were compared to two theoretical correlations, the Hausen correlation [Ref. 10] given by:

$$Nu_m = 3.66 + \frac{0.0668(D/L)Re_D Pr}{1 + 0.04[(D/L)Re_D Pr]^{2/3}} \quad (5.12)$$

and the Shah and London correlation [Ref. 9] given by:

$$Nu_m = 1.93(x^*)^{-1/3} \quad (5.13)$$

The reader is reminded that the Hausen correlation is for a uniform wall temperature boundary condition and was used in Mazzone's condensation experiments [Ref. 6]. The Shah and London correlation is for a constant wall heat flux condition. It should also be noted that equation 5.13 is used since x^* for the test section was always less than 0.03.

For the twisted tape insert the experimental mean Nusselt number was compared to the correlation developed by Hong and Bergles [Ref. 15]:

$$Nu_m = 0.383Pr^{0.35}(Re/y)^{0.622} \quad (5.14)$$

Equation 5.14 is used because values for Re/y were always greater than 10.

For the HEATEX insert, the data were compared to the two correlations developed by Mazzone [Ref. 6]. For the 13.26 mm inside diameter tube, the equation is given by:

$$Nu_m = 0.226 Re^{0.65} Pr^{0.46} \quad (5.16)$$

and for the 10.16 mm inside diameter tube by:

$$Nu_m = 0.063 Re^{0.76} Pr^{0.46} \quad (5.16)$$

B. ADDITIONAL TUBE LENGTHS

In addition to the above calculations for the entire tube length, mean Nusselt numbers for three additional tube "lengths" could be determined. This was accomplished by sectioning the heated length of the tube into four cells as shown in Figure 5.3. Each cell contained one longitudinal thermocouple position. Three additional tube lengths were then determined by adding cell lengths together. The first length, L_1 , consisted of cell 1 alone, L_2 consisted of cells 1 and 2 and L_3 consisted of cells 1, 2 and 3. The fourth length was actually the entire heated length as previously discussed.

The coolant temperature rise along the heated length of the tube was assumed to be linear. The correction to the wall heat flux to account for variation in electrical resistance with temperatures was assumed to be negligible. Therefore, the temperature rise along each cell could be determined by:

SECTIONED TUBE

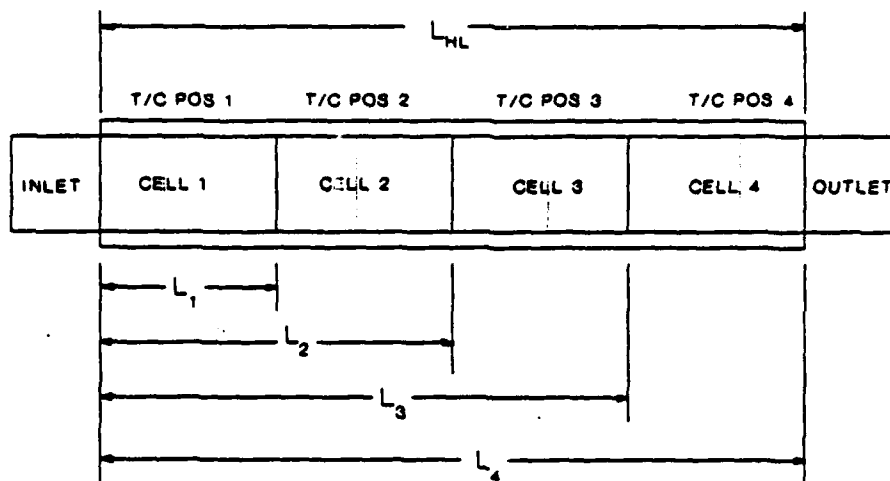


Figure 5.3 Additional Tube Lengths.

$$\Delta T_{cell} = \frac{\Delta T_{HL}}{4} \quad (5.17)$$

Average inside wall temperatures were based on the thermocouples within that tube "length." Therefore, the temperature rise, heat flux and average inside wall temperatures were all known for each tube length. Applying the same calculation method as before, the mean Nusselt number for these three additional tube "lengths" could be calculated.

This adaption to the program was not done until after the smooth tube experiments had been completed; however, this extra data were taken for the remaining two tubes.

C. LOCAL NUSSELT NUMBERS

The program was also adapted to determine local inside heat transfer coefficients at the four axial thermocouple positions. Corrections discussed earlier to determine the temperatures at the inlet and outlet of the heated length were first accounted for. Exact thermocouple longitudinal positions were entered into the program as L/D ratios so that a local x^* could also be calculated. Again, the temperature rise along the heated length was assumed to be linear; therefore, the bulk coolant temperature at the particular thermocouple position could be determined by the simple ratio method discussed earlier (equation 5.10).

The local heat transfer coefficient, h_x , was then determined by:

$$h_x = \frac{q''}{T_{wi} - T_c} \quad (5.13)$$

where \bar{T}_{wi} is the average inside wall temperature based on the three thermocouples at that position and T_c is the bulk coolant temperature at that position. The local Nusselt number was then given by:

$$Nu_x = \frac{h_x D_i}{k} \quad (5.19)$$

The local Nusselt number for all four thermocouple positions was then determined.

For the smooth tube experiments, local Nusselt numbers were calculated only for position 1. The program was later adapted to include local calculations at positions 2, 3, and 4 for the Cu/Ni finned tube and Korodense tube.

VI. RESULTS AND DISCUSSION

A. GENERAL

The experimental heat transfer results are initially presented in terms of the mean Nusselt and Reynolds numbers for all insert conditions. From these graphs, it can be seen how the Nusselt number is inlet temperature dependent, indicating the need for a Prandtl number (raised to an exponent) in the final correlation. However, although not specifically shown, the data shows no dependence on the heat flux setting. In addition, the Nu vs. Re graphs for the no insert condition show when a transition to turbulent flow occurs.

The heat transfer results are then compared to existing correlations based upon the insert condition. For the no insert condition, the Nusselt number is plotted against x^* (dimensionless x coordinate). Note that for a given tube, L/D is constant and x^* varies due to Re and Pr changes. The data are then compared to the Hausen [Ref. 10] correlation (equation 2.10) and the Shah and London [Ref. 9] correlation (equation 2.14). Recall that the Hausen correlation is for a uniform wall temperature boundary condition and was used by Mazzone [Ref. 6] in the refrigerant condensation experiments. Since the present data were taken under a constant heat flux boundary condition, comparison with the Shah and London correlation was also required. The twisted tape insert data are compared to the correlation developed by

Hong and Bergles [Ref. 15] (equation 2.20) which was also used by Mazzone. The HEATEX insert data are compared to the two correlations developed from the limited data received from CAL-GAVIN by Mazzone (equations 2.27 and 2.28).

Correlations are developed for each tube and insert condition based upon a least squares linear regression. An r-squared value, a measure of the accuracy of the least squares curve fitting to the data, is used to determine the uncertainty of the correlation. The correlations and the corresponding r-squared values are summarized in Table 6.1. Note that the 0.2 m/s and 0.3 m/s data were eliminated prior to developing all correlations due to the high degree of uncertainty in these data points.

TABLE 6.1 SUMMARY OF CORRELATIONS

SUMMARY OF CORRELATIONS

	NO INSERT	TWISTED TAPE	HEATEX
SMOOTH TUBE	$Nu = 4.137Xstar^{-0.234}$ $r-sq = 71.9\%$	$Nu = .512Pr^{.35}(Res/y)^{.568}$ $r-sq = 99.5\%$	$Nu = .164Pr^{.46}Re^{.641}$ $r-sq = 98.9\%$
EXT FINNED TUBE	$Nu = 1.84Xstar^{-0.341}$ $r-sq = 93.0\%$	$Nu = .148Pr^{.35}(Res/y)^{.687}$ $r-sq = 96.7\%$	$Nu = .126Pr^{.46}Re^{.657}$ $r-sq = 95.9$
KORODENSE TUBE	$Nu = 2.047Xstar^{-0.326}$ $r-sq = 89.2\%$	$Nu = .569Pr^{.35}(Res/y)^{.498}$ $r-sq = 98.9\%$	$Nu = .282Pr^{.46}Re^{.499}$ $r-sq = 94.3\%$

B. SMOOTH TUBE

1. Smooth Tube - No Insert

The first tube tested was the copper smooth tube with no insert. Heat transfer data is presented in Figure 6.1 in terms of the Nusselt number as a function of Reynolds number for each nominal inlet temperature. The first thing to notice is the sudden increase in Nu at a Re number of about 2300. This is indicative of a change from laminar to transition flow where the heat transfer is greatly increased due to improved mixing. This contradicts Mazzone's [Ref. 6] assumption of a transition to turbulence occurring at $Re > 4000$. The data in the transition region was primarily for the $+20^{\circ}\text{C}$ and $+10^{\circ}\text{C}$ nominal inlet temperatures. Figure 6.1 also shows distinct groupings of data at given inlet temperatures, indicating a Prandtl number effect. These groupings are shown more clearly in Figure 6.2 which represent data under laminar flow conditions only ($Re \leq 2300$) and Figure 6.3 for data in the transition region only ($Re > 2300$).

To develop a useful heat transfer correlation, the mean Nusselt number is plotted as a function of x^* in Figure 6.4. Recall that x^* can be determined by:

$$x^* = \frac{L/D}{Re_D Pr} \quad (2.9)$$

For a given tube, L/D is a fixed quantity. Therefore, for a given Prandtl number (essentially fixed inlet temperature), x^* is dependent only upon the Reynolds number.

Figure 6.4 also shows a comparison of the experimental data with the Hausen correlation (equation 2.10) for a uniform wall temperature (used by Mazzone) and the Shah and London correlation (equation 2.14) for a constant heat flux. The Hausen correlation appears to significantly underestimate the heat transfer coefficient found in the present experimental data, i.e., the present experimental data indicate a lower inside thermal resistance. This is consistent with Mazzone's [Ref. 6] results in that the Hausen correlation was predicting larger inside resistances than the overall measured resistance. However, it must always be remembered that the Hausen correlation is for a uniform wall temperature boundary condition and this would indeed lead to lower heat-transfer coefficients.

The data also fall slightly above (but parallel to) that predicted by the Shah and London correlation. Due to the constant heat flux boundary condition used by Shah and London, one may expect better agreement (as seen). However, the fact that the data fall slightly above can be attributed to secondary flow induced by the apparatus inlet conditions (90° bend due to the thermocouple well). Also, as before, a departure from laminar flow can be seen in Figure 6.4. Since the transition data forms two distinct lines (+20°C and +10°C), it indicates that x^* is not a good correlating parameter for transitional flow.

After removal of the transitional flow data, a correlation was developed based upon the form of the Shah and London correlation. The resulting present

correlation for the mean Nusselt number for laminar flow with no insert is given by:

$$Nu_m = 4.137(x^*)^{-0.234} \quad (6.1)$$

Equation 6.1 and the Hausen correlation, equation 2.10, are both shown in Figure 6.5 with the present laminar flow data. The general form of Figure 6.5 is explained by the fact that at low x^* (high Re) the heat transfer is improved due to slightly better mixing. As x^* increases (coolant velocity decreases), the heat transfer decreases.

Figure 6.5 also shows a high degree of scatter in the data. Initially, it was thought that this scatter was due to the flow not being hydrodynamically fully developed. However, it is seen to be more pronounced at large x^* . Recall that for a given nominal inlet temperature, large x^* represents a low Reynolds number. For a low Reynolds number, the hydrodynamic entry length (given by $X/D = 0.05Re$) is the shortest. Also, since we are dealing with relatively large Prandtl numbers (30-140), the assumption that the velocity profile is fully developed throughout the thermal entry region should be fairly valid. Therefore, it is felt that this scatter is not due to the flow being hydrodynamically undeveloped.

This scatter is believed to be due to the effects of the different inlet temperatures, indicating that x^* is not an ideal correlating parameter. That is to say, the Prandtl number exponent needs to be adjusted to account for the different inlet temperatures. It should also be noted that due to the high degree of detail in Figure

6.5, the scatter appears more pronounced. However, in Figure 6.4 with larger scale increments, the scatter seems minimal.

2. Smooth Tube - Twisted Tape

Results for the smooth tube with a twisted tape insert are shown in Figures 6.6 and 6.7. A definite Prandtl number dependence can be seen in Figure 6.6 where the mean Nusselt number is presented as a function of Reynolds number. Following the guidance of Hong and Bergles [Ref. 15] the dimensionless parameters Re , and y were combined as one parameter Re/y and the mean Nusselt number and Prandtl number were combined as $Nu/Pr^{0.35}$. The final correlation shown in Figure 6.7 is:

$$Nu_m = 0.512Pr^{0.35}(Re/y)^{0.568} \quad (6.2)$$

This correlation is in close agreement with the Hong and Bergles correlation (equation 2.20). The slight differences can be attributed to differences in the experimental apparatus (including the insert itself) and the possible existence of secondary flows. Figure 6.7 shows little inlet temperature dependence, indicating that the Prandtl number exponent of 0.35 is probably fairly accurate. Furthermore, there is little experimental data scatter, giving increased confidence in this correlation.

3. Smooth Tube - HEATEX Insert

HEATEX insert results for a smooth tube are shown in Figures 6.8 and 6.9. Again, on a Nu vs. Re basis, it can be seen from Figure 6.8 that there is a definite dependence on the inlet temperature. Using the same form as the

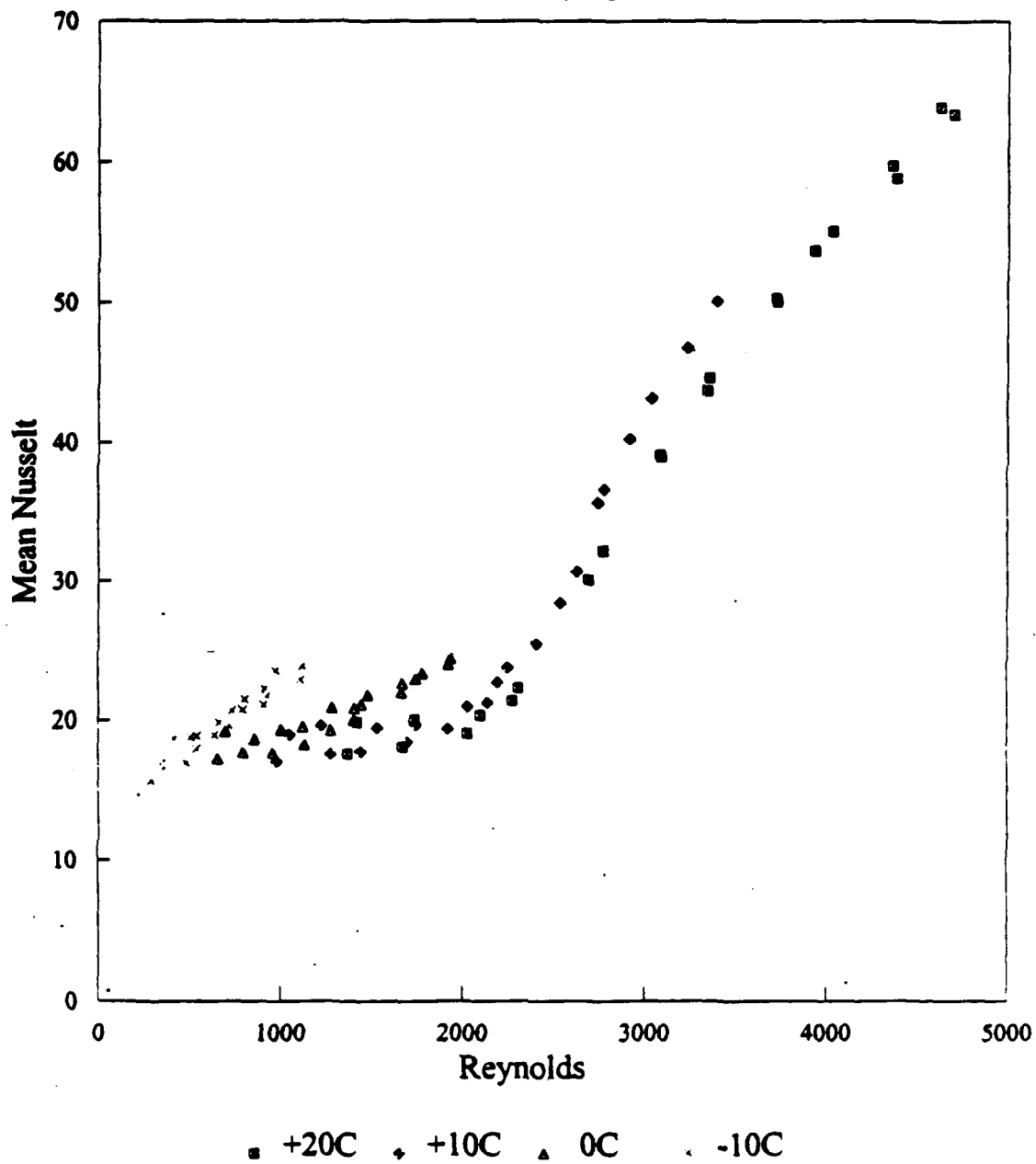
correlation of Oliver and Aldington [Ref. 20], the resulting correlation for the mean Nusselt number is:

$$Nu_m = 0.164 Pr^{0.46} Re^{0.641} \quad (6.3)$$

This is compared in Figure 6.9 to the correlation developed and used by Mazzone (equation 2.23). It is clearly evident that Mazzone's correlation underpredicts the inside thermal resistance and therefore gives a larger inside heat transfer coefficient. Again, Figure 6.9 shows little dependence on inlet temperature indicating that the Prandtl number exponent is fairly accurate. Comparisons of the enhancement in heat transfer gained by the use of HEATEX and twisted tape insert, over the no insert condition are given section F of this chapter.

SMOOTH TUBE - NO INSERT

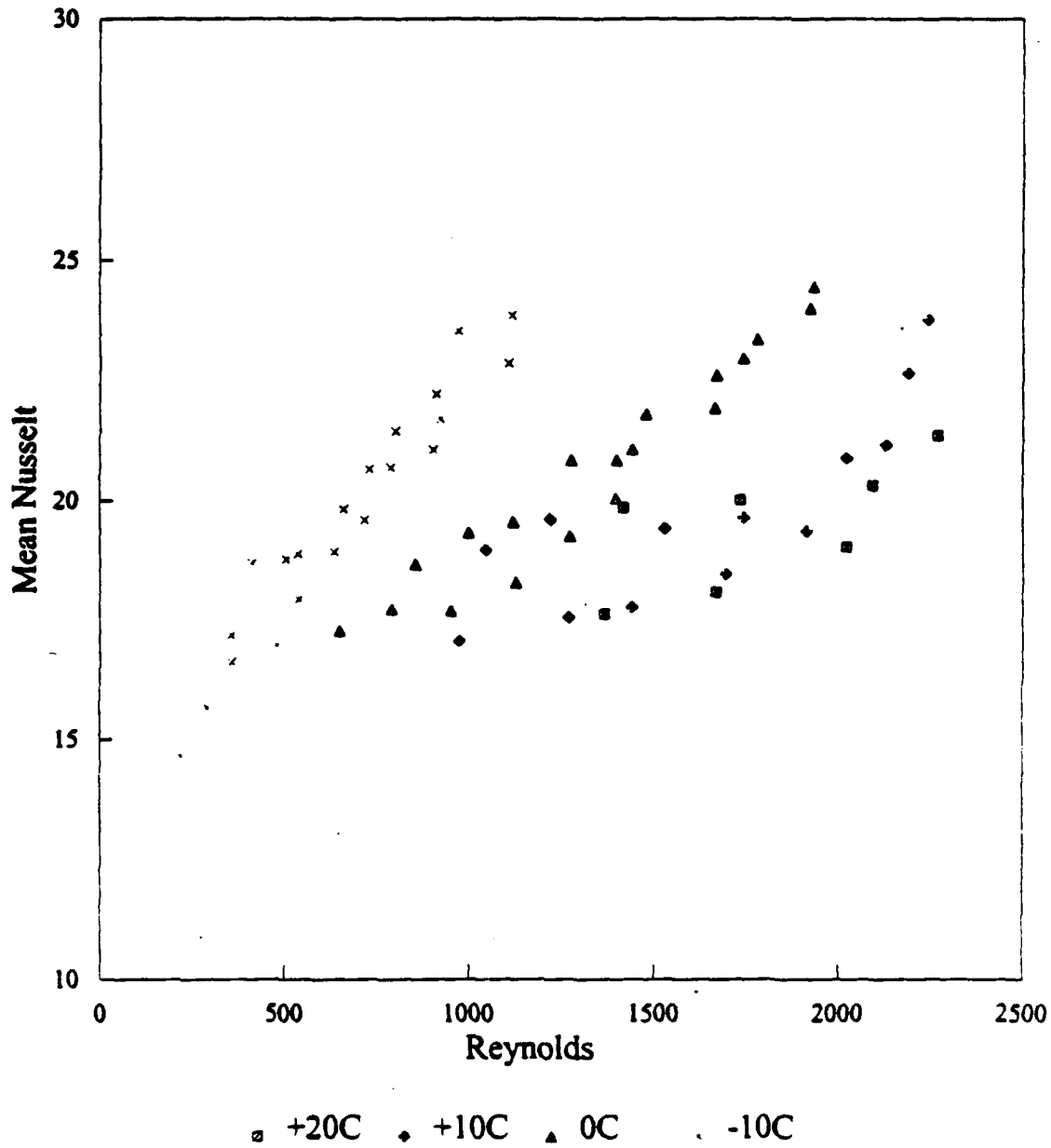
Nu vs Re



SMNIRENU

Figure 6.1 Smooth tube - No insert (Nu_m vs. Re) results.

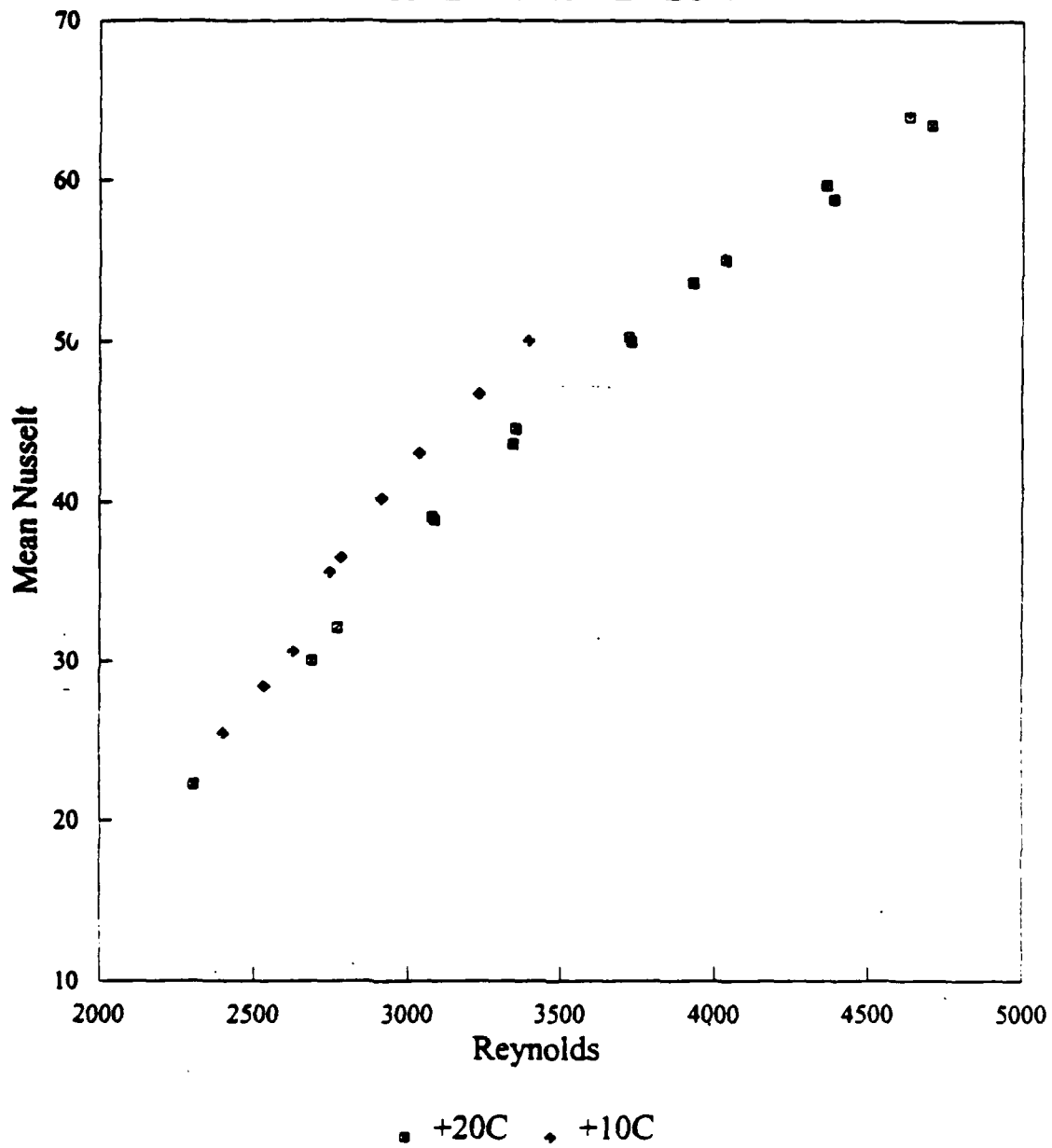
SMOOTH TUBE - NO INSERT LAMINAR FLOW



Nu vs Re
SMNINURELAM

Figure 6.2 Smooth tube - No insert (Nu_m vs. Re) laminar flow results.

SMOOTH TUBE - NO INSERT TRANSITIONAL FLOW

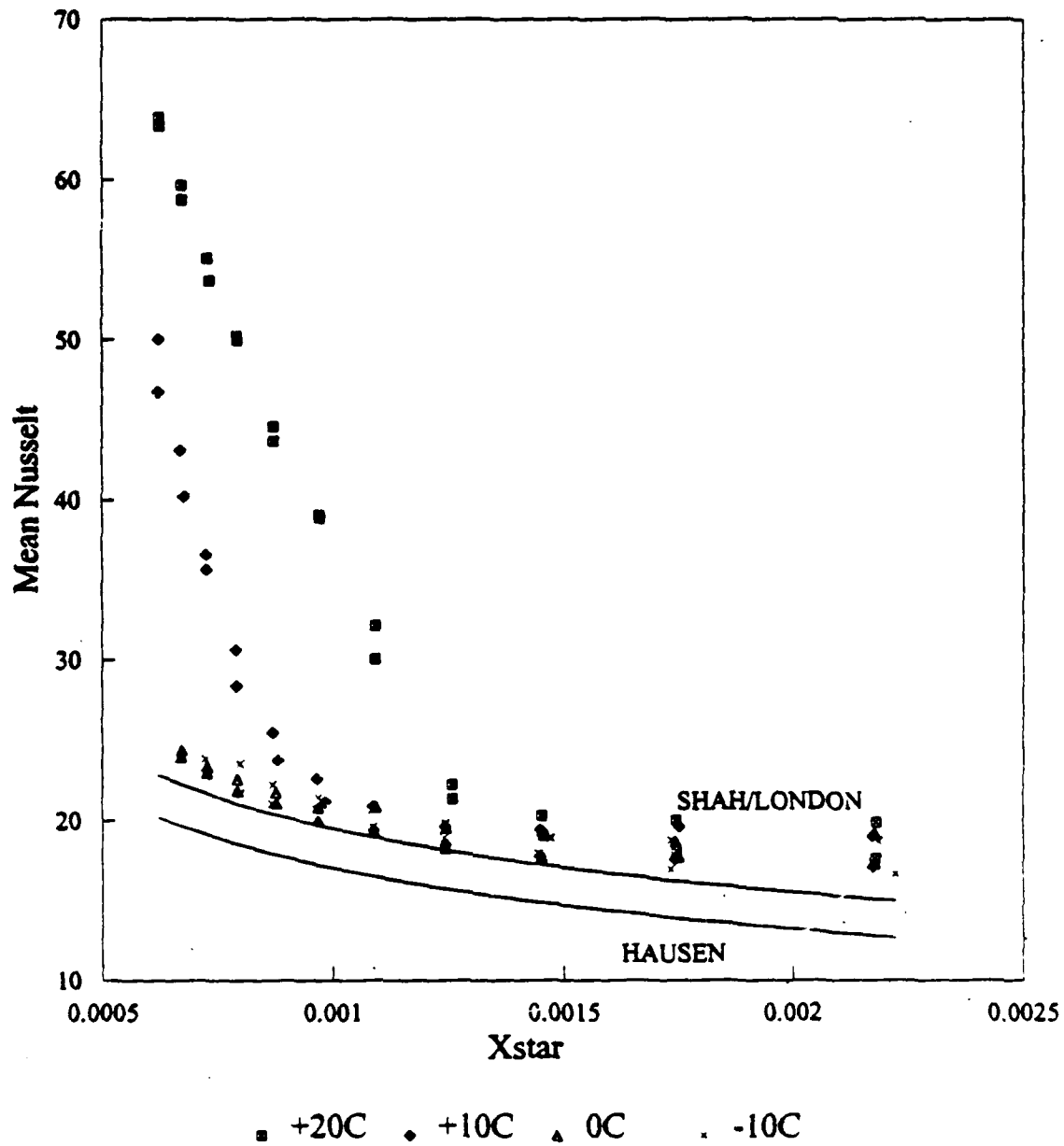


Nu vs Re
SMNINURETRAN

Figure 6.3 Smooth tube - No insert (Nu_m vs. Re) transitional flow results.

SMOOTH TUBE - NO INSERT

Nu vs Xstar



$Xstar = (L/D)/PrRe$
SMNIXNU

Figure 6.4 Smooth tube - No insert (Nu_m vs. x^*) results.

SMOOTH TUBE - NO INSERT LAMINAR FLOW

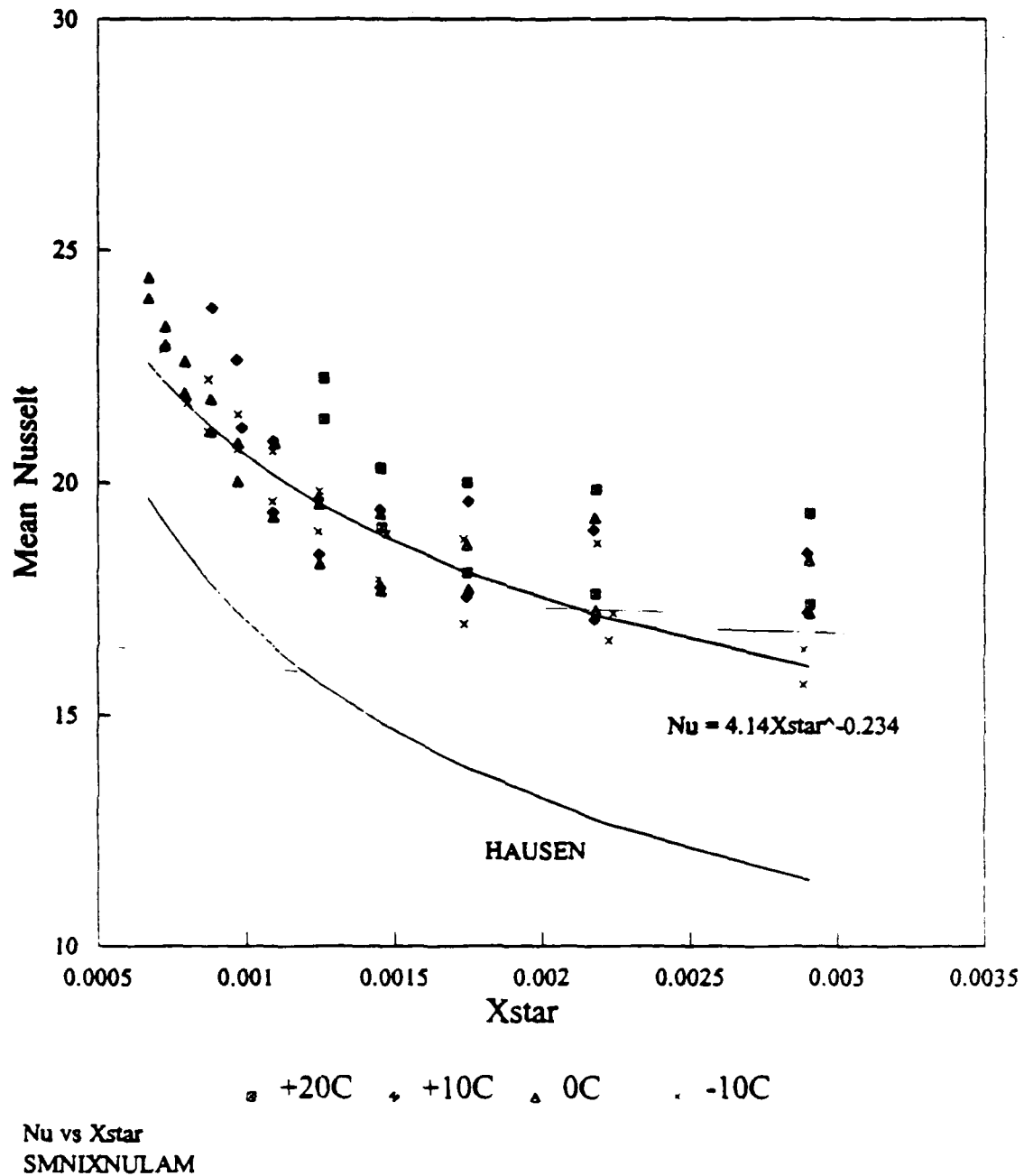
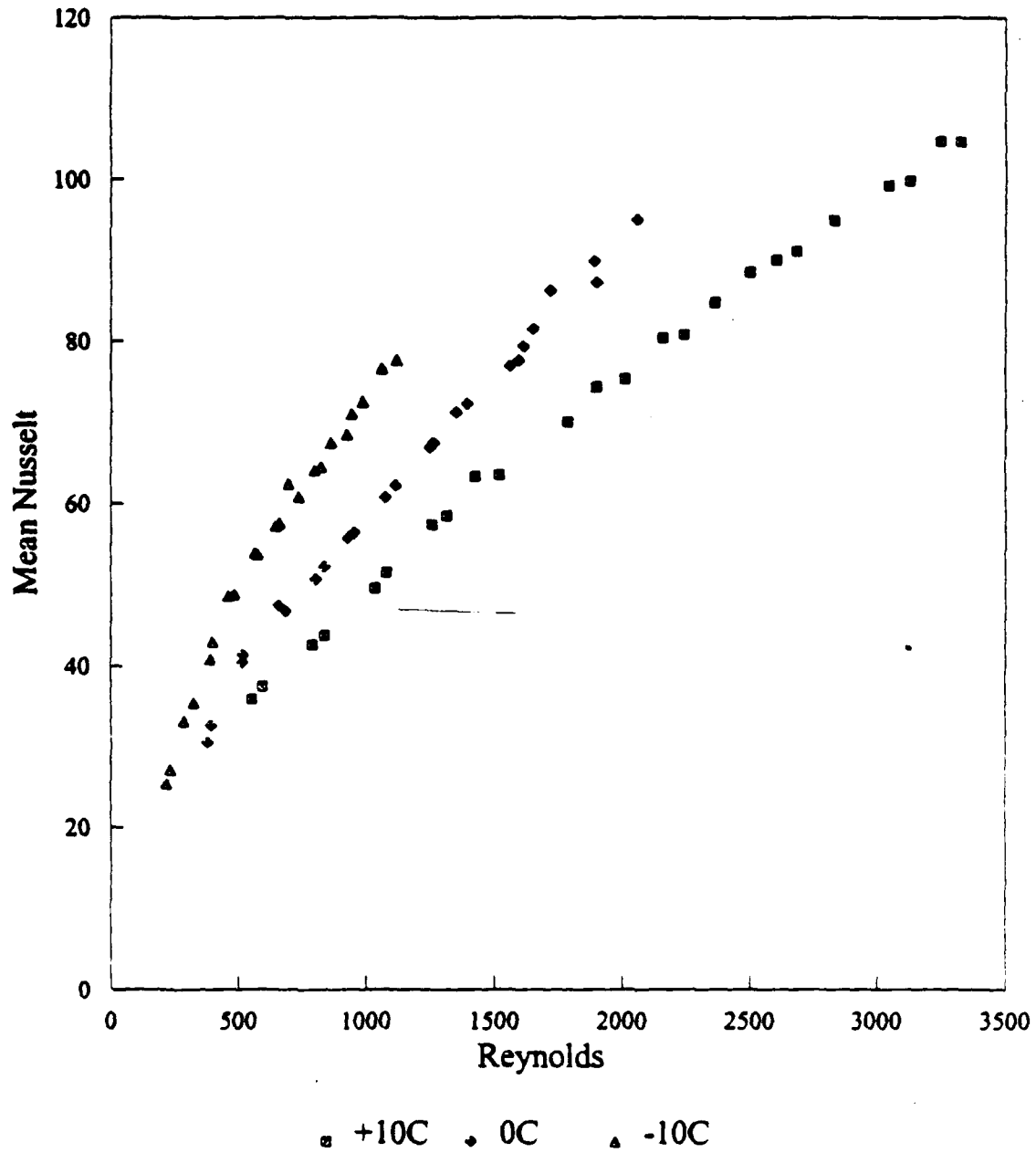


Figure 6.5 Smooth tube - No insert laminar flow correlation results.

SMOOTH TUBE - TWISTED TAPE

Nu vs Re

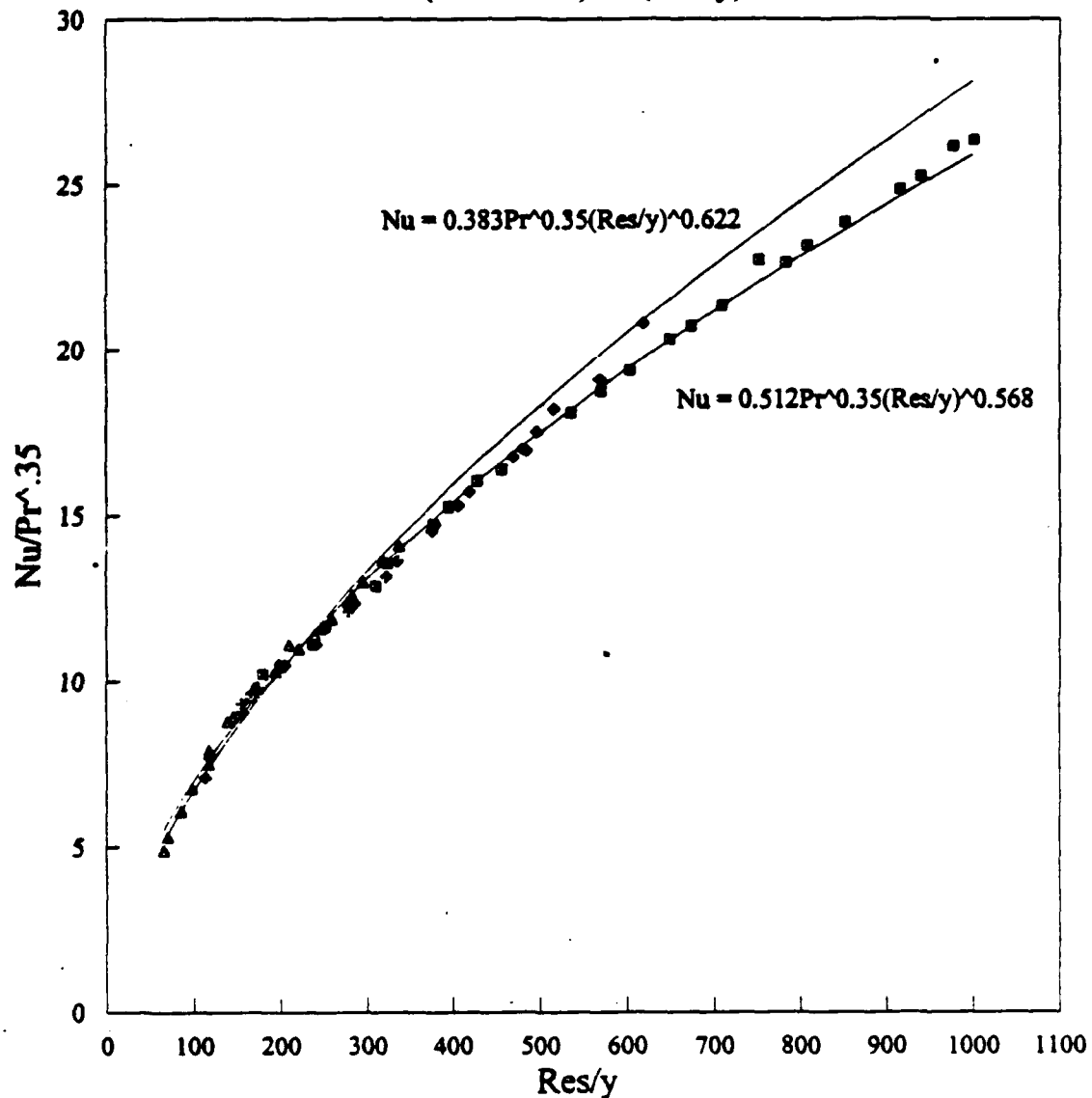


SMITTURE

Figure 6.6 Smooth tube - Twisted tape (Nu_m vs. Re) results.

SMOOTH TUBE - TWISTED TAPE

(Nu/Pr^{.35}) vs (Res/y)

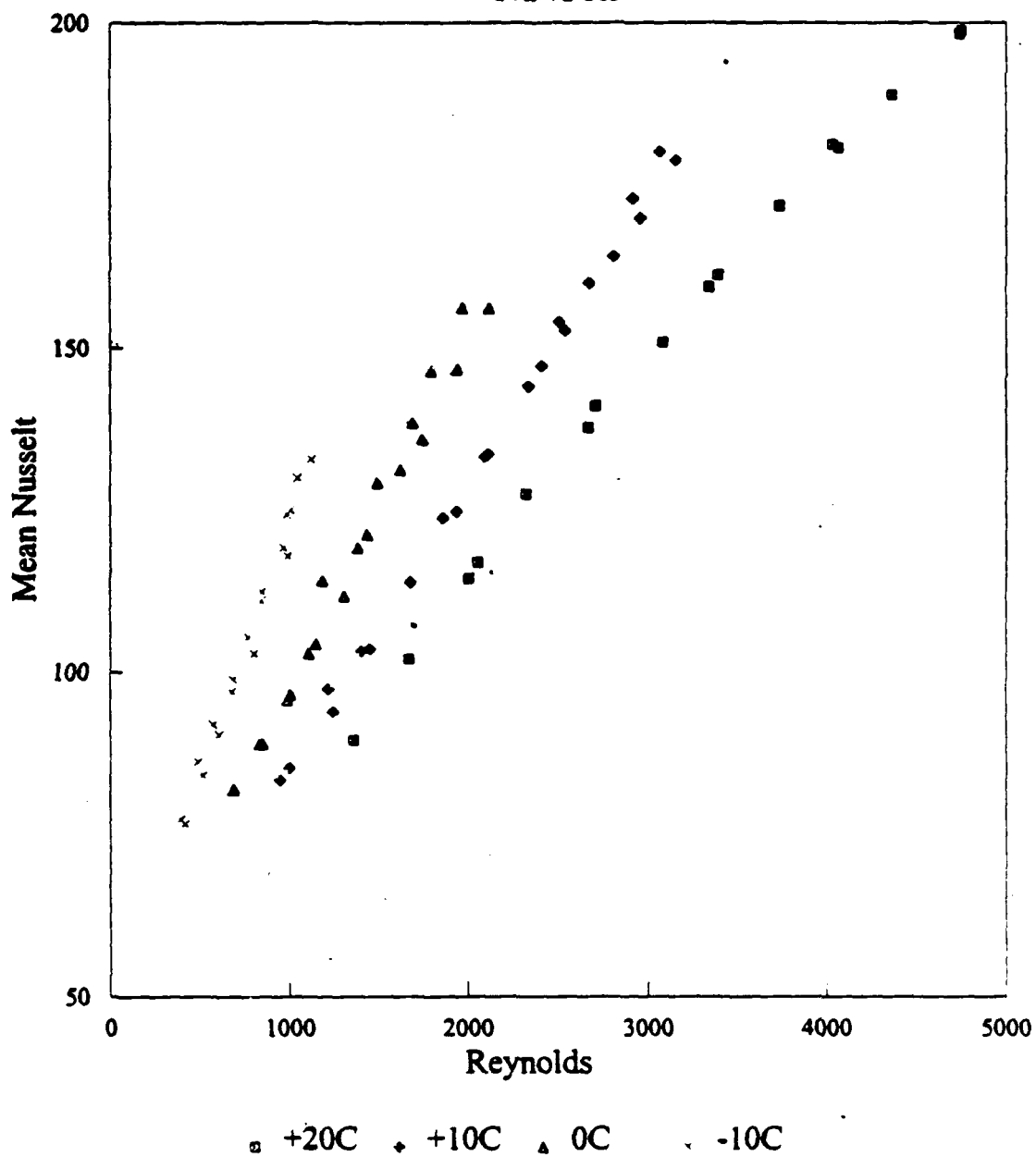


Res = (ṁDi)/(Asu) , y = H/Di
SMTNUPR

Figure 6.7 Smooth tube - Twisted tape correlation results.

SMOOTH TUBE - HEATEX

Nu vs Re

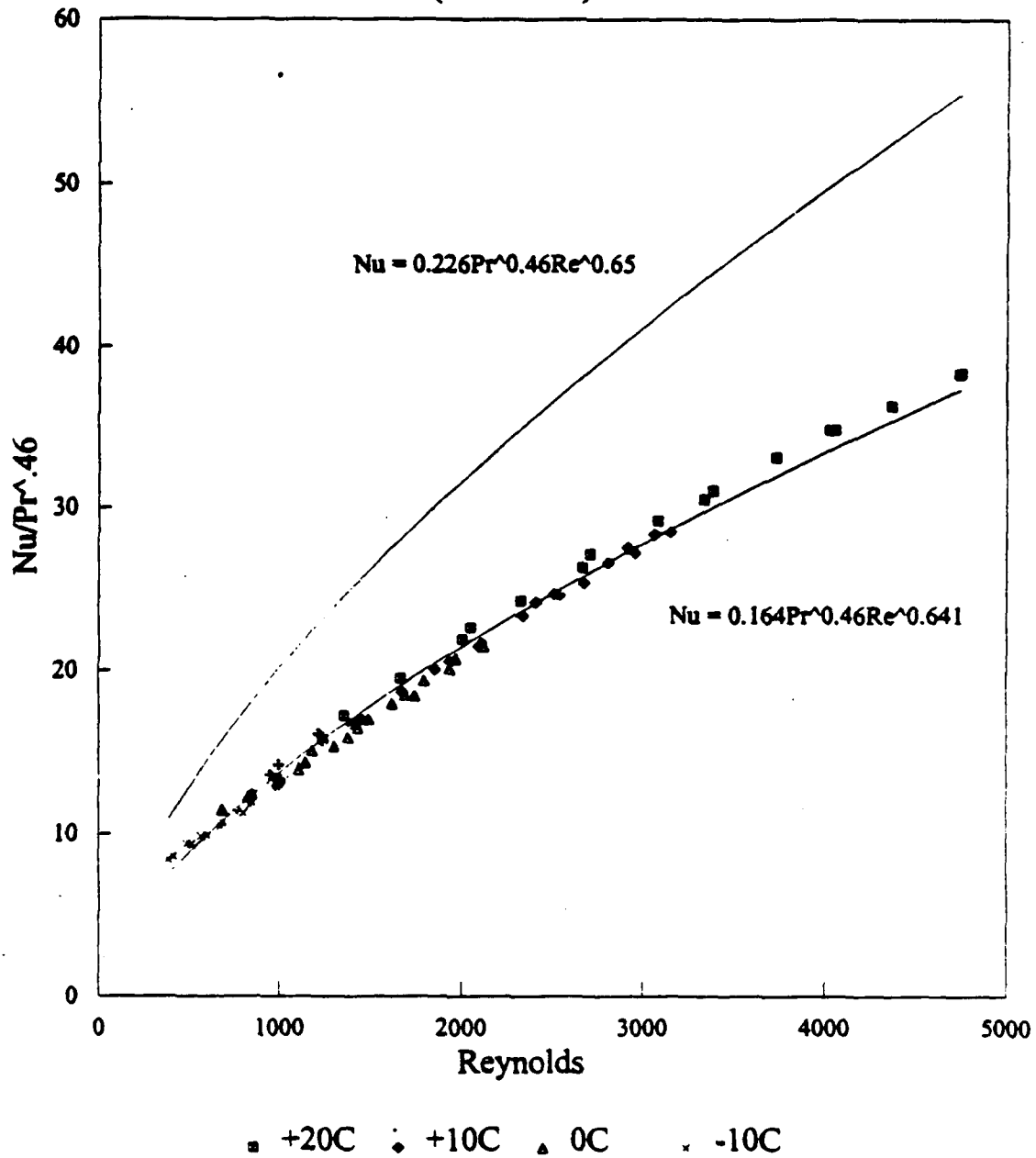


SMHXNURE

Figure 6.8 Smooth tube - HEATEX (Nu_m vs. Re) results.

SMOOTH TUBE - HEATEX

(Nu/Pr^{.46}) vs Re



SMHXNUPR

Figure 6.9 Smooth tube - HEATEX correlation results.

C. CU/NI EXTERNALLY FINNED TUBE

1. Cu/Ni Finned Tube - No Insert

The second tube tested was the Cu/Ni externally finned tube. Recall that this tube has a smaller inside smooth diameter than the smooth tube (10.15 mm vs. 13.26 mm). The no insert results for the mean Nusselt number as a function of Reynolds number are shown in Figure 6.10 and in more detail in Figures 6.11 and 6.12 for laminar and transitional flows, respectively. It can be seen that a slightly higher Reynolds number ($Re \approx 2700$) for the departure from laminar flow exists for this tube. Again, the dependence on inlet temperature is clearly evident.

The data are compared to the Hausen correlation (equation 2.10) and the Shah and London correlation (equation 2.14) in Figure 6.13. As expected, the Hausen correlation again underpredicts the inside heat transfer coefficient. However, the laminar flow data is in closer agreement with the Shah and London correlation than they were for the smooth tube. This can be attributed to the different diameter affecting the thermal boundary layer development. The resulting correlation for the laminar flow mean Nusselt number is shown in Figure 6.14 and is given by:

$$Nu_m = 1.84(x^*)^{-0.341} \quad (6.4)$$

The same conclusions about data scatter can be drawn as for the smooth tube results, although in general the scatter seems to be less.

2. Cu/Ni Finned Tube - Twisted Tape Insert

Figures 6.15 and 6.16 show the results for the Cu/Ni finned tube using a twisted tape to enhance tubeside heat transfer. The inlet temperature dependence in Figure 6.15 seems to be reduced, but still evident. The form of the correlation was again that of Hong and Bergles' correlation. It was developed in the same manner as for the smooth tube and is given by:

$$Nu_m = 0.148Pr^{0.35}(Re/y)^{0.687} \quad (6.5)$$

The data and resulting correlation are compared to the Hong and Bergles correlation (equation 2.20) in Figure 6.16 where the latter is seen to overpredict the mean Nusselt number. This difference can be attributed to several factors. A small diameter tube with a larger diameter smooth entrance length could cause severe secondary flows. Also, because of the smaller diameter tube a different size twisted tape (twist ratio, $y=3$) was used, which had a slightly looser fit than the tape used with the smooth tube. Additionally, Prandtl number effects need to be investigated more closely, as Figure 6.16 shows a definite trend with inlet temperature.

3. Cu/Ni Finned Tube - HEATEX Insert

Data for the Cu/Ni finned tube using the HEATEX insert are presented in Figures 6.17 and 6.18. Figure 6.17 (Nu vs. Re) again shows a dependence of the data on the coolant inlet temperature. Since the HEATEX element used for this tube was a smaller diameter (10.16 mm) with a different loop density than that used for the smooth tube, a new correlation needed to be developed. Again, using the

form of the correlation proposed by Oliver and Aldington, the final proposed correlation is given by:

$$Nu_m = 0.126 Pr^{0.46} Re^{0.657} \quad (6.6)$$

The data and resulting correlation are compared to the correlation developed by Mazzone (equation 2.24) for this insert in Figure 6.18. It can be seen that Mazzone's correlation is adequate for predicting the inside heat transfer coefficients at low Reynolds number ($Re < 1400$), where both correlations merge. However, at higher Reynolds numbers, Mazzone's correlation overpredicts the present experimental data. The differences in the two correlations are primarily due to the limited amount of data available to Mazzone when developing his correlation. Furthermore, the data he used were taken on a different experimental facility (by the manufacturers). As seen before, the data shown in Figure 6.18 still indicate a dependence on inlet temperature and hence the value of 0.46 for the Prandtl number exponent needs to be reinvestigated and optimized.

Cu/Ni FINNED TUBE - NO INSERT

Nu vs Re

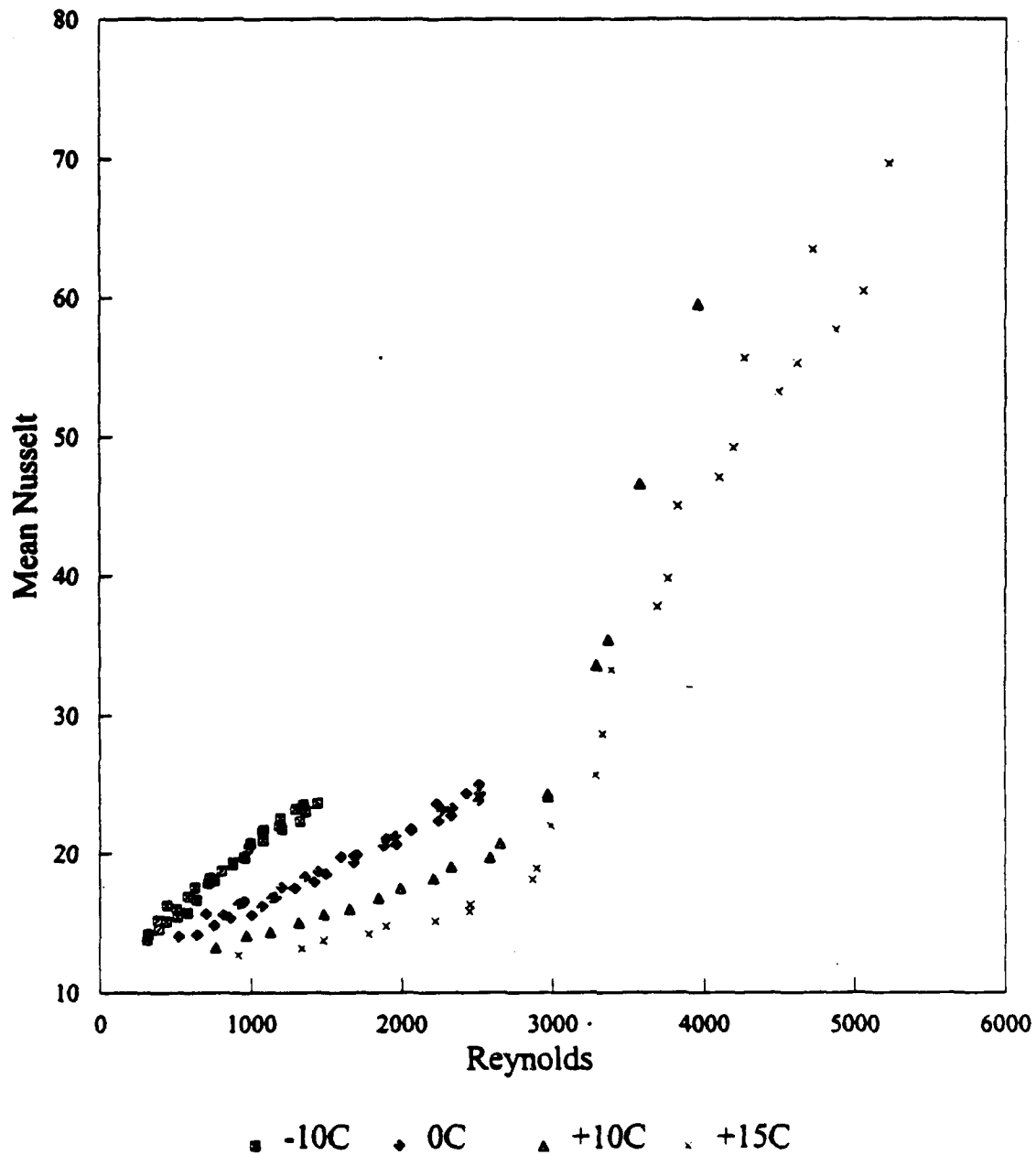
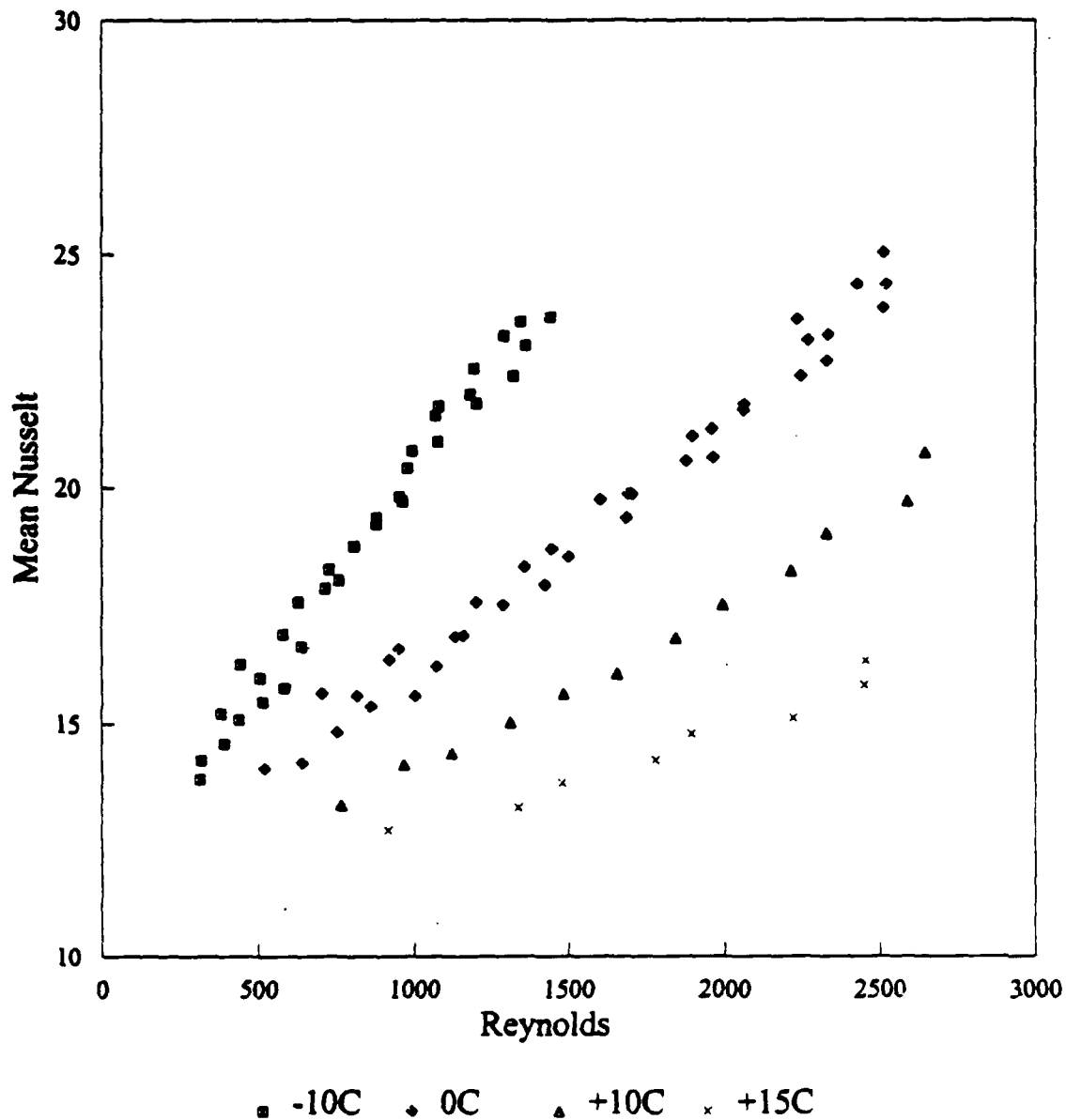


Figure 6.10 Cu/Ni externally finned tube - No insert (Nu_m vs. Re) results.

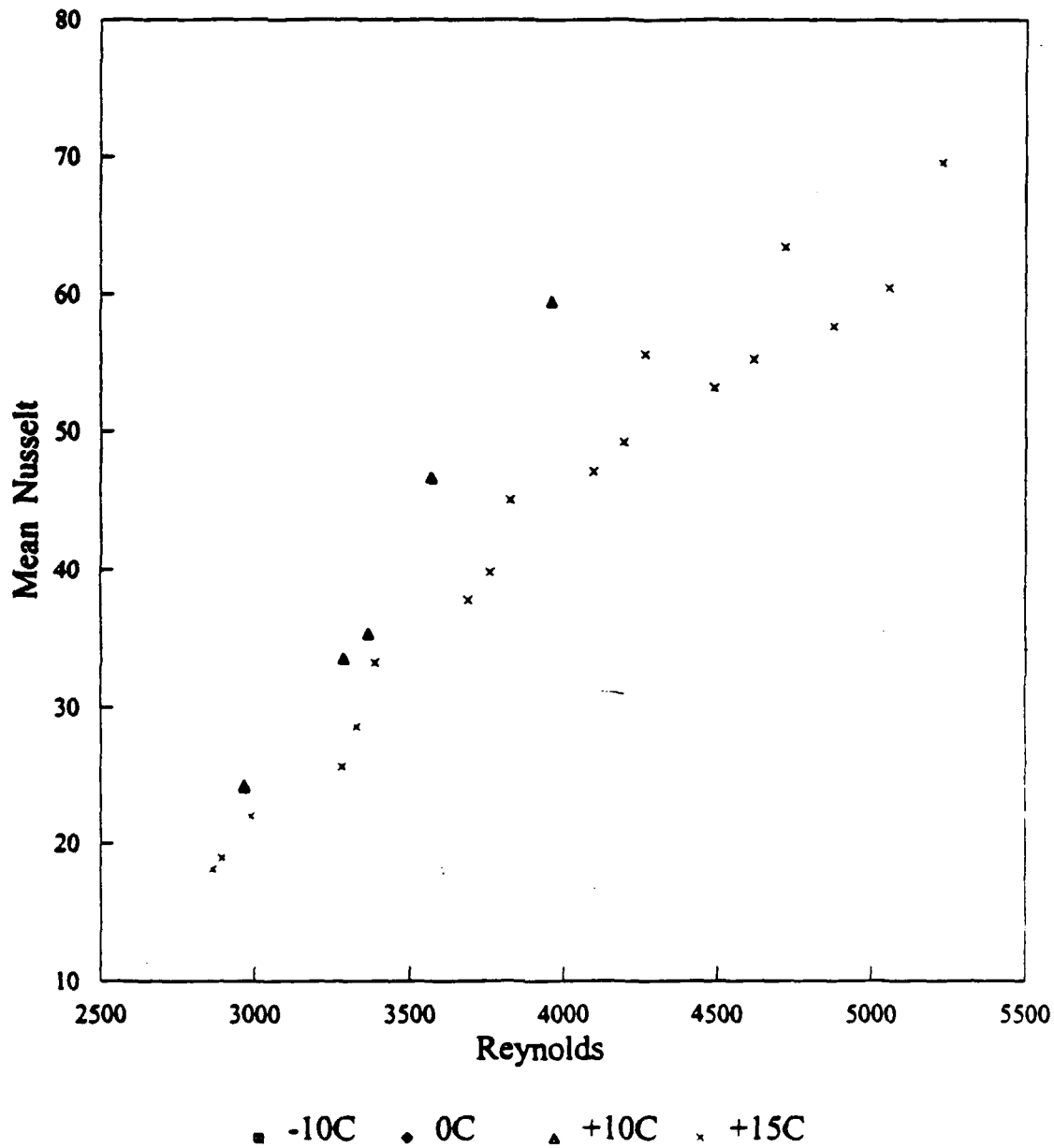
Cu/Ni FINNED TUBE - NO INSERT LAMINAR FLOW



Nu vs Re
CFNINURELAM

Figure 6.11 Cu/Ni externally finned tube - No insert (Nu_m vs. Re) laminar flow results.

Cu/Ni FINNED TUBE - NO INSERT **TRANSITIONAL FLOW**

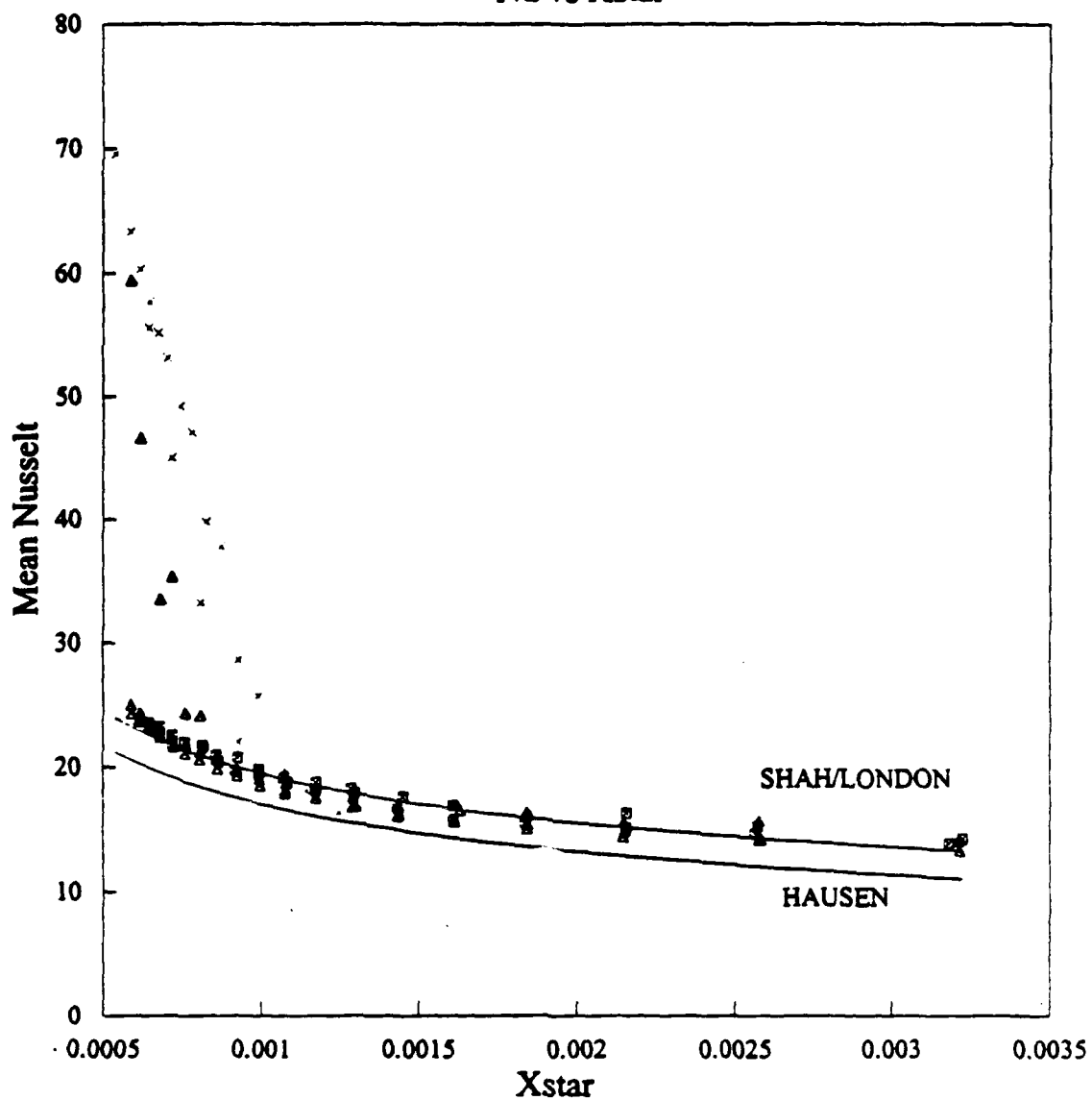


Nu vs Re
CFNINURETRAN

Figure 6.12 Cu/Ni externally finned tube - No insert (Nu_m vs. Re) transitional flow results.

Cu/Ni FINNED TUBE - NO INSERT

Nu vs Xstar



□ -10C ♦ 0C ▲ +10C × +15C

Xstar = (L/D)/RePr
CFNIXNU

Figure 6.13 Cu/Ni externally finned tube - No insert (Nu_m vs. x^*) results.

Cu/Ni FINNED TUBE - NO INSERT LAMINAR FLOW

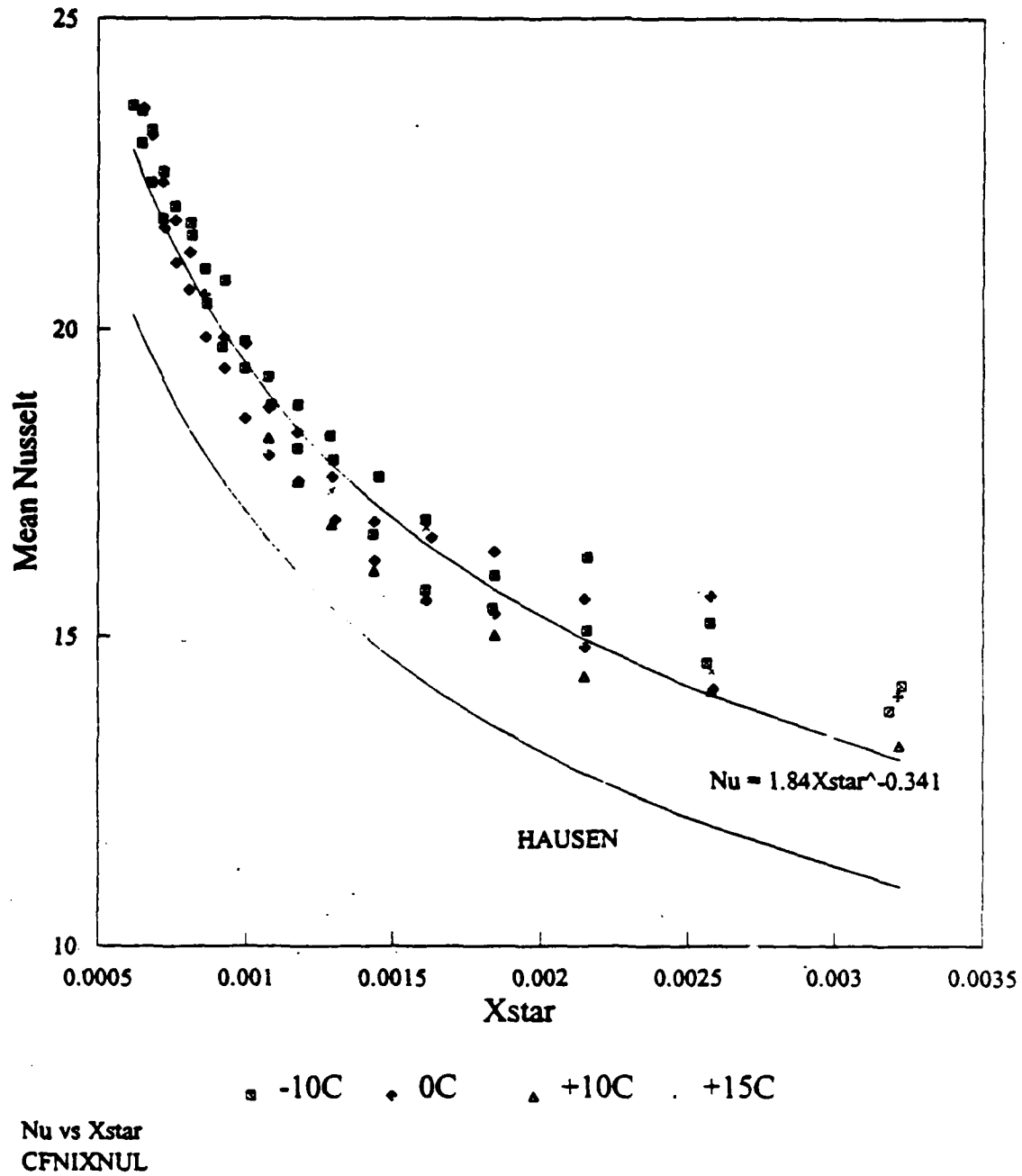
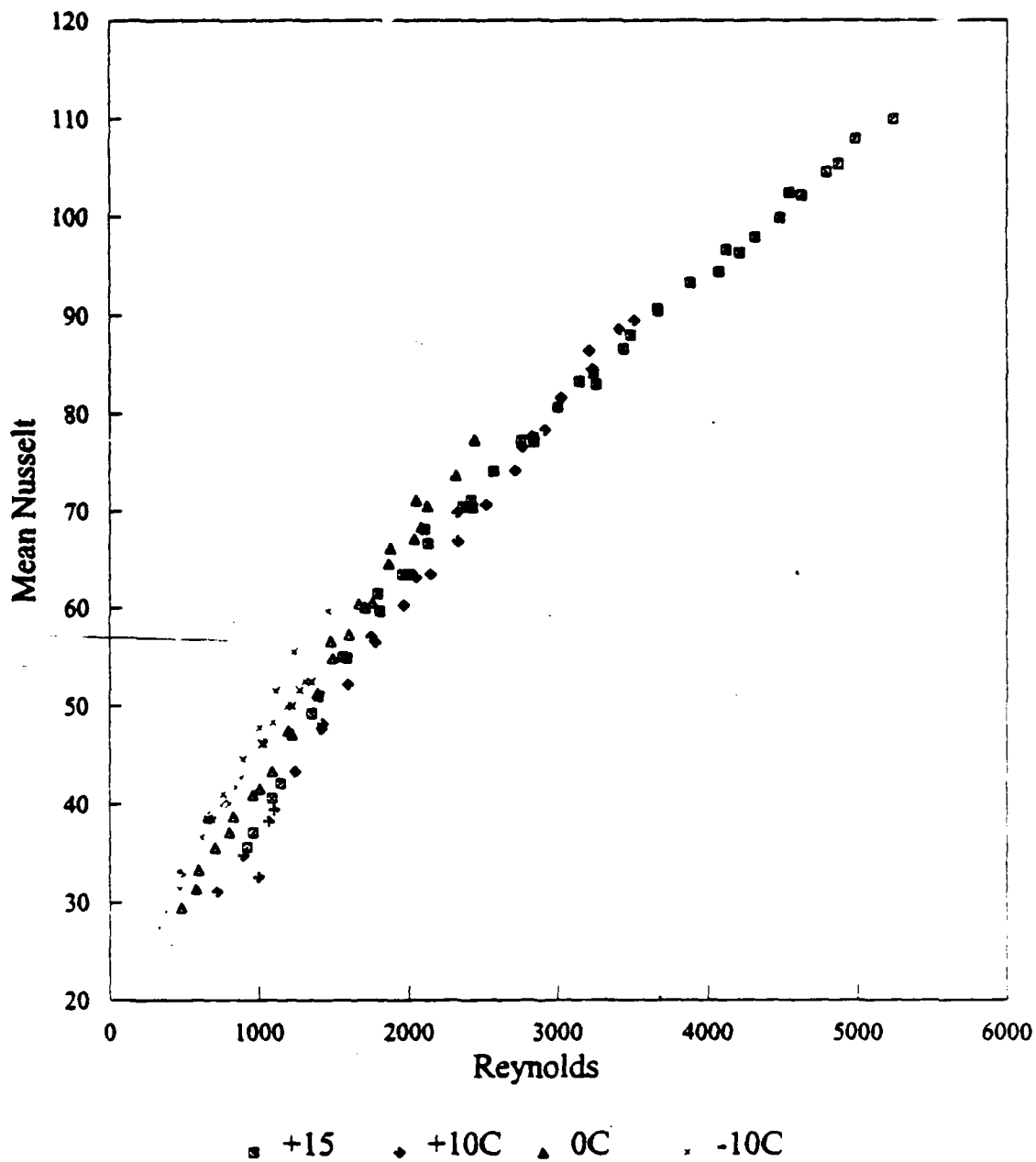


Figure 6.14 Cu/Ni externally finned tube - No insert laminar flow correlation results.

Cu/Ni FINNED TUBE - TWISTED TAPE

Nu vs Re

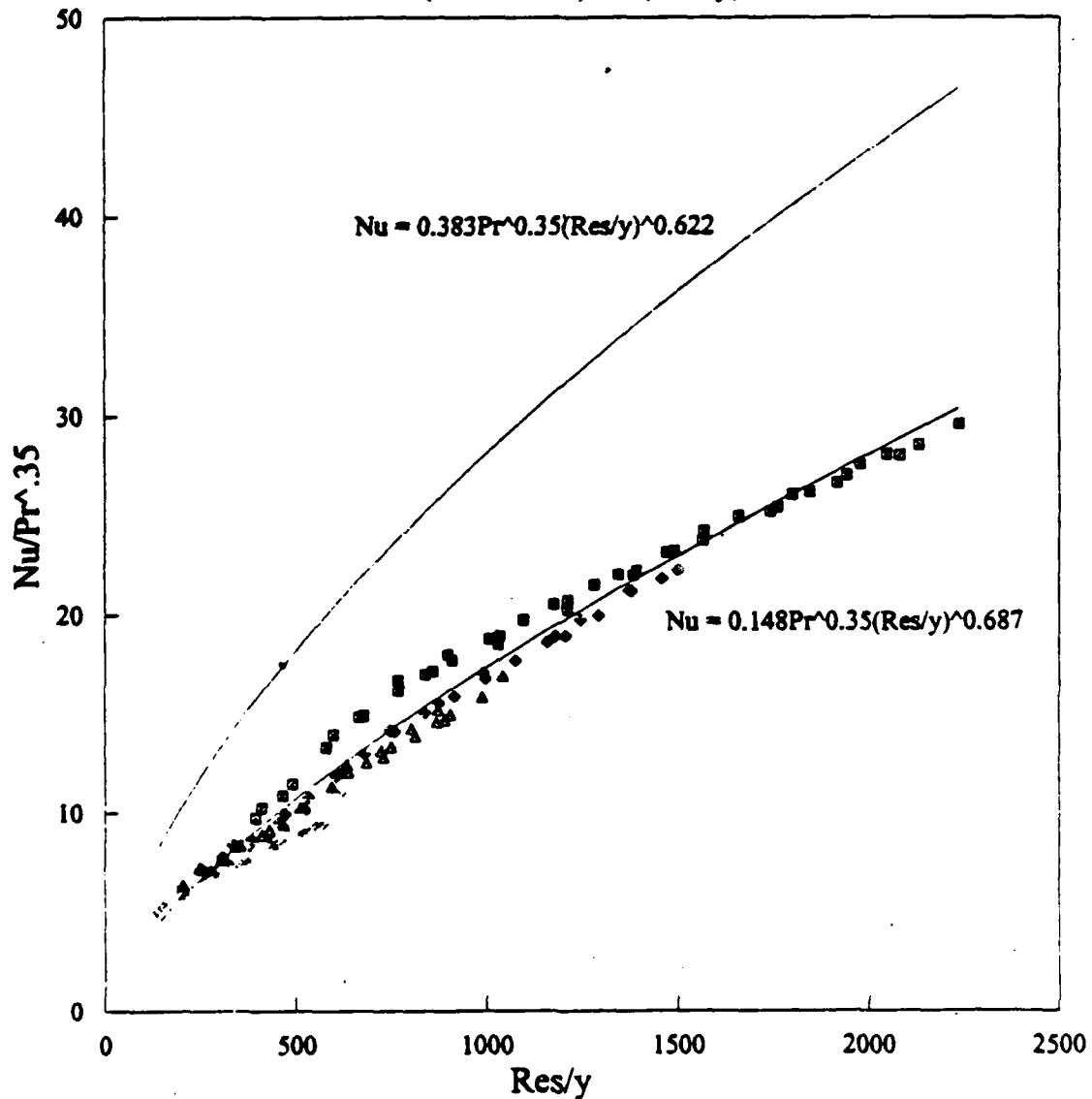


CFTTNURE

Figure 6.15 Cu/Ni externally finned tube - Twisted tape (Nu_m vs. Re) results.

Cu/Ni FINNED TUBE - TWISTED TAPE

(Nu/Pr^{.35}) vs (Res/y)



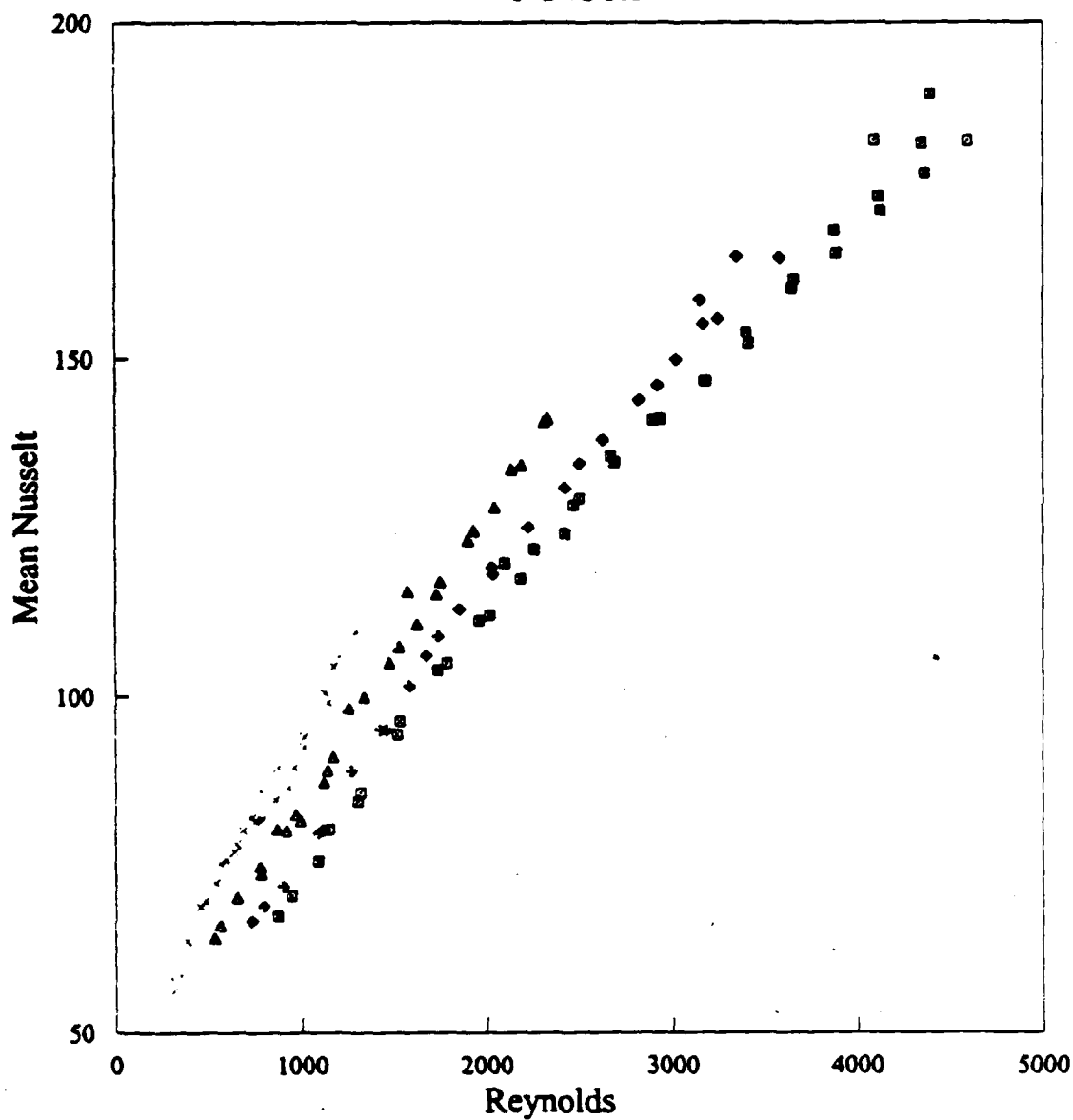
Res = (mDi)/(Asu), y = H/Di

CFTTNUPR

Figure 6.16 Cu/Ni externally finned tube - Twisted tape correlation results.

Cu/Ni FINNED TUBE - HEATEX

Nu vs Re



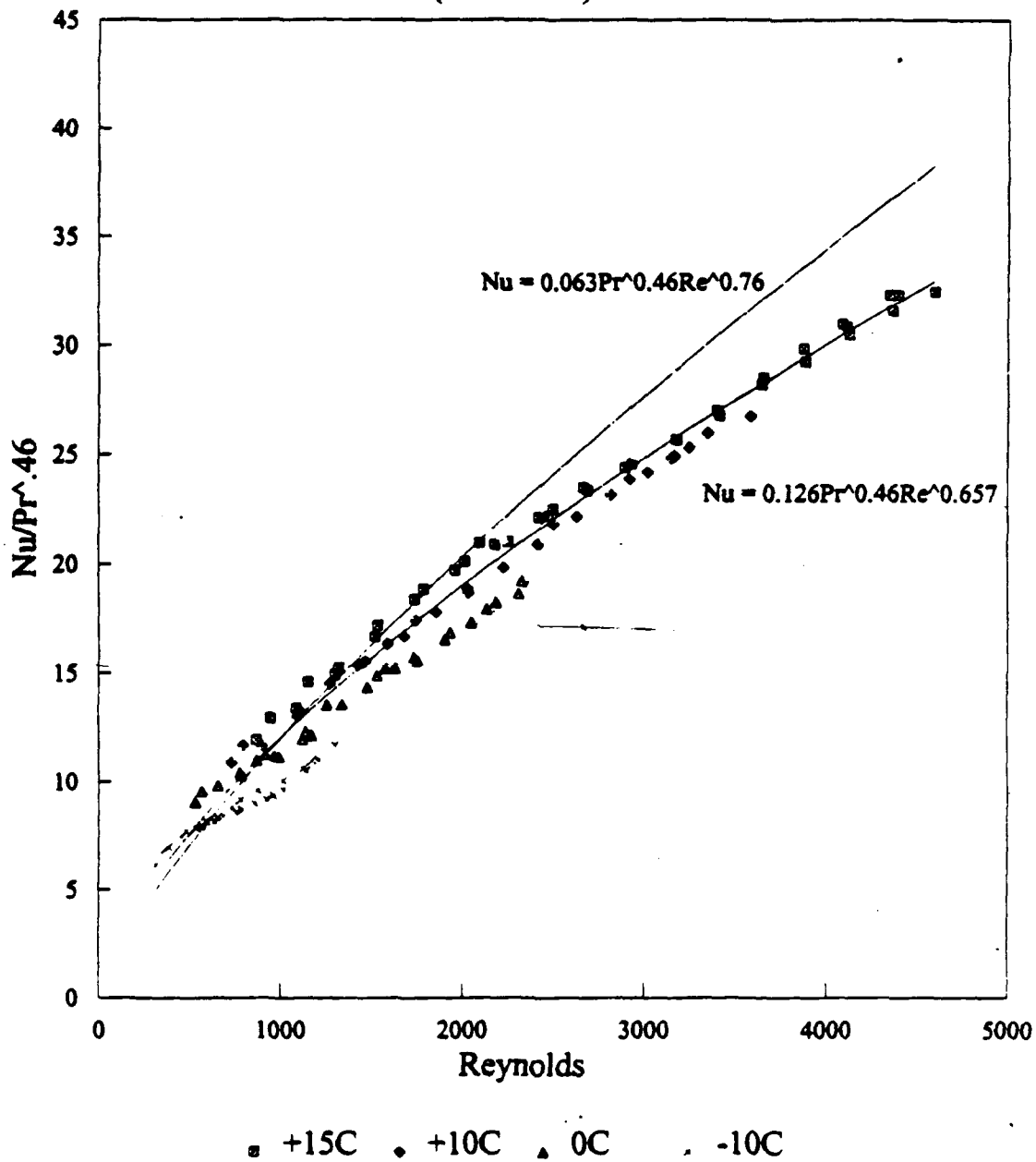
□ +15C ♦ +10C ▲ 0C × -10C

CFHXNURE

Figure 6.17 Cu/Ni externally finned tube - HEATEX (Nu_m vs. Re) results.

Cu/Ni FINNED TUBE - HEATEX

(Nu/Pr^{.46}) vs Re



CFHXNUPR

Figure 6.18 Cu/Ni externally finned tube - HEATEX correlation results.

D. KORODENSE TUBE

1. Korodense Tube - No Insert

The final tube tested was the Korodense tube. This tube was first tested with no insert. The results for the mean Nusselt number as a function of Reynolds number are shown in Figure 6.19 and in more detail for laminar and transitional flow in Figures 6.20 and 6.21, respectively. As was seen in the smooth tube case, a transition to turbulent flow occurred at a Reynolds number of approximately 2300.

Figure 6.22 compares the data to Hausen's correlation (equation 2.10) and the Shah and London correlation (equation 2.14). As before, the transitional flow data are seen as two distinct lines for data taken at +20°C and +10°C nominal inlet temperatures. Under laminar flow conditions, the data are seen to fall very closely to Shah and London's correlation, but significantly above Hausen's correlation. This was also found for the other two tubes. This result was expected since a mildly corrugated wall is not good in enhancing laminar flow and the tube behaves essentially like a smooth tube. Significant enhancement for Korodense tubes is not expected until $Re_D > 10^4$ [Ref. 21].

The resulting correlation for laminar flow data is shown on Figure 6.23 and given by:

$$Nu_m = 2.05(x^*)^{-0.326} \quad (6.7)$$

The Hausen correlation (equation 2.10) used by Mazzone again under predicts the present measured inside heat transfer coefficient. It was expected that the mean

Nusselt number would be the same (or maybe slightly higher) as for the smooth tube case for the reasons already mentioned. However, the Korodense data fall slightly below the smooth tube data and closer to Shah and Londons' smooth tube correlation (equation 2.14). No explanation can be given for this result. Data scatter explanations given for the other tubes also apply for the Korodense tube.

2. Korodense Tube - Twisted Tape Insert

The results for the Korodense tube with a twisted tape insert are shown in Figures 6.24 and 6.25. The same twisted tape that was used for the smooth tube was used for the Korodense tube. Note that the Korodense tube nominal inside diameter (13.35 mm) is slightly larger than the smooth tube inside diameter (13.26 mm). This small difference in inside diameters (together with corrugation in the Korodense tube) led to a looser fit for the twisted tape insert.

The mean Nusselt number as a function of Reynolds number is shown in Figure 6.24 which again clearly indicates the inlet temperature dependence. The data were again correlated using the form of Hong and Bergles' correlation. The present data were compared to their correlation (equation 2.20) in Figure 6.25. The correlation developed for the present data is:

$$Nu_m = 0.569Pr^{0.35}(Re_f/y)^{0.498} \quad (6:8)$$

This correlations falls below the Hong and Bergles correlation (equation 6.20) as well as for the smooth tube. This result is thought to be primarily due to the looser fit of the twisted tape inside the Korodense tube. The corrugations also leave areas of no

contact between the tape and the inside wall of the tube. Stagnant flow or even air bubbles may form in these gaps, especially at low Reynolds numbers, causing an interruption of the swirled flow. The thermal boundary layer, therefore, is not as efficiently mixed as in the smooth tube. For these reasons, lower inside heat transfer coefficients than those assumed by Mazzone should be expected.

3. Korodense Tube - HEATEX Insert

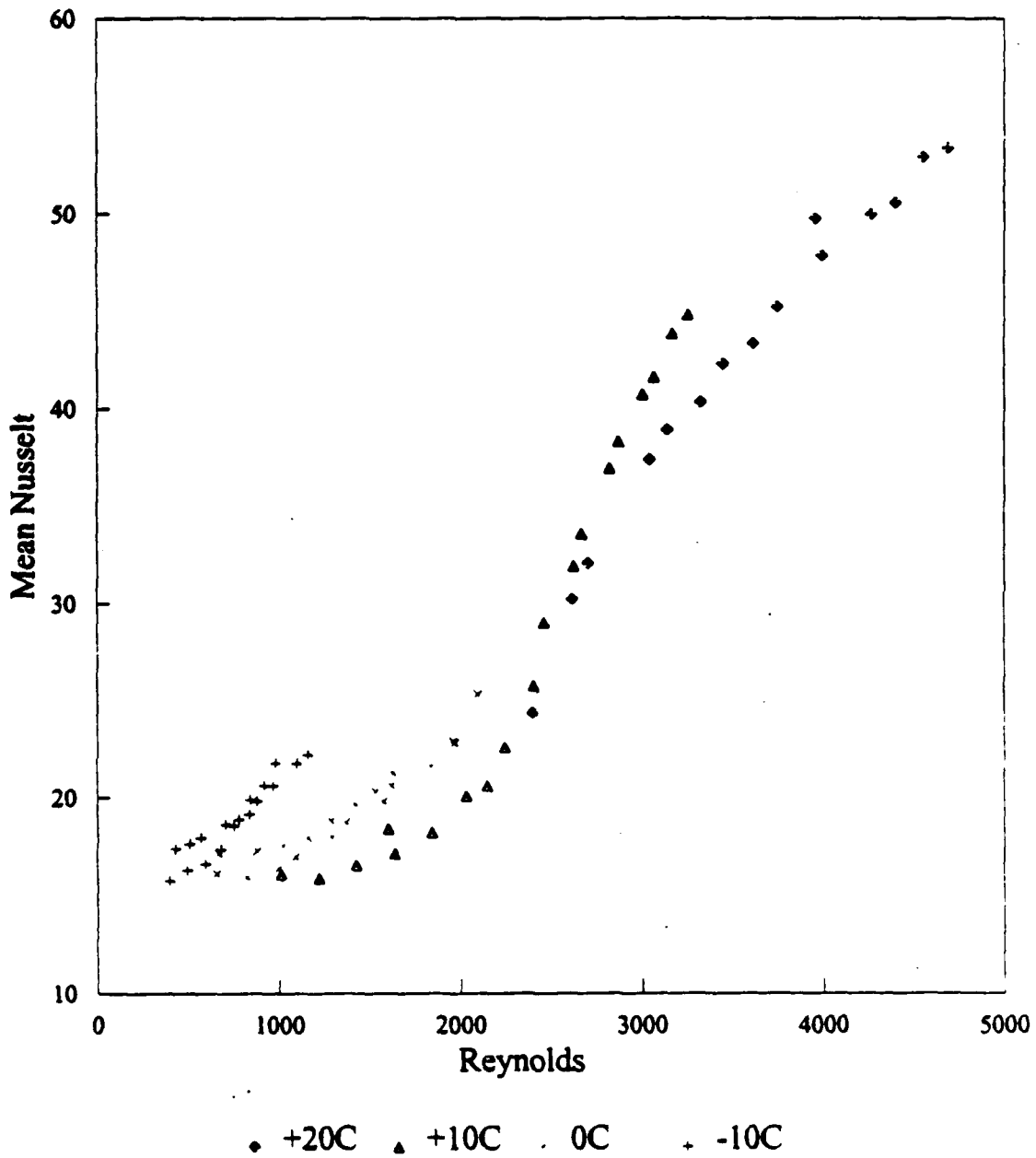
The last tube-insert condition tested was the Korodense tube with the HEATEX insert. The same HEATEX insert used for the smooth tube was used here. Figure 6.26 shows the mean Nusselt number as a function of Reynolds number and again shows an inlet temperature dependence. The resulting correlation for the present data is given by:

$$Nu_m = 0.282Pr^{0.46}Re^{0.499} \quad (6.9)$$

The data and this correlation are compared with the correlation Mazzone used (equation 2.23) in Figure 6.27. It is evident that Mazzone's chosen correlation overpredicts the inside heat transfer coefficient significantly. This again is thought to be primarily due to the incomplete mixing of the thermal boundary layer caused by non-contact regions existing between the tube wall and HEATEX petals.

KORODENSE TUBE - NO INSERT

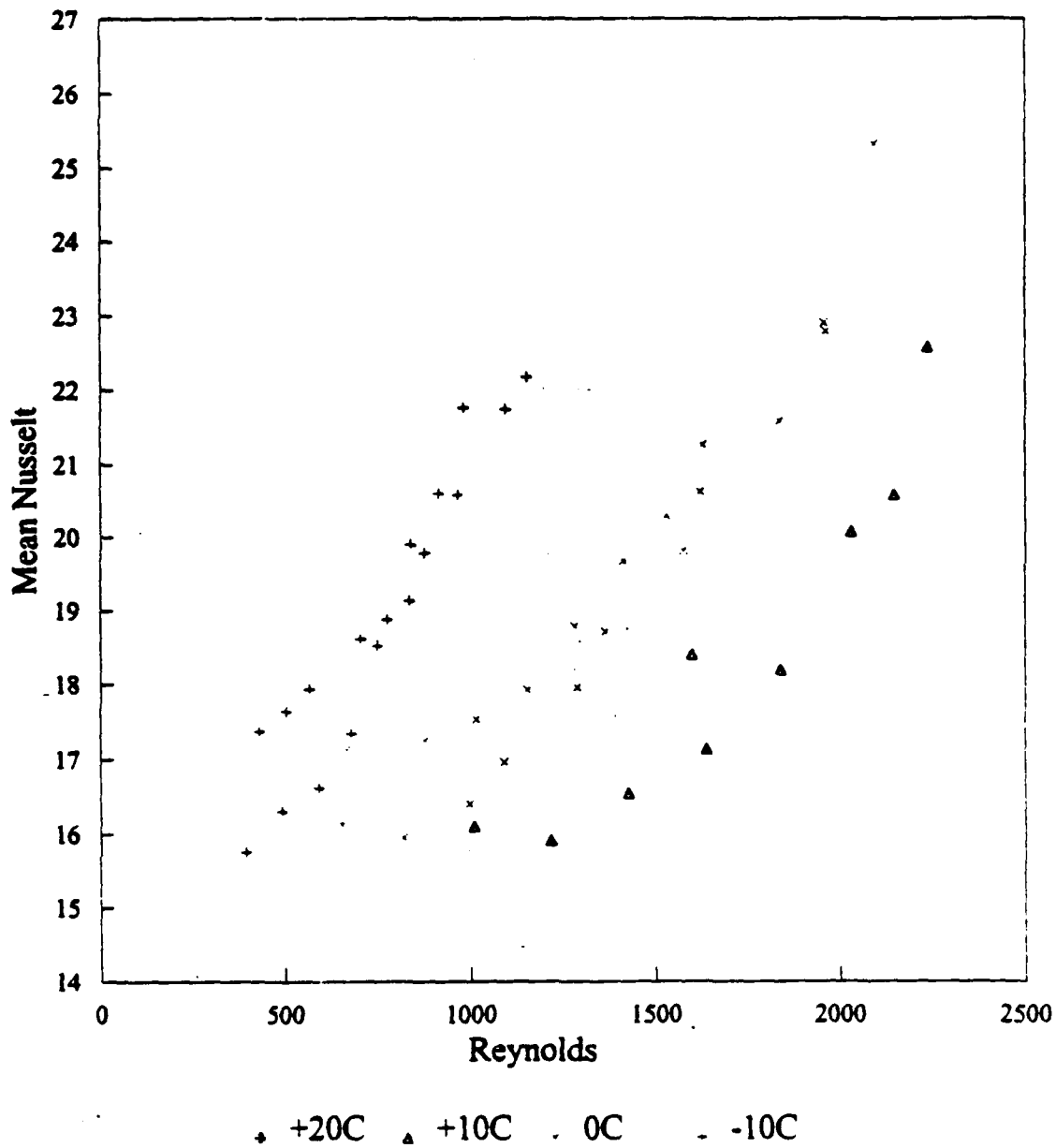
Nu vs Re



KDNIURE

Figure 6.19 Korodense tube - No insert (Nu_m vs. Re) results.

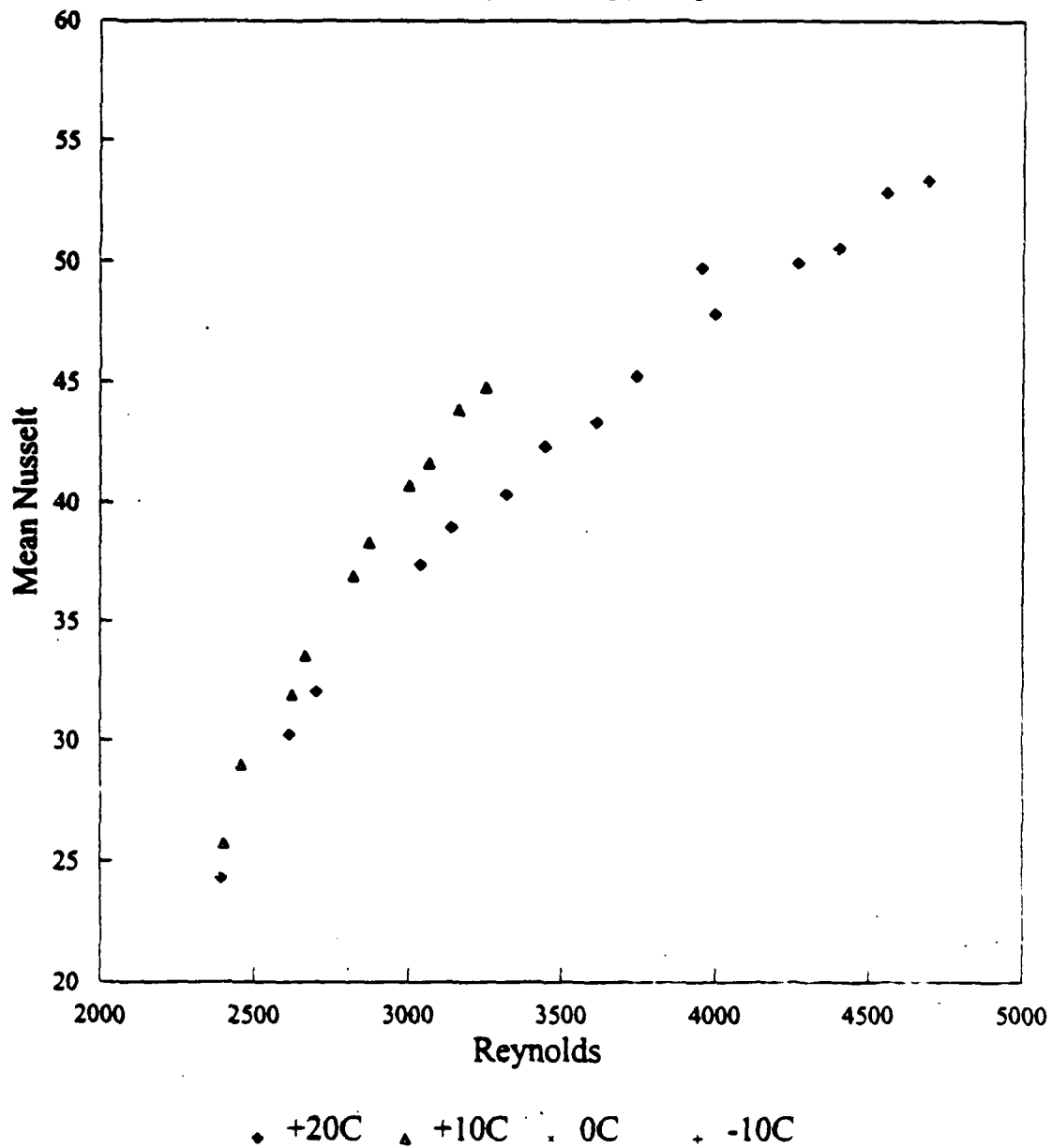
KORODENSE TUBE - NO INSERT LAMINAR FLOW



Nu VS Re
KDNINURELAM

Figure 6.20 Korodense tube - No insert (Nu_m vs. Re) laminar flow results.

KORODENSE TUBE - NO INSERT TRANSITIONAL FLOW

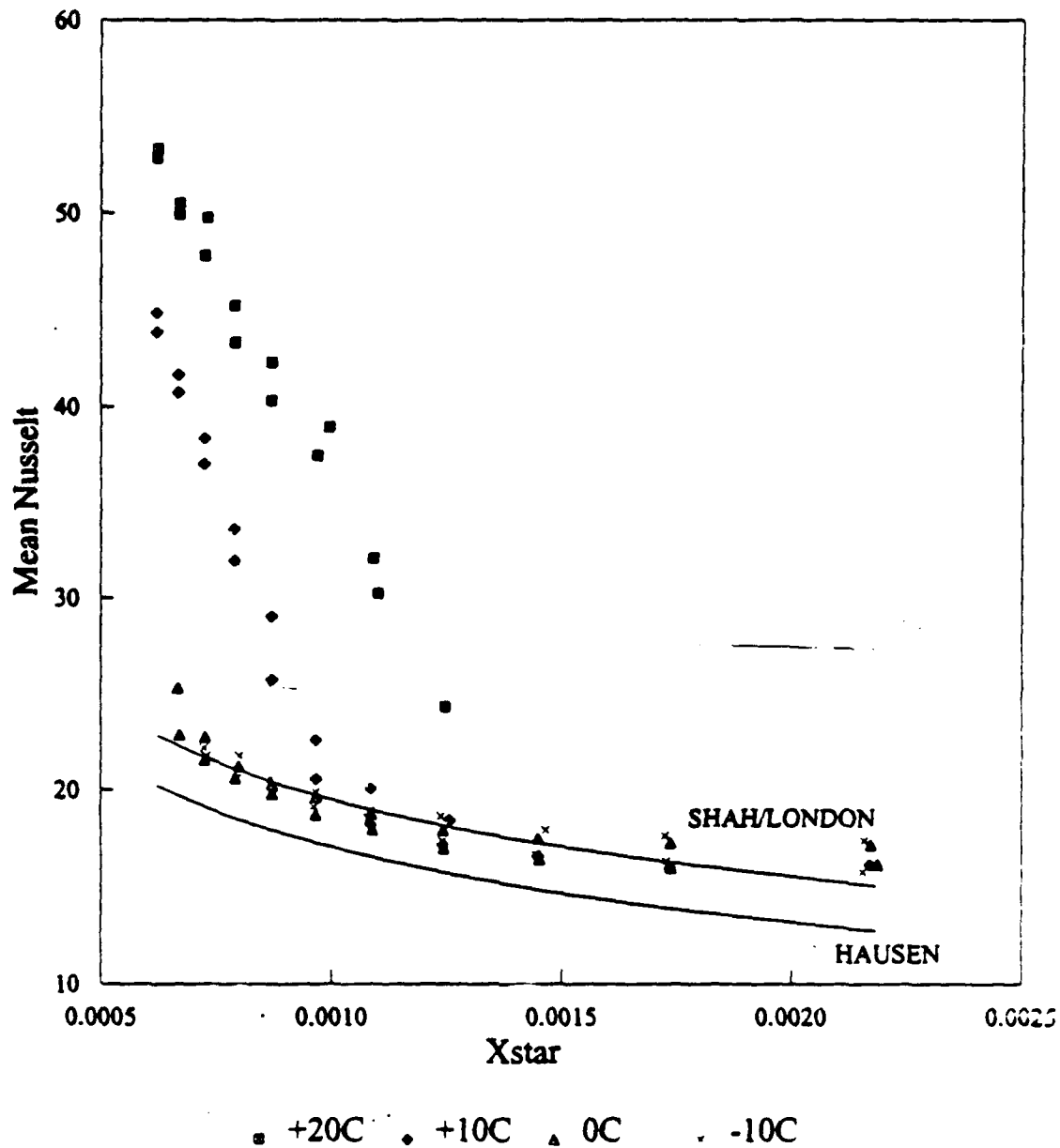


Nu vs Re
KDNINURETRAN

Figure 6.21 Korodense tube - No insert (Nu_m vs. Re) transitional flow results.

KORODENSE TUBE - NO INSERT

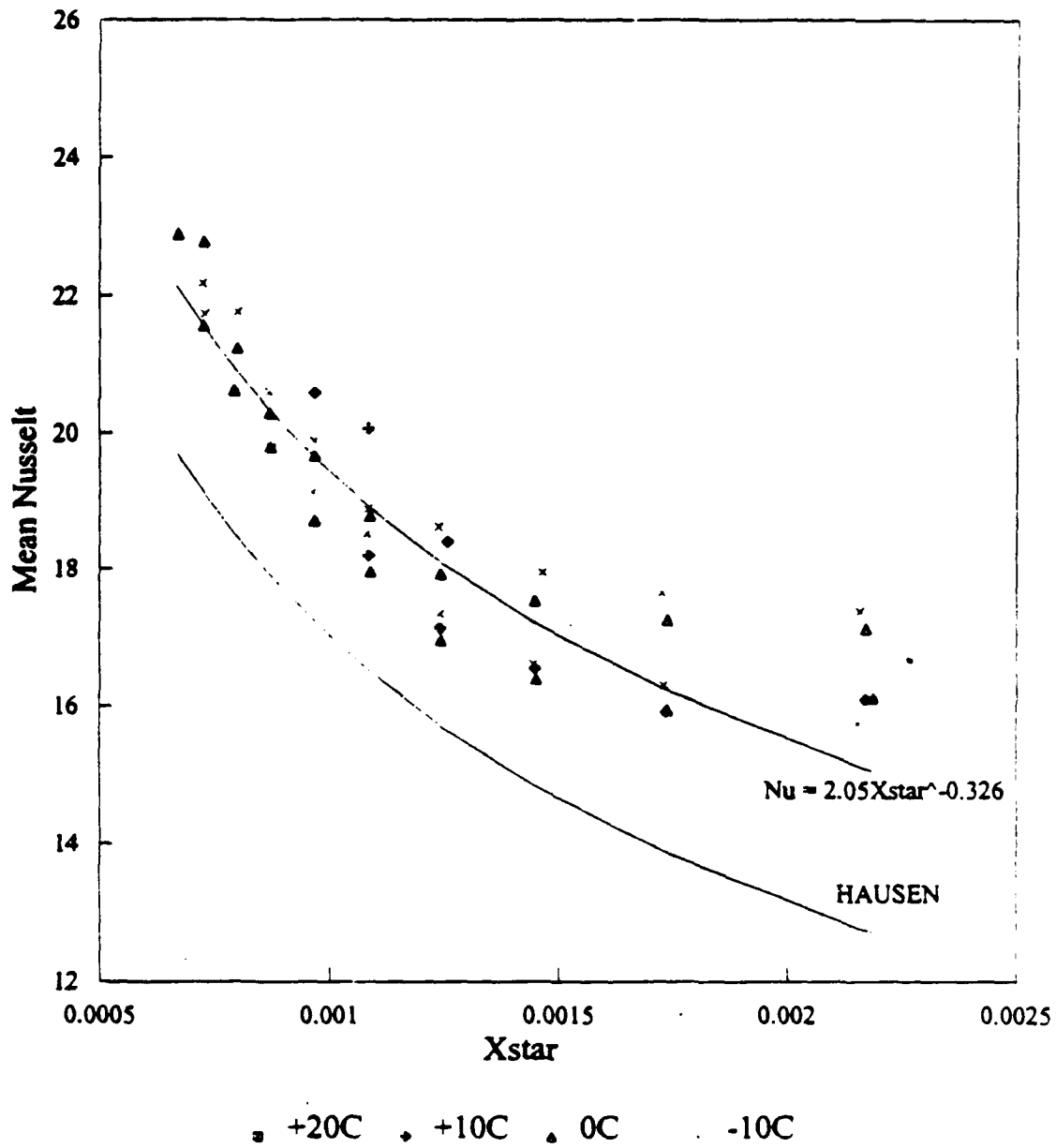
Nu vs Xstar



$X_{star} = (L/D)/PrRe$
KDNIXNU

Figure 6.22 Korodense tube - No insert (Nu_m vs. x^*) results.

KORODENSE TUBE - NO INSERT LAMINAR FLOW



Nu vs Xstar
KDNIXNUL

Figure 6.23 Korodense tube - No insert laminar flow correlation results.

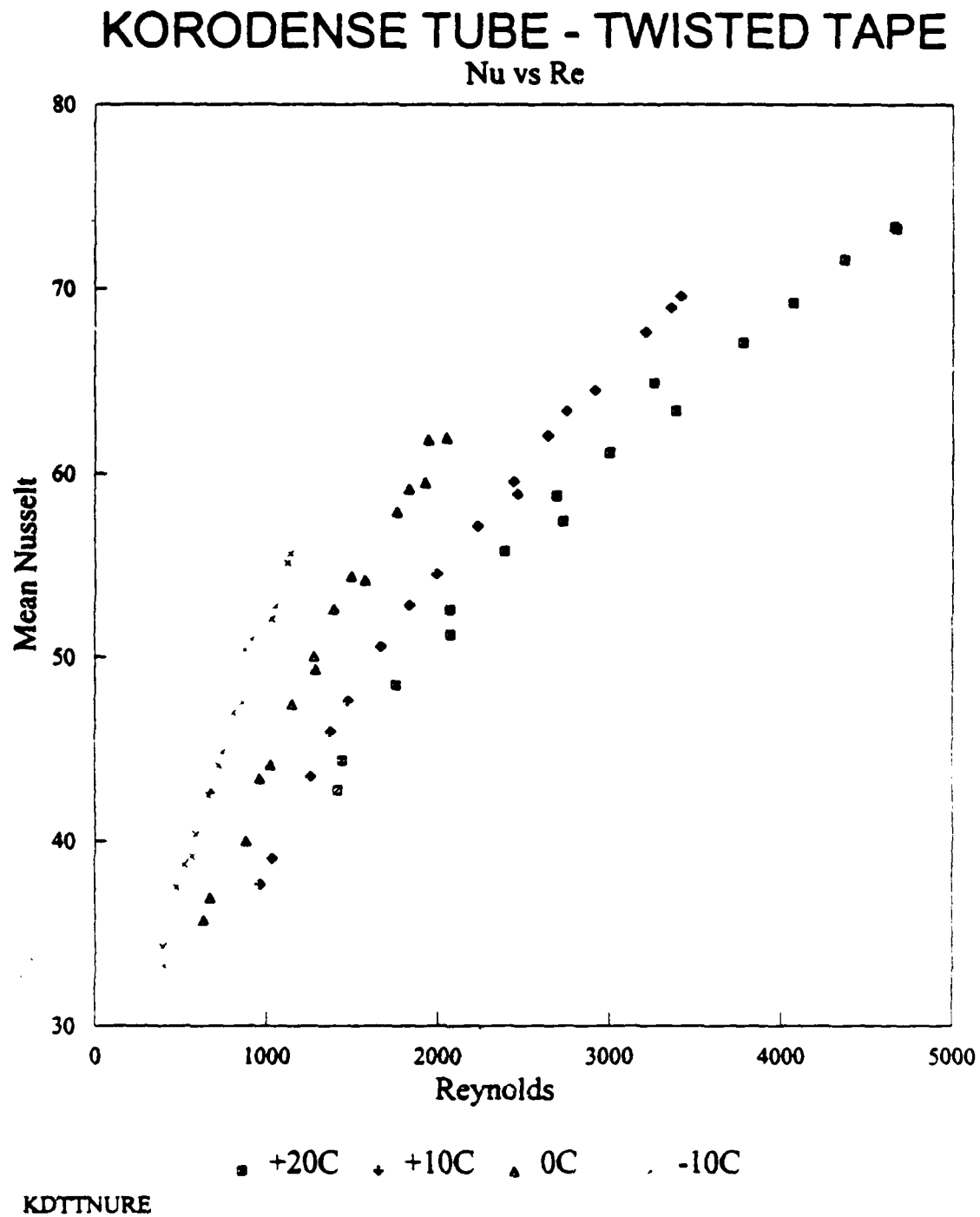


Figure 6.24 Korodense tube - Twisted tape (Nu_m vs. Re) results.

KORODENSE TUBE- TWISTED TAPE

(Nu/Pr^{.35}) vs (Res/y)

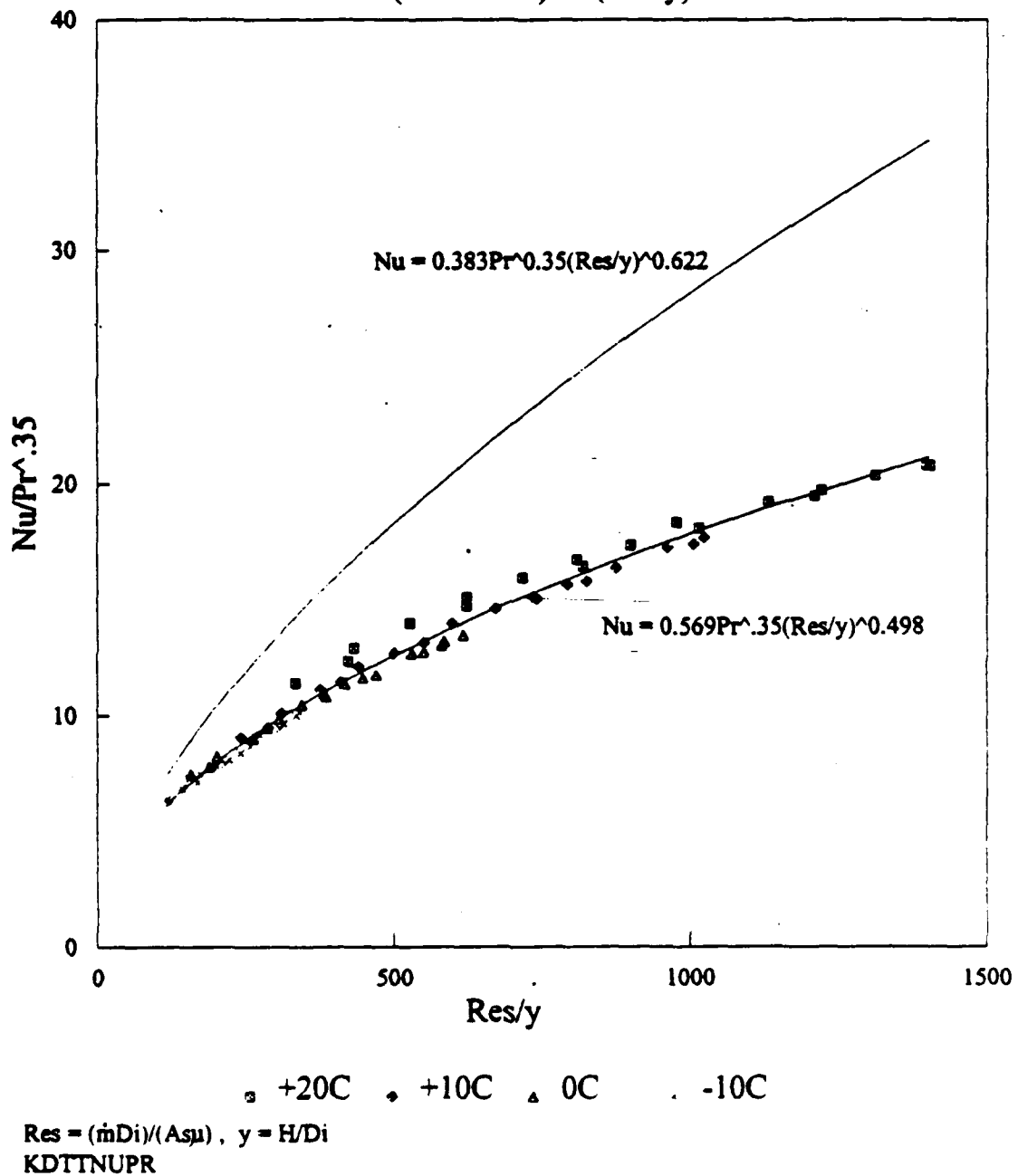
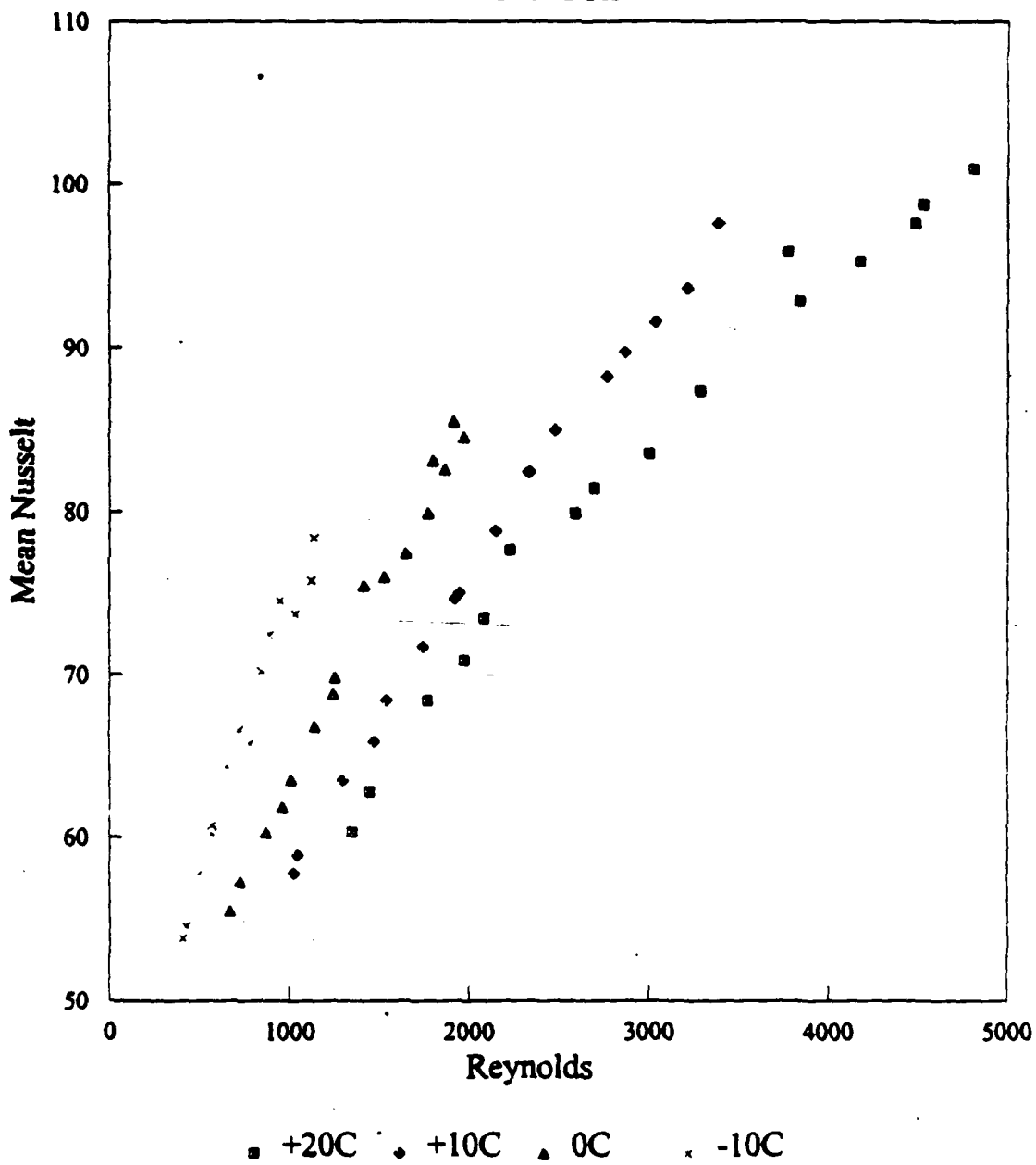


Figure 6.25 Korodense tube - Twisted tape correlation results.

KORODENSE TUBE - HEATEX

Nu vs Re

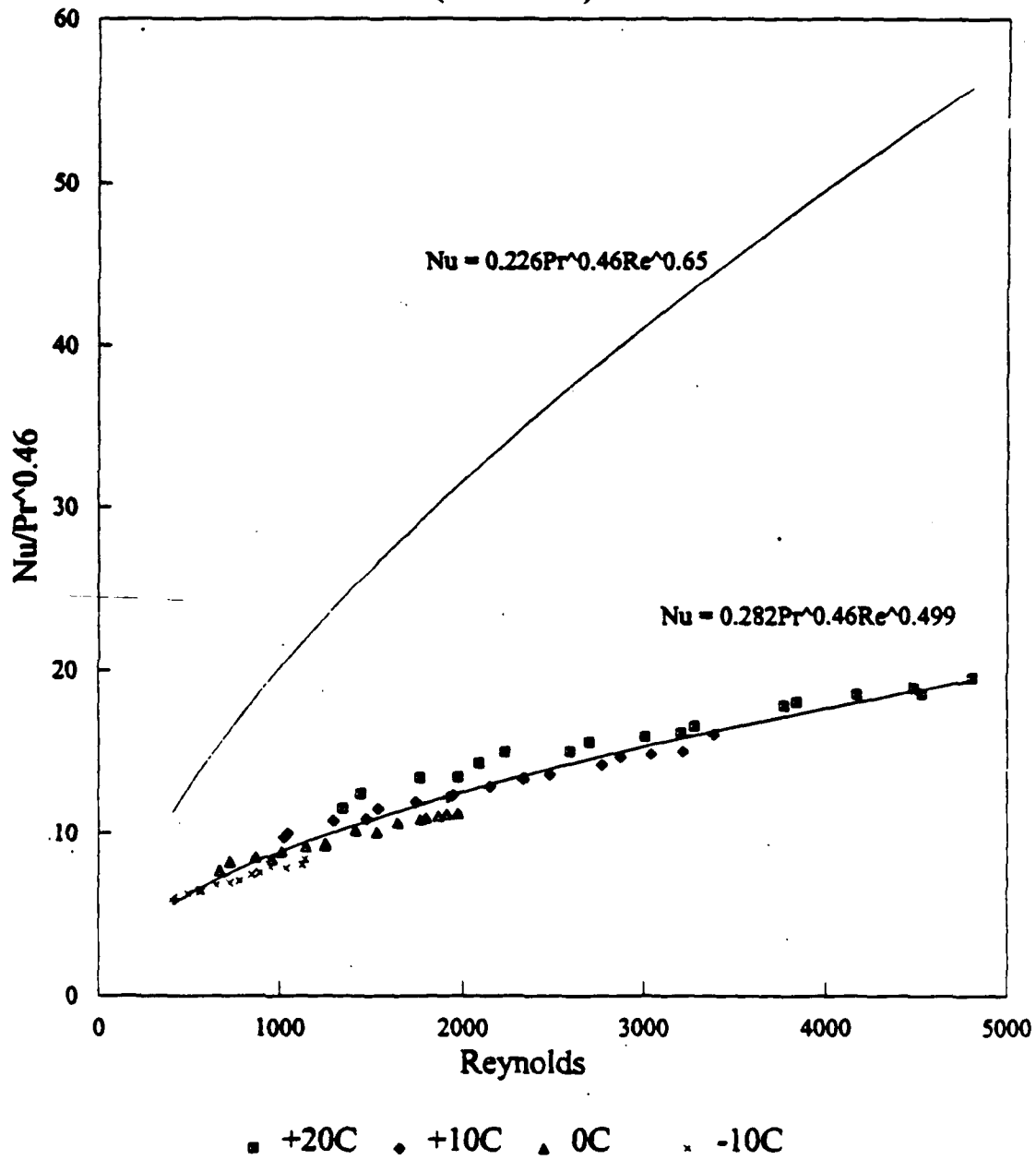


KDHXNURE

Figure 6.26 Korodense tube - HEATEX (Nu_{\square} vs. Re) results.

KORODENSE TUBE - HEATEX

(Nu/Pr^{0.46}) vs Re



KDHXNURE

Figure 6.27 Korodense tube - HEATEX correlation results.

E. INSERT COMPARISON BETWEEN TUBES

Figures 6.28, 6.29 and 6.30 each compare the three correlations for each tube for no insert, twisted tape, and HEATEX inserts, respectively. It can be seen that with no insert (Figure 6.28), the Korodense correlation is about 10% below the smooth tube data. Although one may expect no increase in the heat transfer with a roped tube under laminar flow conditions, one certainly would not expect to find such a decrease with a similar diameter tube. This difference, therefore, can only be attributed to experimental uncertainty, probably in the wall temperature measurement. The finned tube correlation is lower than both the Korodense ($\approx 5\%$) and smooth tube ($\approx 15\%$) correlations; this tube had a smaller inside diameter and it may be that different induced flow patterns are set up causing a reduction in heat transfer. Experimental uncertainty must also not be ruled out as to the cause of the difference.

Figure 6.29 shows the same three tube correlations, but for the twisted tape insert. The smooth tube again has the highest performance. The finned tube is $\approx 20\%$ below at a high Re number and nearly 40% lower at a low Re number. This could be due to a different twist ratio used for the finned tube due to the smaller inside diameter. The Korodense tube is similar to the finned tube, giving slightly lower heat transfer at high Re number and slightly higher heat transfer at low Re. The reason for this tube being significantly lower than the smooth tube is thought to be due to the tape not contacting the inner surface of the tube as well as for the smooth tube,

thereby leaving regions of stagnant flow. These regions would tend to inhibit mixing and lead to a lower heat transfer performance.

For the HEATEX comparison (Figure 6.30), similar conclusions can be made, although the finned tube seems to have better relative performance indicating that the small diameter HEATEX insert used in the small diameter tube is more effective than the twisted tape. The difference between the smooth and Korodense tubes are of similar magnitude to that shown in Figure 6.29 (about 40% at high Re).

NO INSERT COMPARISON UNDER LAMINAR FLOW

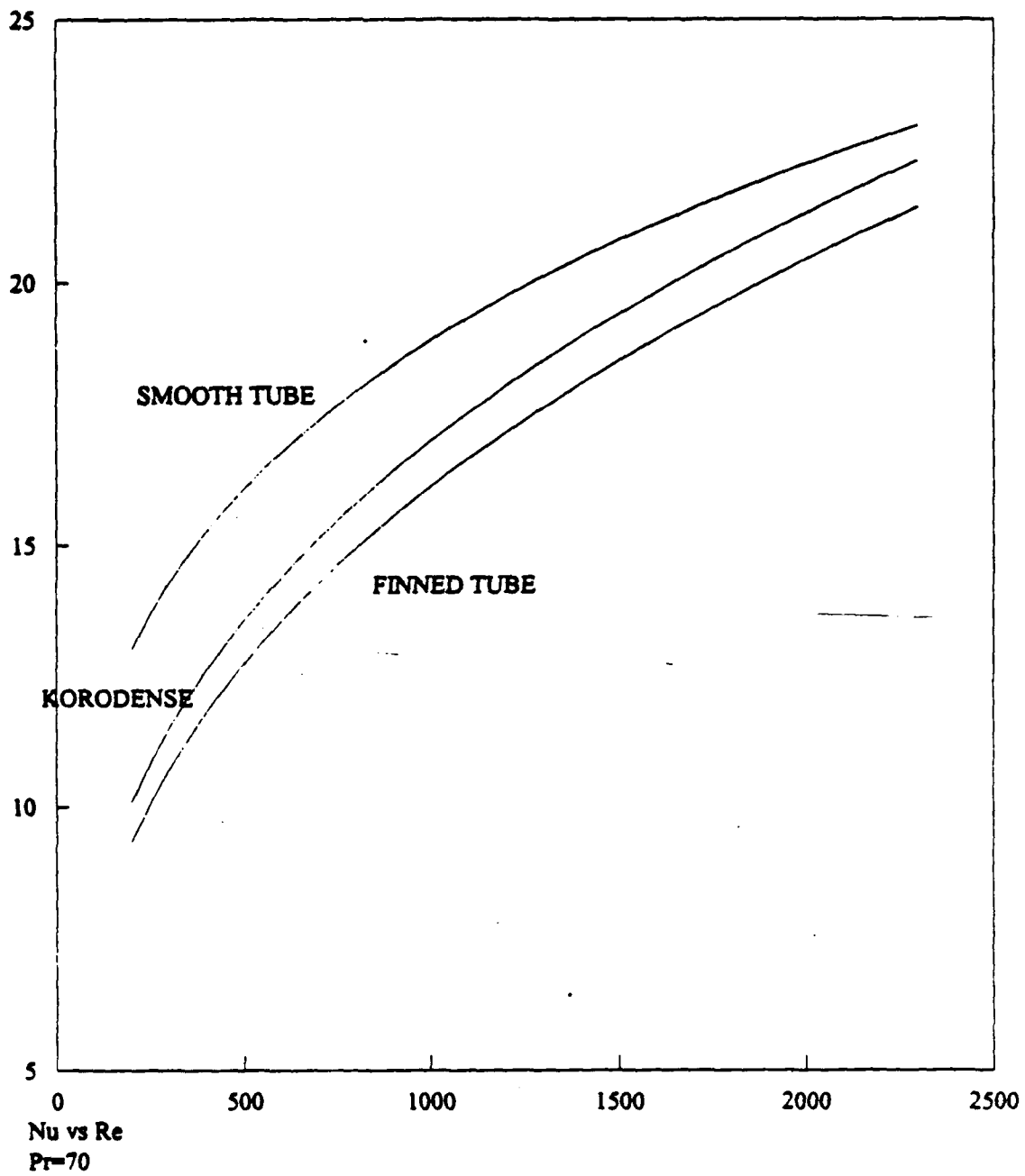


Figure 6.28 No insert comparison under laminar flow for all three tubes.

TWISTED TAPE INSERT COMPARISON UNDER LAMINAR FLOW

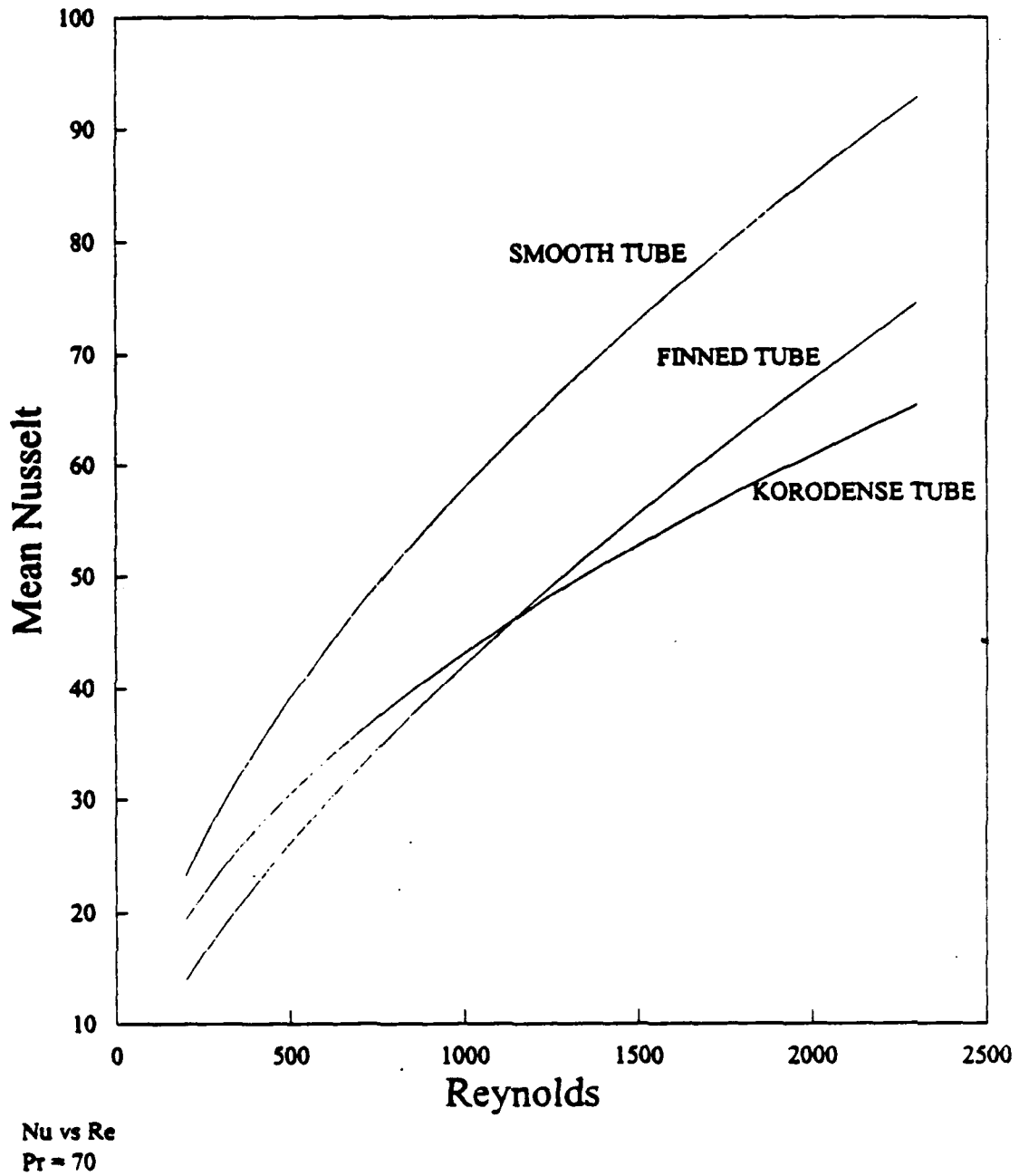


Figure 6.29 Twisted tape insert comparison under laminar flow for all three tubes.

HEATEX INSERT COMPARISON UNDER LAMINAR FLOW

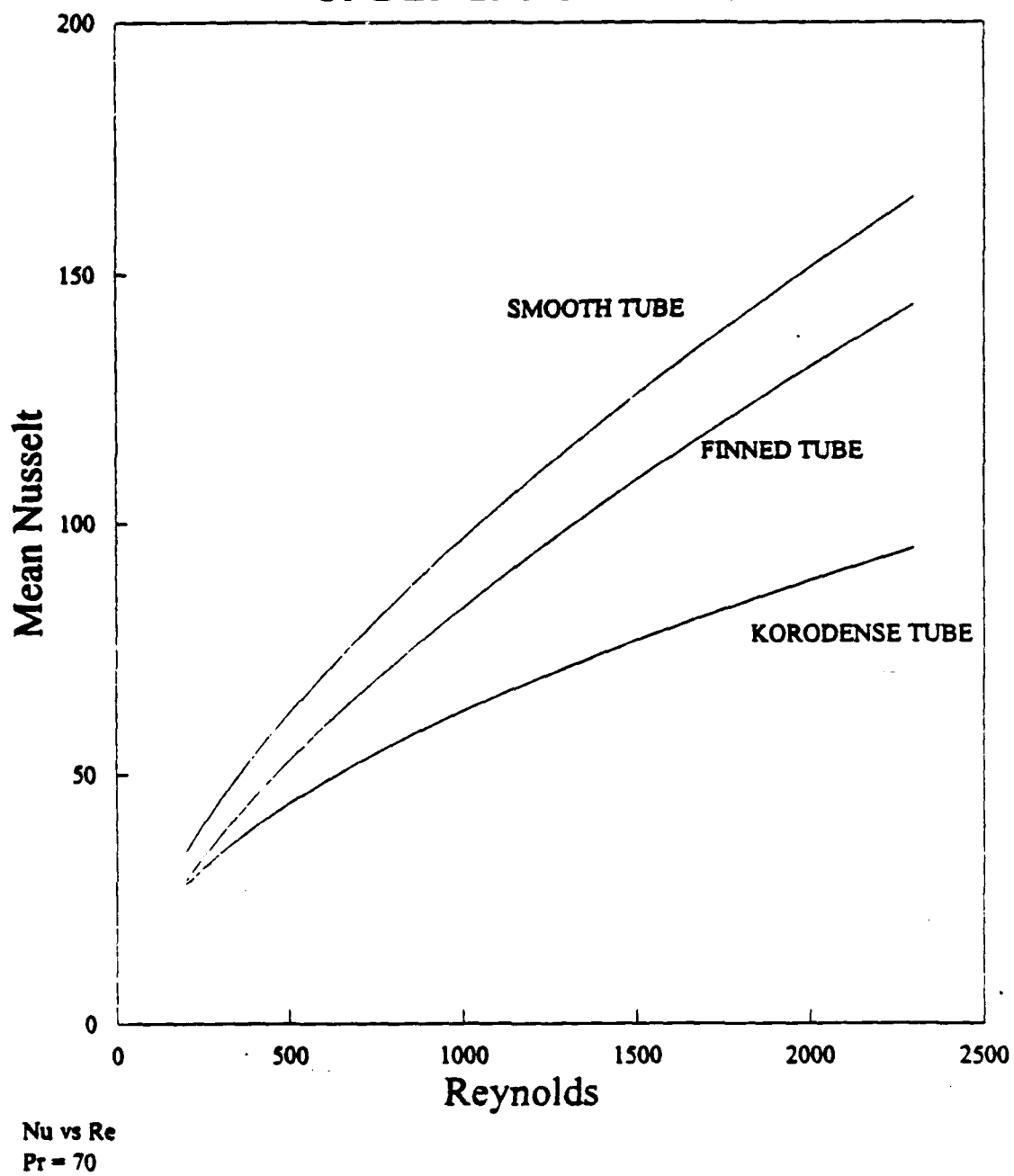


Figure 6.30 HEATEX insert comparisons under laminar flow for all three tubes.

F. LAMINAR FLOW ENHANCEMENT RATIO

The comparisons made in Figures 6.28 through 6.30 are made more complicated by the fact that the uncertainty associated with the wall temperature measurement is unknown and most likely different for each tube. For this reason, it is not known how much of the divergence seen in these figures is due to differences in thermocouple attachment (giving uncertainty to the wall temperature measurement) and how much is an actual flow induced phenomenon. A comparison of the relative effects of the three inserts for a given tube is more accurate, however, due to the fact that any uncertainty for a given tube wall thermocouple attachment combination would be the same.

To determine the degree of tubeside heat transfer enhancement achieved by the use of the twisted tape and HEATEX inserts under laminar flow, an enhancement ratio of the mean Nusselt number for the insert condition (Nu_{insert}) to that for the no insert condition ($Nu_{no\ insert}$) was calculated. The enhancement ratio is therefore defined as:

$$\epsilon = \frac{Nu_{insert}}{Nu_{no\ insert}} \quad (6.10)$$

Figures 6.31 through 6.33 present mean Nusselt number as a function of Reynolds number under laminar flow conditions for each tube under the three insert conditions. For the purposes of this study, enhancement ratios were calculated at the two extreme Reynolds numbers of 200 and 2300 with a constant Prandtl number of

70 using the correlations developed in the previous sections. Table 6.2 summarizes the enhancement ratios for each tube and insert condition.

It is evident from these figures that the greatest enhancement is achieved using the HEATEX insert. An enhancement factor of over seven was achieved for the smooth tube using the HEATEX insert at $Re = 2300$. This reduced to about 2.6 at low Re . Significantly smaller enhancements were achieved for the twisted tape inset for the smooth tube, indicating that for laminar flow, the stripping and mixing effect of the HEATEX element is considerably more effective than the simple swirl flow effect provided by the twisted tape. It should be mentioned here that HEATEX was developed specifically with laminar flow enhancement in mind. In turbulent flow ($Re > 10^4$), the enhancements obtained are much smaller (around 1.5 to 2) and both twisted tape and HEATEX elements give similar enhancement values.

TABLE 6.2 SUMMARY OF LAMINAR FLOW ENHANCEMENT RATIOS
(defined by equation 6.10)

	SMOOTH TUBE		FINNED TUBE		KORODENSE TUBE	
	TWISTED TAPE	HEATEX	TWISTED TAPE	HEATEX	TWISTED TAPE	HEATEX
Low Re ($Re = 200$)	1.79	2.66	1.49	2.86	1.92	2.58
High Re ($Re = 2300$)	4.04	7.19	3.46	6.71	2.93	4.25

For the finned and Korodense tubes, the HEATEX element also provides the highest enhancements. At high Re , the enhancements provided by the twisted tape and HEATEX inserts are lower than those obtained with the smooth tube for the reasons mentioned previously. However, at low Re , the enhancements for the three tubes are about the same for a given insert, indicating the "stagnant" regions mentioned earlier have less of an effect on the total heat transfer.

INSERT CONDITION COMPARISON LAMINAR FLOW - SMOOTH TUBE

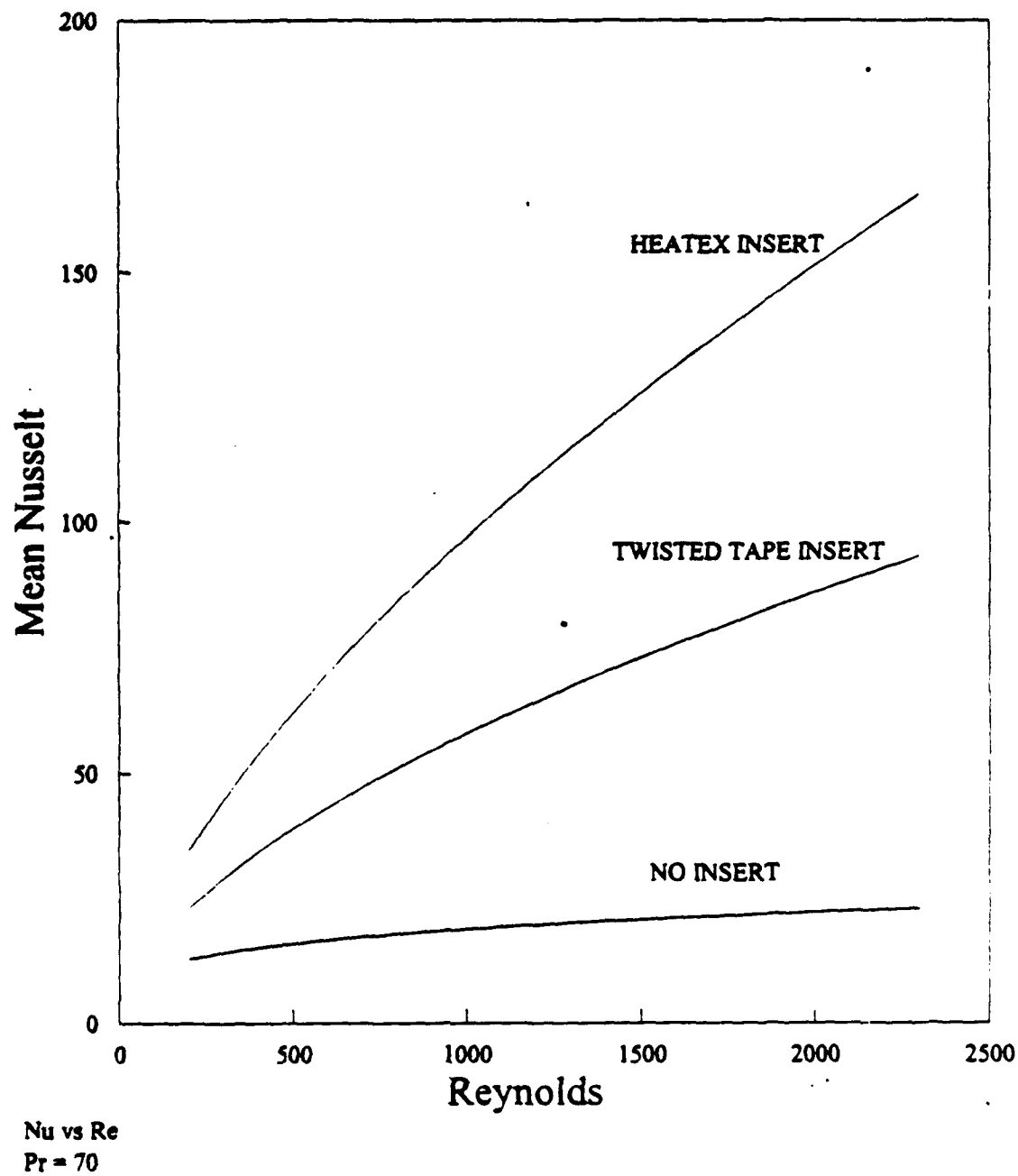
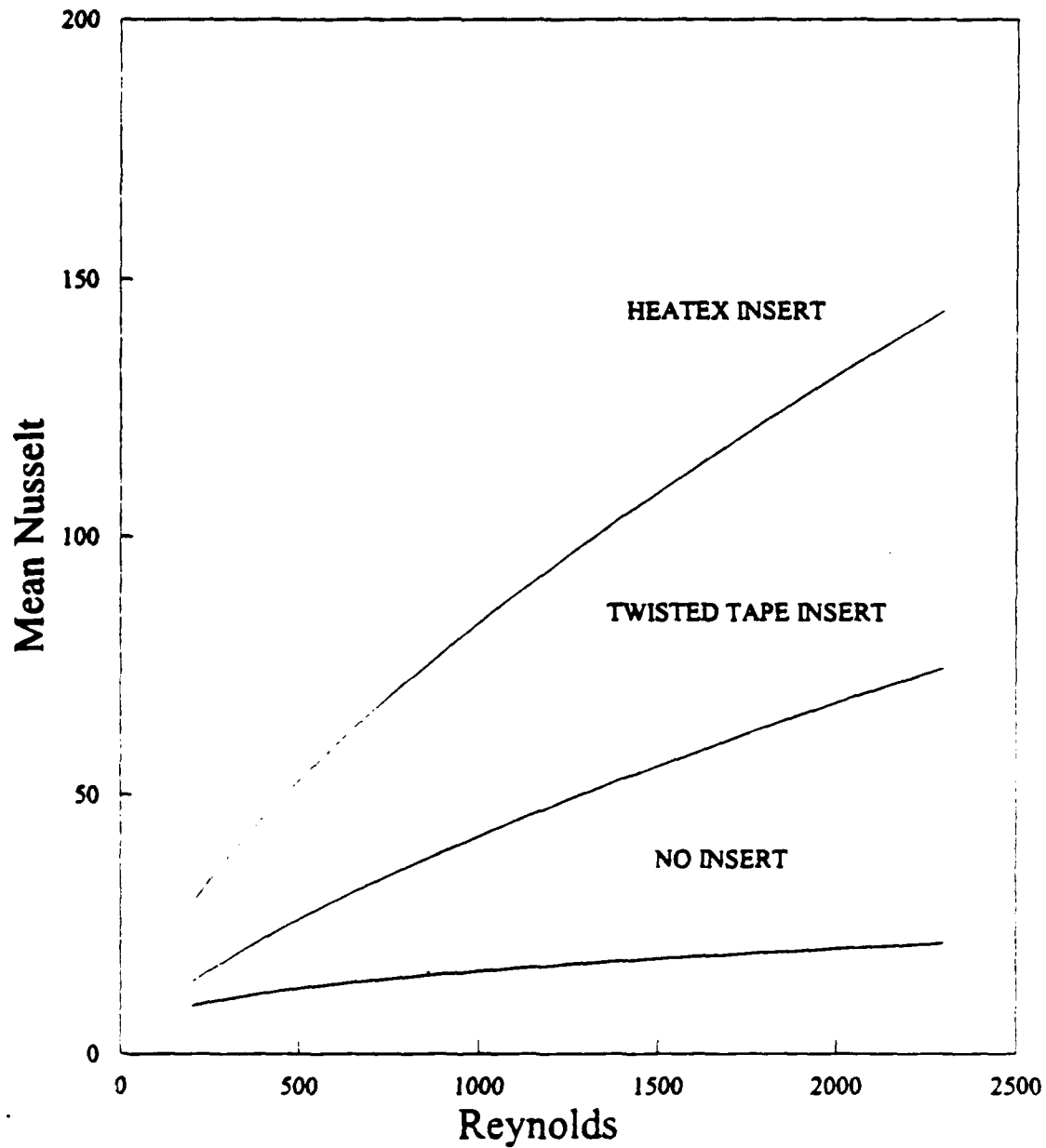


Figure 6.31 Insert condition comparison for laminar flow in a smooth tube.

INSERT CONDITION COMPARISON LAMINAR FLOW - Cu/Ni FINNED TUBE



Nu vs Re
Pr = 70

Figure 6.32 Insert condition comparison for laminar flow in a Cu/Ni externally finned tube.

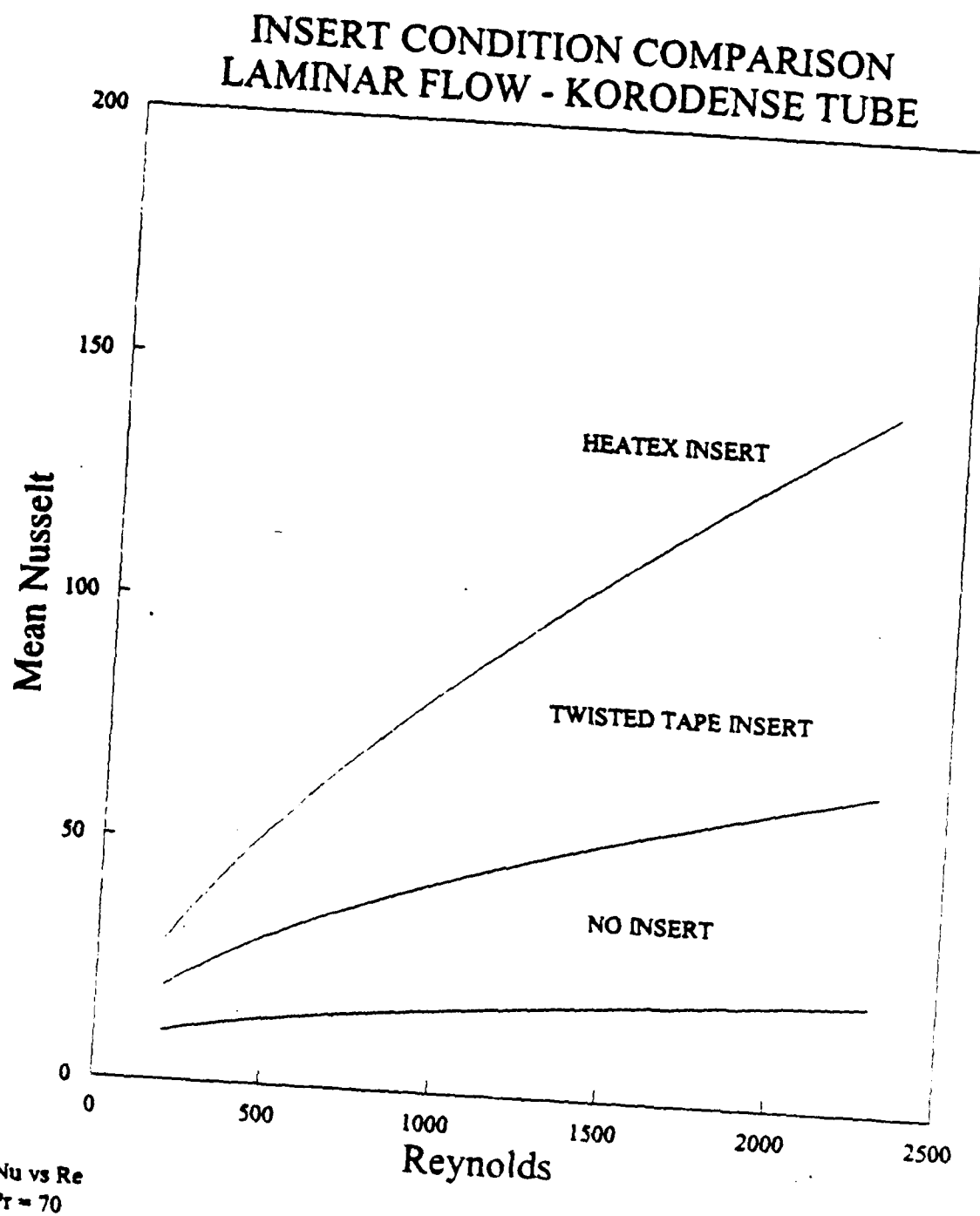


Figure 6.33 Insert condition comparison for laminar flow in a Korodense tube.

G. REPROCESSED REFRIGERANT CONDENSATION DATA

Figure 6.34 shows the condensation data of Mazzone [Ref. 6] with the outside heat transfer coefficient recalculated using the present correlations. The data presented are for the top copper smooth tube. Similar recalculations can also be carried out for the other two tubes (Cu/Ni finned and Korodense tubes) as well as for condensation bundle data. The data of Mazzone are reprocessed using the Modified Wilson Plot Technique (see Mazzone [Ref. 6] for details). This technique essentially lets the leading coefficient of the correlation 'float' to try to smooth out any uncertainty in the correlations being used. As previously stated, the chosen correlation for the no insert condition (even when reprocessing using the Wilson Plot Technique) gave values of inside thermal resistances greater than the measured overall thermal resistance, thereby yielding negative values of the outside heat transfer coefficient, h_o . This explains why Figure 6.34 has no data for Mazzone's no insert condition.

It can be seen that by using the present developed correlations for the no insert condition, the calculated values of h_o are significantly improved (i.e. positive values). In addition, for the other two inserts, the new correlations increase h_o by about 10% for the twisted tape insert and nearly 20% for the HEATEX insert. The newly calculated values of h_o when using these inserts are now very close and just above the Nusselt prediction as may be expected for low vapor velocity film condensation. Mazzone commented that his data were below Nusselt by about 10%

and thought that this was a consequence of the length of his condenser tubes violating the uniform wall temperature assumption of the Nusselt theory. The fact that these data are so close gives confidence in the new correlations, as the insert itself should have no influence on the magnitude of h_o . By significantly reducing the inside resistance, the insert simply increase the accuracy of h_o . Of course, the no insert condition should also give similar values of h_o . Figure 6.34 shows that they are too high, indicative of the fact that the correlation for the no insert condition, although much improved, is still not ideal. If one recalls the scatter obtained in the present data for the no insert case, together with the fact that the inside resistance is still dominating, then the results shown in Figure 6.34 are not too surprising and still very encouraging. It is recommended, therefore, that all future refrigerant condensation experiments carried out on the bundle facility should be conducted with the inserts using the newly formulated correlations.

One final note is the fact that the present correlations were formulated using a constant wall heat flux, whereas for the condensation experiments, one should ideally use correlations developed under uniform wall temperature conditions. One may expect that the inside heat transfer coefficient would increase slightly under constant wall heat flux conditions, thereby decreasing the outside heat transfer coefficient. However, from Figure 6.34 it is clear that the use of the constant wall heat flux correlations seems to increase h_o . Thus it appears that with the inserts, the inside resistance is so reduced that the boundary condition imposed has little

influence. Future investigators should look into this boundary value problem in more detail.

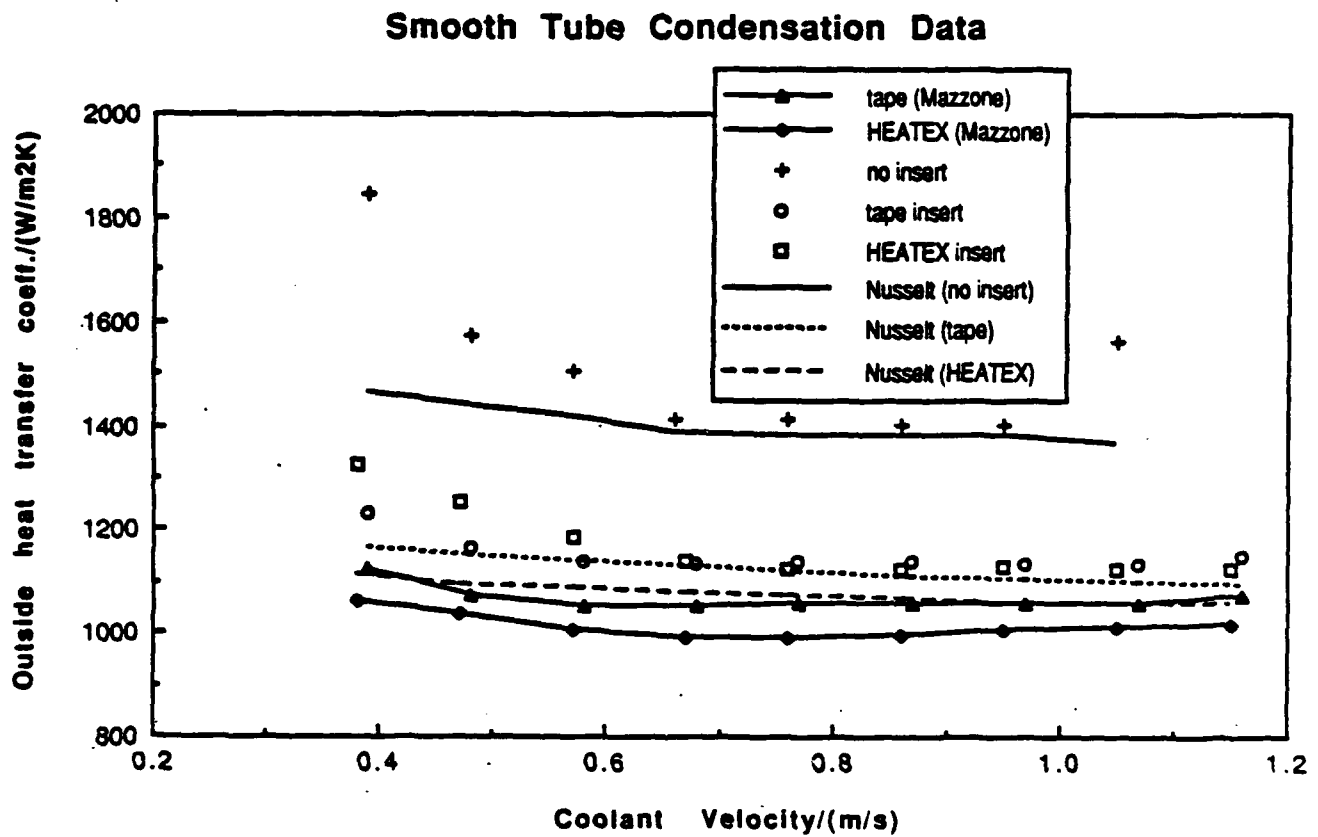


Figure 6.34 Reprocessed refrigerant condensation data using new correlations.

VII. CONCLUSIONS

The following conclusions are based upon results obtained in this study.

A. GENERAL

1. A test apparatus was successfully designed and built to accurately determine inside heat transfer coefficients for the same tubes and insert conditions used in the condensation experiments.
2. Correlations to accurately determine inside heat transfer coefficients under laminar flow conditions both with and without inserts were successfully developed.
3. Reprocessing of Mazzone's [Ref. 6] refrigerant condensation data using these new correlations has yielded more accurate values of the outside heat transfer coefficient. (Note: the name of the program used for the reprocessing is DRPCON7.)

B. SPECIFIC

1. A departure from laminar flow into a transitional flow exists at Reynolds numbers of approximately 2300 for the smooth and Korodense tubes and 2700 for the Cu/Ni finned tube. This contradicts Mazzone's [Ref. 6] assumption of laminar flow up to a Reynolds number of approximately 4000.
2. Laminar flow results for the no insert condition were in close agreement with the Shah and London [Ref. 9] correlation for a constant wall heat flux boundary condition for all three tubes tested.
3. The Hausen [Ref. 10] correlation used by Mazzone [Ref. 6] significantly overpredicted the inside thermal resistance and led to nonsensical results for h_o .

4. The smooth tube/twisted tape data were in close agreement with the Hong and Bergles [Ref. 13] correlation. Since this correlation was used by Mazzone [Ref. 6], his results for outside heat transfer coefficient should be fairly accurate for this tube.
5. For the Cu/Ni finned and Korodense tubes with the twisted tape insert, the Hong and Bergles correlation predicted higher inside heat transfer coefficients than the experimental data over the entire Reynolds number range tested. This could have been due to a different twist ratio (for the Cu/Ni finned tube) and stagnant regions (for the Korodense tube).
6. Experimental data for all three tubes using the HEATEX insert yielded results that were well below the correlations developed and used by Mazzone [Ref. 6] over the entire Reynolds number range tested.
7. HEATEX inserts provided the best inside heat transfer enhancement for all three tube. Enhancement ratios of over a factor of seven were found.

VIII. RECOMMENDATIONS

Based on the results of this study, the following recommendations are made:

1. Further refinement of the correlations to better account for different coolant inlet temperatures should be made by optimizing the Prandtl number exponent.
2. These correlations should be used to reprocess all refrigerant condensation data and should be used in future refrigerant condensation experiments conducted at NPS. Note that since these correlations were developed by omitting coolant velocities of 0.2 and 0.3 m/s, then the condensation data should do the same.
3. HEATEX inserts provide the best enhancement of tubeside heat transfer. Due to the data reduction technique used, HEATEX inserts should therefore be used in all tubeside refrigerant condensation experiments to increase the accuracy of the outside heat transfer coefficient.
4. Transitional flow correlations can also be developed for the no insert condition since condensation experiments typically move into this flow region. However, since the transition region is not generally well developed, any developed correlations for this region will be useful only for this particular apparatus.

APPENDIX A. FLOW METER CALIBRATION

The flowmeter used to measure flow through the instrumented tube was initially calibrated at 0°C and 24°C by Mazzone [Ref. 6]. However an additional calibration temperature of -15°C was needed for this study. The flowmeter was calibrated using the same procedure as Mazzone and is summarized as follows.

The outlet of the flowmeter was disconnected from the test section and connected to an empty 55 gallon drum. The drum was placed on a scale with a resolution of 0.5 lbs. The coolant pump was started with the flow through a bypass. The flowmeter was initially opened to maximum flow and then throttled back to 10%. The weight of fluid in the drum was recorded and the timer started. The weight was then recorded at the end of the calibration time. This procedure was repeated in 10% increments up to 100% flow. The calibration run was then repeated from the maximum flow back to 10% flow in 10% increments. The mass flow rate was then calculated in kg/s based on an average of the two readings. The data for the flowmeter calibrations as a function of nominal flow rate are shown in Table A.1.

A least squares linear regression was performed for the flowmeter at each of the three temperatures for which the calibration runs were carried out. The linear regression equation takes the following form:

$$\dot{m} = a + bN \quad (\text{A.1})$$

where a is the y-intercept in kg/s, b is the slope in kg/s/% and N is the flowmeter setting in %. The results are shown in Table A.2.

TABLE A.1. MASS FLOW RATE (KG/S) AT -15, 0 AND 24°C

FLOW METER A			
NOMINAL FLOW RATE (%)	MASS FLOW RATE (kg/s)		
	-15°C	0°C	24°C
10	0.0114	0.0149	0.0172
20	0.0295	0.0363	0.0403
30	0.0483	0.0544	0.0621
40	0.0679	0.0794	0.0851
50	0.0866	0.1003	0.1120
60	0.1078	0.1179	0.1339
70	0.1258	0.1388	0.1556
80	0.1453	0.1563	0.1769
90	0.1613	0.1846	0.2028
100	0.1824	0.2019	0.2151

TABLE A-2. FLOWMETER CALIBRATION REGRESSION RESULTS

FLOW METER A			
	-15°C	0°C	24°C
Slope	0.0019	0.00206	0.00225
Y-Intercept	-0.0098	-0.00414	-0.00329

In order to obtain flowrates at any intermediate temperatures, a simple interpolation procedure was incorporated into the data reduction program "DRPSING." The results of the calibrations for this flowmeter are shown in Figure A.1.

FLOWMETER CALIBRATION @ -15, 0, 24C

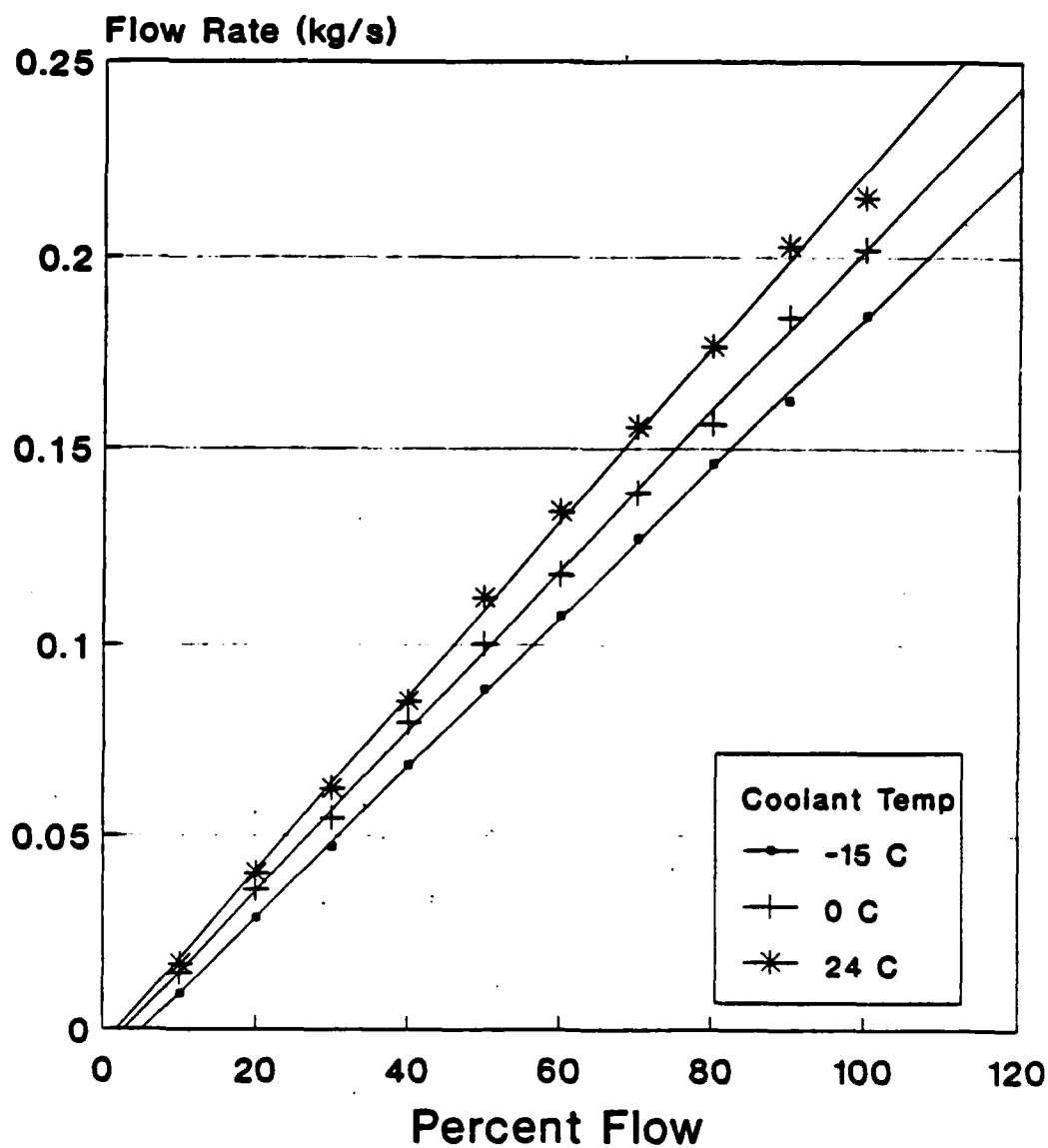


Figure A.1 Flowmeter Calibration.

APPENDIX B. HEAT LOSS TO AMBIENT EXPERIMENT

A series of heat loss experiments were conducted to account for the amount of heat lost to ambient. To accomplish this, the coolant was drained from the test tube and the inlet and outlet capped off to prevent any air flow through the tube. Heater power was set at a desired level and wall temperatures monitored by the DAU. Average wall temperatures were determined every minute for the first 15 minutes and then every four minutes until an equilibrium temperature was reached (after approximately 60 minutes). At that point, any additional heat added could be considered lost to ambient. This procedure was repeated at five nominal power settings, 1W, 3W, 5W, 7W, and 9W. All data were taken at an ambient temperature of 22.0°C.

Figure B.1 is a plot of average wall temperature versus time for the 1W and 7W power settings. It can be seen that an equilibrium average wall temperature was reached after approximately 60 minutes for these two power settings (as it was for the other three power settings.) This graph shows that if the average wall temperature in the experiments reached 46°C or 74°C, then the heat lost to the atmosphere was 1W or 7W, respectively.

Table B.1 shows the data for the equilibrium average wall temperature as a function of the actual power setting (\dot{q}_{tube}). The data are shown graphically in Figure B.2. A least squares linear regression was performed and the resulting equation was:

$$\dot{q}_{loss} = \frac{(T_w - 44.15)^\circ\text{C}}{4.39 \text{ W}^\circ\text{C}} \quad (\text{B.1})$$

Therefore, for a given average wall temperature, the amount of heat lost to ambient could be determined. Equation B.1 was incorporated into the data reduction program "DRPSING."

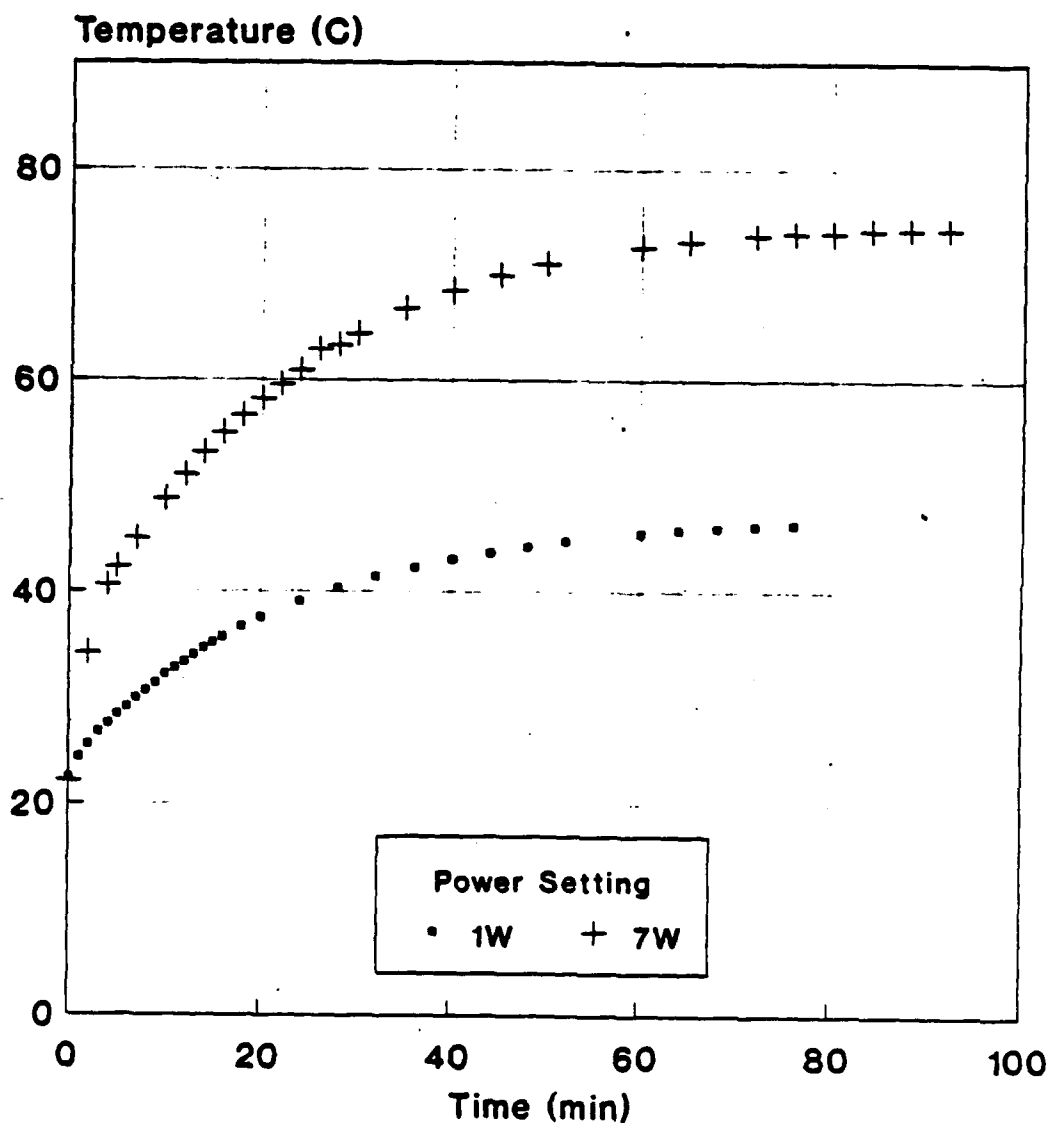
TABLE B.1 EQUILIBRIUM AVERAGE WALL TEMPERATURE RESULTS

NOMINAL POWER	ACTUAL POWER (W)	EQUILIBRIUM \bar{T}_w ($^\circ\text{C}$)
1W	0.9412	46.47
3W	3.122	59.23
5W	5.126	67.90
7W	6.790	74.34
9W	9.560	84.85

HEAT LOSS TO AMBIENT

Temperature vs Time

1W and 7W

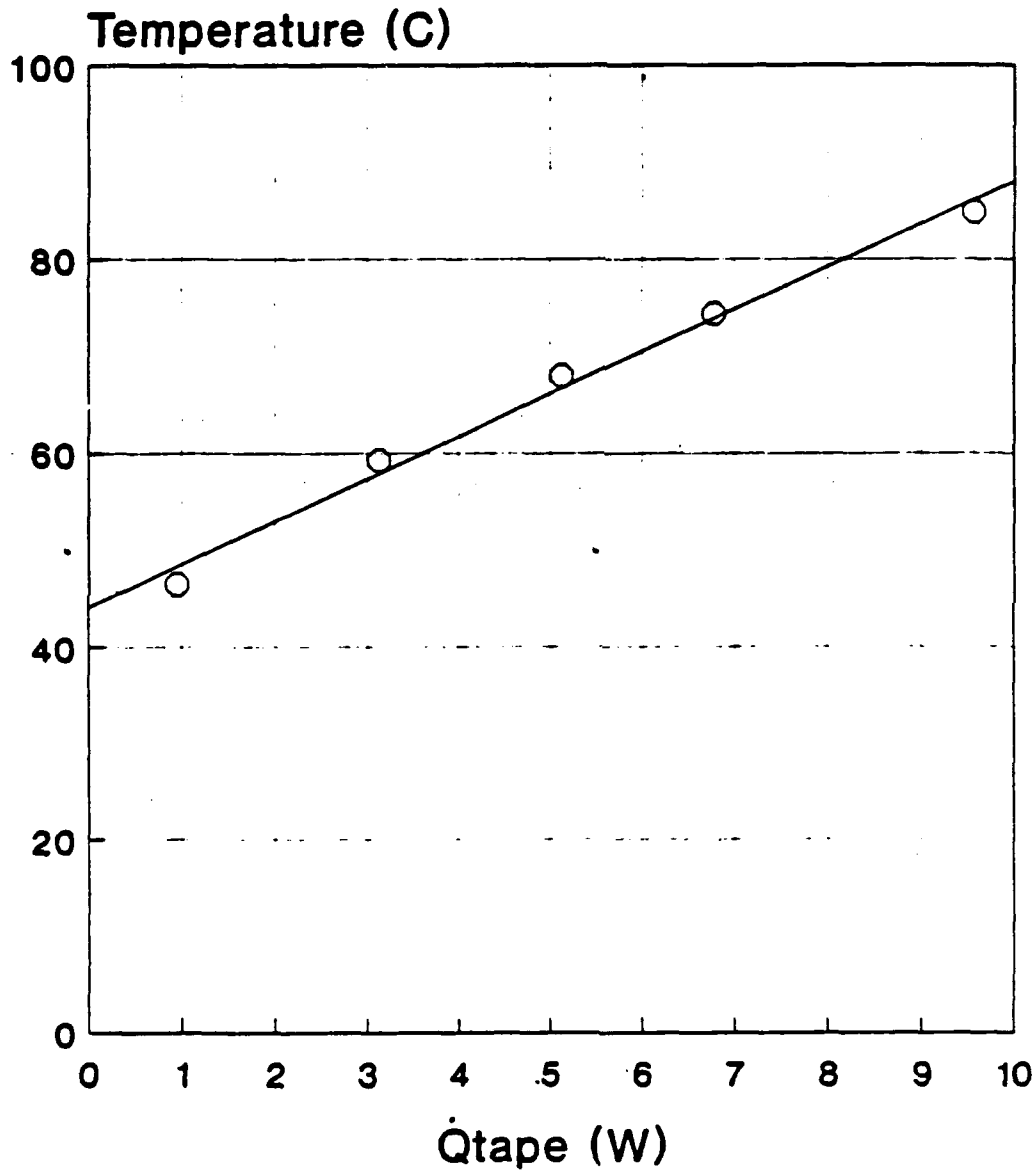


$T_{amb} = 22.0$

Figure B.1 Heat loss to ambient; Average wall temperature versus time for 1W and 7W.

HEAT LOSS TO AMBIENT

Temperature vs Heat Input



Tamb = 22:0

Figure B.2 Heat loss to ambient; Average wall temperature versus heat input.

APPENDIX C. FRICTIONAL/HEAT LEAKAGE EXPERIMENT

As coolant flows through the thermocouple wells/mixing box and along the tube, a small temperature rise results from frictional dissipation. When the coolant inlet temperature drops below ambient, an additional temperature rise can be attributed to heat leakage into the coolant from ambient. Since there was no means available to determine these terms separately, they were considered as one heat leakage term (\dot{q}_{leak}).

To determine this heat leakage term, the power to the heating elements was secured and coolant passed through the tube being tested at a given flowmeter setting. Any temperature rise detected was therefore due to frictional effects or heat leakage from ambient. This temperature rise was determined at flowmeter settings of 15% and 100% for each tube and insert condition at all four nominal inlet temperatures.

Data showed that flowmeter setting, tube and insert condition had no substantial effect on the temperature rise and that only the coolant inlet temperature made any difference. It can therefore be concluded that the heat leakage term was primarily due to heat addition from ambient. The results are shown in Table C.1.

TABLE C.1 HEAT LEAKAGE RESULTS

INLET TEMPERATURE	TEMPERATURE RISE
+20°C	0.0°C
+10°C	0.07°C
0°C	0.08°C
-10°C	0.18°C

These corrections were incorporated into the data reduction program "DRPSING" by directly subtracting this temperature rise from the measured outlet temperature.

APPENDIX D. POWER CALIBRATION

Actual heating element power (and therefore heat flux) was based upon the applied voltage and total heating element resistance. To measure voltage and current, the Data Acquisition Unit made use of a voltage and current sensing unit. However, a power factor needed to be applied to these sensed values to determine actual values required for the power/heat flux calculation.

Voltage and current meters were placed in the circuit downstream of the power source and prior to the first heating element as shown in Figure D.1. The voltage rheostat was varied over its entire range and voltage and current sensed by the meters and in the DAU were recorded (Table D.1). For each setting, actual power was calculated by:

$$P = VI \quad (D.1)$$

and total heating element resistance by:

$$R = \frac{V}{I} = \frac{P}{I^2} \quad (D.2)$$

In addition, voltage (PF_v) and current (PF_i) power factors were determined by:

$$PF_v = \frac{V_{ACTUAL}}{V_{CH29}} \text{ and } PF_i = \frac{I_{ACTUAL}}{I_{CH25}} \quad (D.3)$$

where the subscripts "CH25" and "CH29" refer to the DAU sensing unit channel assignments and "actual" to the meter readings. All the above readings and calculations were done for five rheostat settings as shown in Table D.1.

An average heater resistance (\bar{R}), current (\bar{PF}_i) and voltage (\bar{PF}_v) power factors were then calculated. Heater power could then be calculated by one of the following forms of equation:

$$P = (\bar{PF}_i)(\bar{PF}_v)V_{CH29} I_{CH25} \quad (D.4)$$

or

$$P = (\bar{PF}_v V_{CH29})^2 / \bar{R} \quad (D.5)$$

The current power factor varied too much to be utilized in a simple calculation. Therefore, it was decided to make use of equation (D.5). The final equation to determine the average heating element power (\dot{q}_{tape} in Watts) for a given rheostat setting was:

$$\dot{q}_{tape} = [59.66 V_{CH29}]^2 / 49.6 \quad (D.6)$$

This equation was incorporated into the data reduction program "DRPSING."

TABLE D.1 POWER CALIBRATION RESULTS

POWER (W)	V (VOLTS)	I (AMPS)	R (OHMS)	V _{cms} (VOLTS)	I _{cms} (AMPS)	PF _v	PF _i
31.31	30.7	0.61	50.32	0.5135	0.0106	59.78	57.50
76.14	61.4	1.24	49.51	1.032	0.0430	59.49	28.80
303.30	122.5	2.48	49.39	2.054	0.1050	59.63	23.60
750.36	192.4	3.90	49.30	3.226	0.1746	59.64	22.30
113.84	234.0	4.76	49.51	3.915	0.2170	59.77	21.90

POWER CALIBRATION ELECTRICAL SCHEMATIC

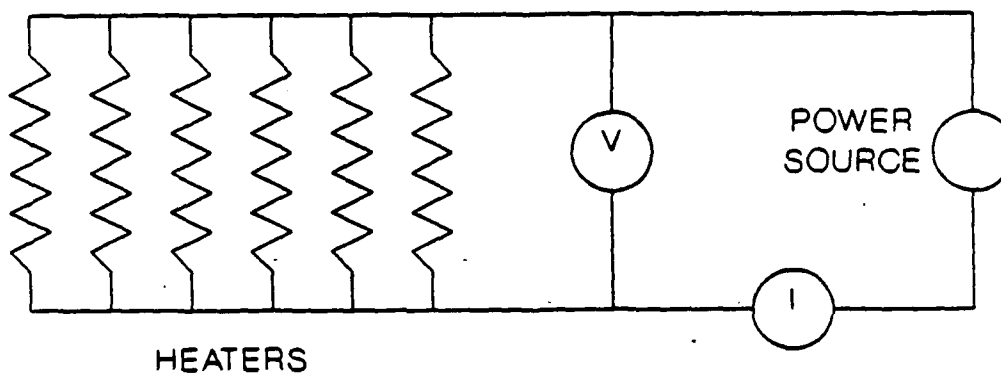


Figure D.1 Electrical schematic of power calibration experiment.

APPENDIX E. TUBE AND INSERT SPECIFICATIONS

TABLE E.1 TUBE CHARACTERISTICS/SPECIFICATIONS

PHYSICAL CHARACTERISTICS	Cu SMOOTH	Cu/Ni FINNED	Cu/Ni KORODENSE
Inside Diameter (D_i)	13.26mm	10.16mm	13.35mm
Outside Diameter (D_o)	15.88mm	14.00mm	15.85mm
T/C Diameter ($D_{t/c}$) t/c	14.36mm	12.62mm	14.53mm
Wall Thickness	1.31mm	1.22mm	1.25mm
Length			
Overall Length (L)	152.4cm	153.7cm	152.7cm
Heated Length (L_H)	140.6cm	143.0cm	142.4cm
Heated Finned Length (L_F)	-	122.3cm	-
Smooth Section Length (L_S)	-	15.7cm	-
T/C Location (1)			
Pos 1	15.2cm	17.8cm	15.6cm
Pos 2	55.9cm	57.2cm	56.2cm
Pos 3	96.5cm	96.5cm	96.8cm
Pos 4	137.2cm	135.9cm	134.5cm
T/C X/D for L_H (2)			
Pos 1	6.77	2.05	7.91
Pos 2	37.41	40.80	38.35
Pos 3	68.06	79.55	68.79
Pos 4	98.71	118.27	96.99
Inside Surface Area for L_H			
A_i	0.0586m ²	0.0340m ² (3)	0.0600m ²
T/C Attachment Method	Silver Solder	Soft Solder	Tach Weld/ Liquid Metal

(1) measured from tube inlet; (2) measured from start of heated length; (3) for finned heated length.

TABLE E.2 INSERT CHARACTERISTICS/SPECIFICATIONS

TWISTED TAPE	NARROW	WIDE
thickness, δ	0.559mm	0.559mm
width, w	10.16mm	13.26mm
180° pitch, H	3.05cm	5.30cm
twist ratio, y	3	4
material	brass	brass
HEATEX	SMALL	LARGE
diameter	10.16mm	13.26mm
material	stainless steel	stainless steel

APPENDIX F. UNCERTAINTY ANALYSIS FOR THE INSIDE HEAT TRANSFER COEFFICIENT

Data file SMNI03 (smooth tube, no insert, +10°C/10kW/m²), was chosen to conduct an uncertainty analysis of the experimental determination of the inside mean heat transfer coefficient, \bar{h}_i . In order to assess the effects of coolant velocity on the uncertainty in the measurement of \bar{h}_i , this uncertainty analysis was performed at coolant velocities of 0.4 and 1.4 m/s (for the same data set). The calculations below are shown for the 0.4 m/s coolant velocity. Table F.1 summarizes the results of the uncertainty analysis for both 0.4 m/s and 1.4 m/s coolant velocities.

The uncertainty analysis utilizes the procedure suggested by Kline and McClintock [Ref. 24]. This procedure states that if

$$R = R(x_1, x_2, x_3, \dots, x_n)$$

then the uncertainty in R, namely, δR is given by the equation:

$$\delta R = \left[\left(\frac{\partial R}{\partial x_1} \delta x_1 \right)^2 + \left(\frac{\partial R}{\partial x_2} \delta x_2 \right)^2 + \dots + \left(\frac{\partial R}{\partial x_n} \delta x_n \right)^2 \right]^{0.5}$$

where x_n is the measured variable and δx_n is the uncertainty in the measured variable.

The uncertainty in the coolant temperature measurements is due to uncertainty in the voltage measured by the thermocouples. For the thermocouples used, this value was assumed to be 4 microvolts or 0.1°C. The uncertainty in ΔT is found from

the uncertainty in the coolant inlet and outlet temperatures, T_a and T_∞ , and can be calculated as follows:

$$T_\infty = \frac{T(14) + T(15)}{2}$$

Taking the partial derivatives we obtain:

$$\frac{\partial T_\infty}{\partial T(14)} = \frac{\partial T_\infty}{\partial T(15)} = \frac{1}{2}$$

The uncertainty in the measurement of T_∞ is thus:

$$\partial T_\infty = \left[\left(\frac{\partial T_\infty}{\partial T(14)} \delta T \right)^2 + \left(\frac{\partial T_\infty}{\partial T(15)} \delta T \right)^2 \right]^{0.5}$$

Based on the thermocouple uncertainty, $\delta T = 0.1^\circ\text{C}$, we obtain:

$$\delta T_\infty = 0.071^\circ\text{C}$$

The coolant inlet temperature is calculated from a single thermocouple. The uncertainty in this measurement is calculated as:

$$\frac{\partial T_a}{\partial T(13)} = 1$$

and

$$\delta T_d = \left[\left(\frac{\partial T_d}{\partial T(13)} \delta T \right)^2 \right]^{0.5} = 0.1^\circ\text{C}$$

or,

$$\delta T_d = 0.1^\circ\text{C}$$

Since,

$$\left(\frac{\partial T_\infty}{\partial \Delta T} \right) = 1, \quad \left(\frac{\partial T_d}{\partial \Delta T} \right) = -1$$

then the uncertainty in ΔT is calculated from:

$$\delta \Delta T = \left[(\delta T_\infty)^2 + (\delta T_d)^2 \right]^{0.5}$$

or,

$$\delta \Delta T = 0.1225^\circ\text{C}$$

For a measured ΔT of 3.7°C , the uncertainty is therefore:

$$\frac{\delta \Delta T}{\Delta T} = 0.0332 = 3.32\%$$

Coolant velocity is calculated from:

$$V_c = \frac{\dot{m}}{\rho_c A_i}$$

For a coolant velocity 0.4 m/s, \dot{m} was calculated to be 0.05954 kg/s. The uncertainty in the reading of the flowmeter is defined as the scale interpolation. This value corresponds to one-half the value of the smallest marked increment. In this case, the scale interpolation factor, $\delta_{\dot{m}}$ is 0.5%, which corresponds to 0.00101 kg/s resolution. In addition, a time-wise jitter, $\delta_{\dot{m}}$ of 0.5% was noted during the runs. Therefore, the uncertainty in \dot{m} is given by:

$$\frac{\delta \dot{m}}{\dot{m}} = \left[\left(\frac{\delta \dot{m}}{\dot{m}} \delta_{\dot{m}} \right)^2 + \left(\frac{\delta \dot{m}}{\dot{m}} \delta_{\dot{m}} \right)^2 \right]^{0.5}$$

For a the measured coolant mass flow rate:

$$\frac{\delta \dot{m}}{\dot{m}} = 0.0239 = 2.39\%$$

The uncertainty in the cross-sectional area of the tubes was estimated from:

$$\frac{\delta A_c}{A_c} = \left[2 \times \left(\frac{\delta D_i}{D_i} \right)^2 \right]^2$$

where δD_i is given as 0.1 mm based on tolerances supplied from the manufacturer.

Therefore, for an inside diameter of 13.26 mm,

$$\frac{\delta A_c}{A_c} = 0.0107 = 1.07\%$$

Assuming that the uncertainty in the evaluation of the fluid properties is negligible, the uncertainty in the coolant velocity is now given by:

$$\frac{\delta V_c}{V_c} = \left[\left(\frac{\delta \dot{m}}{\dot{m}} \right)^2 + \left(\frac{\delta A_i}{A_i} \right)^2 \right]^{0.5}$$

or for a coolant velocity of 0.4 m/s,

$$\frac{\delta V_c}{V_c} = 0.0262 = 2.62\%$$

The uncertainty in the calculation of coolant Reynolds number is given by:

$$\frac{\delta Re_c}{Re_c} = \left[\left(\frac{\delta V_c}{V_c} \right)^2 + \left(\frac{\delta D_i}{D_i} \right)^2 \right]^{0.5}$$

or substituting appropriate numbers we find

$$\frac{\delta Re_c}{Re_c} = 0.0282 = 2.82\%$$

The uncertainty in the calculation of the heat transfer rate to the coolant is related to the uncertainty in the measurements of coolant mass flow rate and coolant

temperature rise where:

$$\frac{\delta \dot{q}}{\dot{q}} = \left[\left(\frac{\delta \dot{m}}{\dot{m}} \right)^2 + \left(\frac{\delta \Delta T}{\Delta T} \right)^2 \right]^{0.5}$$

or

$$\frac{\delta \dot{q}}{\dot{q}} = 0.0409 = 4.09\%$$

The uncertainty in the heat flux is then:

$$\frac{\delta q_i''}{q_i''} = \left[\left(\frac{\delta \dot{q}}{\dot{q}} \right)^2 + \left(\frac{\delta A_s}{A_s} \right)^2 \right]^{0.5}$$

where the uncertainty in A_s is given by:

$$\frac{\delta A_s}{A_s} = \left[\left(\frac{\delta D_i}{D_i} \right)^2 + \left(\frac{\delta L}{L} \right)^2 \right]^{0.5}$$

Here, the uncertainty in the length of the tube, δL , is assumed to be 5 mm while δD_i , is assumed to be 0.1 mm (again from given manufactures tolerances). Substitution of the appropriate numbers yields:

$$\frac{\delta q_i''}{q_i''} = 0.0147 = 1.47\%$$

Finally, since \bar{h}_i is given by:

$$h_i = \frac{q''}{LMTD}$$

the uncertainty in the LMTD must be calculated. The LMTD is given by:

$$LMTD = \frac{\Delta T}{\ln \left[\frac{T_{wi} - T_{ci}}{T_{wi} - T_{co}} \right]}$$

In order to calculate the uncertainty in the measurement of the LMTD, the following equations were used:

$$\frac{\partial LMTD}{\partial \Delta T} = \frac{1}{\ln \left[\frac{T_{wi} - T_{ci}}{T_{wi} - T_{co}} \right]}$$

$$\frac{\partial LMTD}{\partial T_{wi}} = \frac{\Delta T [(T_{wi} - T_{co}) - (T_{wi} - T_{ci})]}{\left[\ln \left[\frac{T_{wi} - T_{ci}}{T_{wi} - T_{co}} \right] \right]^2 (T_{wi} - T_{ci})(T_{wi} - T_{co})}$$

$$\frac{\partial LMTD}{\partial T_{co}} = - \frac{\Delta T}{\left[\ln \left[\frac{T_{wi} - T_{ci}}{T_{wi} - T_{co}} \right] \right]^2 (T_{wi} - T_{co})}$$

$$\frac{\partial LMTD}{\partial T_a} = \frac{\Delta T}{\left[\ln \left[\frac{T_w - T_a}{T_w - T_\infty} \right] \right]^2 (T_w - T_a)}$$

The uncertainty in the LMTD is therefore given by:

$$\delta LMTD = \left[\left(\frac{\partial LMTD}{\partial \Delta T} \delta \Delta T \right)^2 + \left(\frac{\partial LMTD}{\partial T_w} \delta T_w \right)^2 + \left(\frac{\partial LMTD}{\partial T_\infty} \delta T_\infty \right)^2 + \left(\frac{\partial LMTD}{\partial T_a} \delta T_a \right)^2 \right]^{\frac{1}{2}}$$

Before the uncertainty in LMTD can be calculated, the uncertainty in the measured average inside wall temperature must be determined. The average inside wall was determined from a total of twelve thermocouples, three at each of the four longitudinal positions. The uncertainty in a single wall temperature measurement is due to the uncertainty in the voltage measurement of the thermocouple ($\delta T = 0.1^\circ\text{C}$) and the uncertainty due to the influence caused by the various attachment techniques used. Obviously, the variations seen in the wall thermocouple readings were due to this latter uncertainty and some account has to be made of this as this is by far the dominant uncertainty. If the average temperature at a given longitudinal position is assumed to be the required temperature, then the standard deviation of the three thermocouple readings at that position could be assumed to be this latter uncertainty. Therefore, the uncertainty at a given longitudinal position can be represented by:

$$\delta T_{pos(i)} = \frac{\partial T(i)}{\partial T} \delta T$$

where $i = 1,2,3,4$ for each of the four thermocouple longitudinal locations and

$\frac{\partial T(i)}{\partial T}$ is the standard deviation at each of these locations mentioned above.

Since the average inside wall temperature at each position increases along the length of the tube, the average inside wall temperature for the entire tube must be thought of as the average of the four longitudinal positions' average temperatures ($T_{pos(i)}$). The average inside wall temperature is then determined by:

$$T_{wi} = \frac{T_{pos1} + T_{pos2} + T_{pos3} + T_{pos4}}{4}$$

Taking the partial derivatives gives:

$$\frac{\partial T_{wi}}{\partial T_{pos1}} = \frac{\partial T_{wi}}{\partial T_{pos2}} = \frac{\partial T_{wi}}{\partial T_{pos3}} = \frac{\partial T_{wi}}{\partial T_{pos4}} = \frac{1}{4}$$

Therefore, the uncertainty in the average inside wall temperature measurement is:

$$\delta T_{wi} = \left[\left(\frac{\partial T_{wi}}{\partial T_{pos1}} \delta T_{pos1} \right)^2 + \left(\frac{\partial T_{wi}}{\partial T_{pos2}} \delta T_{pos2} \right)^2 + \left(\frac{\partial T_{wi}}{\partial T_{pos3}} \delta T_{pos3} \right)^2 + \left(\frac{\partial T_{wi}}{\partial T_{pos4}} \delta T_{pos4} \right)^2 \right]^{0.5}$$

Considering position 1, the average inside wall temperature is:

$$T_{pos1} = \frac{T(10) + T(11) + T(12)}{3}$$

For the three thermocouple readings of

$$T(10) = 25.99^{\circ}\text{C}, T(11) = 25.74^{\circ}\text{C} \text{ and } T(12) = 26.01^{\circ}\text{C},$$

the average inside wall temperature for position 1 is

$$T_{pos1} = 25.91^{\circ}\text{C}$$

The standard deviation at this location is given by:

$$S.D. = \delta T_{pos1} = (\sum (T_n - T_{avg})^2 / n)^{0.5} = 0.123^{\circ}\text{C}$$

Therefore,

$$\frac{\delta T_{pos1}}{\bar{T}_{pos1}} = 4.7 \times 10^{-3} = 0.47\%$$

Repeating this for the other three locations gives:

$$\delta T_{pos2} = 0.497^{\circ}\text{C}$$

$$\delta T_{pos3} = 0.634^{\circ}\text{C}$$

$$\delta T_{pos4} = 0.145^{\circ}\text{C}$$

Therefore, the uncertainty in the measurement of average inside wall temperatures is:

$$\delta T_{wi} = \left[[(0.25)(0.123)]^2 + [(0.25)(0.497)]^2 + [(0.25)(0.634)]^2 + [(0.25)(0.145)]^2 \right]^{0.5} = 0.207$$

After substituting the appropriate values for $\partial LMTD/\partial \Delta T$, $\partial LMTD/\partial \bar{T}_{wi}$, $\partial LMTD/\partial T_{co}$ and $\partial LMTD/\partial T_{ci}$ the uncertainty in the measurement of LMTD is:

$$\delta LMTD = 1.122^\circ C$$

and

$$\frac{\delta LMTD}{LMTD} = \frac{1.122}{24.13} = 0.0465 = 4.65\%$$

The uncertainty in the overall heat transfer coefficient, U_o , is then given by:

$$\frac{\delta \bar{h}_i}{\bar{h}_i} = \left[\left(\frac{\delta q_o''}{q_o''} \right)^2 + \left(\frac{\delta LMTD}{LMTD} \right)^2 \right]^{\frac{1}{2}}$$

or

$$\frac{\delta h_i}{h_i} = \left[(0.0417)^2 + (0.0463)^2 \right]^{\frac{1}{2}}$$

$$\frac{\delta h_i}{h_i} = 0.0625 = 6.25\%$$

$$\frac{\delta h_i}{\delta h_i} = 0.0625 = 6.25\%$$

Table F.1 summarizes the results of the uncertainty analysis for the smooth copper tube with no insert for coolant velocities of 0.4 and 1.4 m/s, respectively at a nominal inlet coolant temperature of +10°C.

The uncertainty analysis neglects any uncertainty in the physical properties of the coolant. For the most part, this is probably a reasonable assumption. The exception to this may be the viscosity due to its sensitivity to temperature. Hence, the uncertainty reported here is likely to be conservative.

It is curious that the relative magnitudes of the uncertainty for the low and high coolant velocities are nearly the same. Two different mechanisms dominate in this calculated uncertainty at low and high coolant velocities. In terms of the mass flow rate, the time-wise jitter and scale interpolation terms are the same for both coolant velocities. However, the actual mass flow rate is less at the lower flow rates. Hence, the uncertainty in the mass flow rate calculation is more significant at the lower coolant velocities. At higher coolant flow rates, the uncertainty in the calculation of LMTD becomes the dominant term. This is because the coolant temperature rise is smaller at high coolant velocities but the uncertainty in the temperature measurements remains the same.

TABLE F.1 SUMMARY OF RESULTS FOR SAMPLE UNCERTAINTY ANALYSIS

Variable	$V_c = 0.4 \text{ m/s}$	$V_c = 1.4 \text{ m/s}$
$\frac{\delta T_d}{T_d}$	0.98%	0.87%
$\frac{\delta T_{co}}{T_{co}}$	0.51%	0.56%
$\frac{\delta \Delta T}{\Delta T}$	3.32%	10.67%
$\frac{\delta \dot{m}}{\dot{m}}$	2.39%	0.69%
$\frac{\delta A_i}{A_i}$	1.07%	1.07%
$\frac{\delta V_c}{V_c}$	2.62%	1.27%
$\frac{\delta Re_c}{Re_c}$	2.32%	1.47%
$\frac{\delta \dot{q}}{\dot{q}}$	4.09%	10.69%

$\frac{\delta T_{wi}}{T_{wi}}$	0.57%	0.71%
$\frac{\delta q_o''}{q_o''}$	4.17%	10.72%
$\frac{\delta LMTD}{LMTD}$	4.65%	16.32%
$\frac{\delta \bar{h}_i}{\bar{h}_i}$	6.25%	19.53%

APPENDIX G. PROGRAM LISTING

```

1000 | FILE   DRPSING
1005 | PURPOSE This program collects and processes single instrumented tube da
      ta.
1015 | CREATED: APRIL 1, 1992 (S. MEMORY)
1030 | BEEP
1035 | PRINTER IS 1
1040 | PRINT USING "4X," "SELECT OPTION"
1045 | PRINT USING "6X," "0 TAKING DATA OR REPROCESSING PREVIOUS DATA"
1065 | PRINT USING "6X," "1 PURGE FILES"
1080 | PRINTER IS 701
1085 | INPUT Icall
1090 | IF Icall=0 THEN CALL Main
1095 | IF Icall=1 THEN CALL Purge
1125 | END
1130 | SUB Main
1135 | COM /Cc/ C(7)
1140 | COM /Fld/ Ifl
1145 | COM /Nus/ Iin,Tset,Qdpl,Hnus,Kf,Rhof,Hfg,Muf,Do,Itube
1150 | COM /W11/ Qoa(4),Qia(4),Kma(4),Iact,Droot(4),Ld(3)
1155 | COM /W12/ Delta,Iset,Nsets,Hod,Cia(4),Alpaal(3)
1160 | DIM Enf(17),Tp(4),T(17),Ho(4),Qdp(4),Uo(4),Pc(4),Xstar(4),Nux(4),Nuss(4)
1170 | DIM Xxx1(4),Xxx2(4),Xxx3(4),Xxx4(4),Xxx5(4),Xxx6(4)
1180 | DIM Num(4),Nueg(4),Ldd(4),Nu(4),Xs(4)
1215 | DATA 1.0,5.172,0.226,0.063,5.172
1220 | READ Cia(*)
1225 | DATA 0.10086091,25727.94369,-767345.8295,78025595.81
1230 | DATA -9247486589,6.97680E11,-2.66192E13,3.94078E14
1235 | READ C(*)
1240 | DATA 0.015875,0.014000,0.015850,0.0159,0.0
1245 | DATA 0.013259,0.010160,0.013350,0.01346,0.0
1250 | DATA 386.0,42.98,42.98,21.9,0.0
1255 | DATA 0.0005588,3
1260 | READ Qoa(*),Qia(*),Kma(*),Delta,Hod ! Hod=M/Do
1261 | IF Itube=0 THEN
1263 | DATA 6.765,37.41,68.06,99.71
1264 | READ Ld(*) ! LENGTH/DIAMETER RATIO FOR 4 T/C LOCS (SMOOTH)
1265 | L=1.406 ! Heated length of smooth tube
1266 | END IF
1267 | IF Itube=1 THEN
1268 | DATA 2.05,40.80,79.55,118.29
1269 | READ Ld(*) ! FIN LENGTH/DIAMETER RATIO FOR 4 T/C LOCS (CU/NI FIN)
1270 | L=1.223 ! Heated finned length of Cu/Ni fin tube
1271 | END IF
1273 | IF Itube=2 THEN
1274 | DATA 7.908,38.35,68.792,96.987
1275 | READ Ld(*) ! LENGTH/DIAMETER RATIO FOR 4 T/C LOCS (KORODENSE)
1276 | L=1.422 ! Heated length of Korodense tube
1277 | END IF
1283 | Jset=0
1284 | Okacct=1
1285 | BEEP
1286 | INPUT "ENTER MONTH, DATE AND TIME (MM:DD:MM:SS)",Otg8
1287 | OUTPUT 709:"TO":Otg8
1290 | BEEP
1300 | Ihard=1
1310 | INPUT "WANT A HARDCOPY PRINTOUT (1=DEF=YES,0=N)",Ihard
1315 | BEEP
1325 | Iin=1
1345 | IF Ihard=1 THEN PRINTER IS 701
1355 | BEEP

```

```

1360      INPUT "GIVE A NAME FOR THE NEW DATA FILE",File$
1365      CREATE BOAT File$,20
1370      ASSIGN @File TO File$
1375      BEEP
1380      INPUT "ENTER TUBE CODE (0=SMOOTH CU,1=FINNED CU/Ni,2=KORODENSE,3=TIT
FIN )",Itube
1383      BEEP
1384      INPUT "0=NO INSERT, 1=TWISTED TAPE (WIDE), 2=HEATEX (L), 3=HEATEX (S)
, 4=TWISTED TAPE (NARROW)",Insert
1385      IF Insert=1 THEN Mod=4
1386      IF Insert=4 THEN Mod=3
1388      BEEP
1389      INPUT "NOMINAL SUMP TEMP. 0=-10 C, 1=0 C, 2=+10 C, 3=+20 C",Itemp
1390      BEEP
1391      Egrat=54
1392      INPUT "ENTER EG CONCENTRATION (WT PERCENT),DEFAULT = 54%",Egrat
1393      BEEP
1395      ENTER 709:Otg$
1400      OUTPUT @File:Otg$
1405      OUTPUT @File:Itube,Egrat,Od1,Od2,Od3,Od4,Od5
1430      PRINT USING "10X,""FILE NAME: """,I2A":File$
1435      PRINT
1595      Iout=1
1600      BEEP
1605      INPUT "WANT TO CREATE AN OUTPUT FILE? (1=DEF=YES,0=N0)",Iout
1610      IF Iout=1 THEN
1615          BEEP
1620          INPUT "ENTER A NAME FOR OUTPUT FILE",Fout$
1625          CREATE BOAT Fout$,5
1630          ASSIGN @Fout TO Fout$
1635      END IF
1640
1646      IF Itube=0 THEN Dtc=.01436      | DIAMETER TO T/C BURIAL (SMOOTH)
1647      IF Itube=1 THEN Dtc=.0126      | DIAMETER TO T/C BURIAL (CU/Ni FIN)
1649      IF Itube=2 THEN Dtc=.01453      | DIAMETER TO T/C BURIAL (KORODENSE)
1650      Do=Doa(Itube)
1651      Od1=Doa(Itube)
1653      Oi=Oia(Itube)
1655      Km=Kma(Itube)
1660      Ax=PI*Oi^2/4      | Cross-sectional area
1661      IF Itube=2 THEN Ax=.00014      | BASED ON WOLVERINE DESIGN DATA
1665      Ao=PI*Do*L
1666      Ai=PI*Oi*L
1667      IF Itube=2 THEN Ao=.05*L      | BASED ON WOLVERINE DESIGN DATA
1668      IF Itube=2 THEN Ai=Ao/1.186      | BASED ON WOLVERINE DESIGN DATA
1670      Perim=PI*Oi
1671      Anarea=PI*(Do^2-Oi^2)/4.
1672      Ldd(1)=L/(4.*Oi)
1673      Ldd(2)=L/(2.*Oi)
1674      Ldd(3)=3.*L/(4.*Oi)
1675      Ldd(4)=L/Oi
1676      IF Itube=0 THEN
1677          Ulen1=.0627      | UNHEATED INLET END OF COPPER SMOOTH TUBE ONLY
1678          Ulen2=.0572      | UNHEATED OUTLET END OF COPPER SMOOTH TUBE ONLY
1679      END IF
1680      IF Itube=1 THEN
1681          Ulen1=.045      | UNHEATED INLET END OF CU/Ni FIN TUBE ONLY
1682          Ulen2=.06      | UNHEATED OUTLET END OF CU/Ni FIN TUBE ONLY
1683      Dcuo=.015875      | UNHEATED OUTSIDE DIAMETER OF CU/Ni FIN TUBE
1684      Dcui=.013259      | UNHEATED INSIDE DIAMETER OF CU/Ni FIN TUBE

```

```

1685 Lcui=.112      I HEATED INLET SMOOTH END OF CU/NI FIN TUBE
1686 Lcuo=.097      I HEATED OUTLET SMOOTH END OF CU/NI FIN TUBE
1687 Perim=PI*Qcui
1688 Anarea=PI*(Qcuo^2-Qcui^2)/4.
1689 END IF
1690 IF Itube=2 THEN
1691 Ulen1=.050      I UNHEATED INLET END OF CU/NI KORODENSE TUBE ONLY
1692 Ulen2=.055      I UNHEATED OUTLET END OF CU/NI KORODENSE TUBE ONLY
1693 END IF
1694 Hr=S0           I HEATER RESISTANCE
1700 !
1701     PRINTER IS 1
1702     BEEP
1703     INPUT "WHAT IS REQUIRED NOMINAL COOLANT VELOCITY IN m/s (MAX. = 1.4 m
/s)?" ,Vegst
1704     OUTPUT 709:"AR AF13 AL13 VRS"
1705     OUTPUT 709:"AS SA"
1706     Vsum=0
1707     FOR J=1 TO 5
1708         ENTER 709:E
1709         Vsum=Vsum+E
1710     NEXT J
1711     Enf(13)=Vsum/5
1712     T(13)=FNTVsv(Enf(13))
1713     Tavgl=T(13)
1714     IF Tavgl<-15 OR Tavgl>24 THEN
1715         PRINT "COOLANT TEMP. NOT IN RANGE -15 TO 24 C"
1716         GOTO 1703
1717     END IF
1718     Rhoegl=FNRhoeg(Tavgl,Egrat)
1719     Mdot1=khoegl*Ax*Vegst
1720     Pcal5=(Mdot1+.0098)/.0019
1721     Pca0=(Mdot1+.00414)/.00206
1722     Pca24=(Mdot1+.00329)/.00225
1723     IF Tavgl<0 THEN
1724         Pc(0)=Pcal5+((Tavgl+15)*(Pca0-Pcal5))/15
1725     ELSE
1726         Pc(0)=Pca0+(Tavgl*(Pca24-Pca0))/24
1727     END IF
1728     PRINT "SET FLOWMETER READINGS CORRESPONDING TO:"
1729     PRINT USING "6X,"% OF METER A = ",000.0":Pc(0)
1730     PRINT
1731     PRINT "HIT CONTINUE WHEN READY"
1732     PAUSE
1733 Repeat:
1734     PRINTER IS 701
1735     Ido=1
1736     ON KEY 0,15 RECOVER 1734
1737     PRINT USING "4X,""SELECT OPTION ""
1738     PRINT USING "6X,""0=TAKE DATA ""
1739     PRINT USING "6X,""1=SET Heater Tape Heat Flux (DEFAULT) ""
1740     PRINT USING "6X,""2=CHECK FLOWMETER % SETTING ""
1741     PRINT USING "4X,""NOTE: KEY 0 = ESCAPE""
1742     Ido = desired option
1743     BEEP
1744     INPUT Ido
1745     Set default value for input
1746     IF Ido>2 THEN Ido=2
1747     Take data option
1748     IF Ido=0 THEN 1816

```

```

1752 IF Ido=2 THEN 1703
1754 Loop to set heat flux and check temperatures
1755 IF Ido=1 THEN
1756 INPUT "ENTER DESIRED HEAT FLUX",Qdpwan
1758 PRINT USING "4X, " Qdp (wanted) Qdp (actual) Tin Delt""
1759 PRINT USING "4X, " (W/m^2) (W/m^2) (C) (C) ""
1761 Read thermocouple voltages
1762 OUTPUT 709:"AR AF1 AL15 VRS"
1764 FOR I=1 TO 15
1765 OUTPUT 709:"AS SA"
1766 Usum=0
1767 FOR J=1 TO 20
1768 ENTER 709:E
1769 Usum=Usum+E
1770 NEXT J
1771 Emf(I)=Usum/20
1772 T(I)=FNTvsv(Emf(I))
1773 NEXT I
1784 Compute average temperature of coolant outlet
1785 Tout=(T(14)+T(15))/2
1789 Delt=Tout-T(13)
1793 OUTPUT 709:"AR AF25 AL25 VRS"
1794 OUTPUT 709:"AS SA"
1795 ENTER 709:Amp
1796 OUTPUT 709:"AR AF29 AL29 VRS"
1797 OUTPUT 709:"AS SA"
1798 ENTER 709:Volt
1799 Qtape=(60*Volt)^2/H-
1800 Qdptape=Qtape/Ao
1801 PRINT
1803 PRINT USING "4X,5(MZ.3DE,3X)":Qdpwan,Qdptape,T(13),Delt,Qtape
1804 PRINT
1805 PRINT USING "4X, " TEMPS AT POSITION 1",3(000.00,3X)":T(10),T(11),T
(12)
1806 PRINT
1807 PRINT USING "4X, " TEMPS AT POSITION 2",3(000.00,3X)":T(7),T(8),T(9)
)
1808 PRINT
1809 PRINT USING "4X, " TEMPS AT POSITION 3",3(000.00,3X)":T(4),T(5),T(6)
)
1810 PRINT
1811 PRINT USING "4X, " TEMPS AT POSITION 4",3(000.00,3X)":T(1),T(2),T(3)
)
1812 WAIT 2
1813 GOTO 1752
1814 END IF
1815 TAKE DATA IF Im=0 LOOP
1816 Twm=0
1818 Twl=0
1819 PRINTER IS 701
1820 OUTPUT 709:"AR AF1 AL15 VRS"
1821 FOR I=1 TO 15
1822 OUTPUT 709:"AS SA"
1823 Usum=0
1824 FOR J=1 TO 20
1825 ENTER 709:E
1826 Usum=Usum+E
1827 NEXT J
1828 Emf(I)=Usum/20
1829 NEXT I

```



```

1840 !
1845 ! DATA ANALYSIS
1850 !
1860 FOR I=1 TO 15
1865 T(I)=FNTvsv(Emf(I))
1870 NEXT I
1871 FOR I=1 TO 12
1872 Tw1=Tw1+T(I)
1873 NEXT I
1874 Tw1av=Tw1/12.
1876 Tout=(T(14)+T(15))/2
1880 Delt=Tout-T(13)
1881 Hlc=0. ! Heat leakage correction
1883 IF Itube=0 THEN
1884 IF Itemp=0 THEN Hlc=.18 ! HEAT LEAKAGE CORRECTION AT -10 C
1885 IF Itemp=1 THEN Hlc=.08 ! HEAT LEAKAGE CORRECTION AT 0 C
1886 IF Itemp=2 THEN Hlc=.07 ! HEAT LEAKAGE CORRECTION AT +10 C
1887 IF Itemp=3 THEN Hlc=0. ! NO HEAT LEAKAGE CORRECTION AT +20 C
1888 Delt=Delt-Hlc
1890 END IF
1891 Tout=Tout-Hlc
1893 OUTPUT 709;"AS SA"
1894 ENTER 709:Amp
1895 OUTPUT 709;"AR AF29 AL29 VRS"
1896 OUTPUT 709;"AS SA"
1897 ENTER 709:Volt
1898 Qtape=(60*Volt)^2/Hr
1923 Qdptape=Qtape/Ao
1925 Jset=Jset+1
1926 IF Okaccpt=0 THEN Jset=Jset-1
1930 PRINT
1935 PRINT USING "10X","Data set number = ",00":Jset
1940 PRINT
1941 IF Itube=0 THEN PRINT USING "10X","Smooth tube"
1942 IF Itube=2 THEN PRINT USING "10X","Korodense tube"
1943 IF Itube=1 THEN PRINT USING "10X","Copper/Nickel fin"
1945 IF Itemp=0 THEN PRINT USING "10X","Nominal sump temp. = -10 C"
1946 IF Itemp=1 THEN PRINT USING "10X","Nominal sump temp. = 0 C"
1948 IF Itemp=2 THEN PRINT USING "10X","Nominal sump temp. = +10 C"
1949 IF Itemp=3 THEN PRINT USING "10X","Nominal sump temp. = +20 C"
1951 IF Insert=0 THEN PRINT USING "10X","No insert used"
1952 IF Insert=1 THEN PRINT USING "10X","Wide twisted tape insert used"
1953 IF Insert=4 THEN PRINT USING "10X","Narrow twisted tape insert used"
1954 IF Insert=2 THEN PRINT USING "10X","Large HEATEX insert used"
1955 IF Insert=3 THEN PRINT USING "10X","Small HEATEX insert used"
1956 PRINT USING "10X","Nominal set heat flux = ",MZ.30E".Qdptape
1960 PRINT USING "10X","Nominal set coolant velocity = ",0.0".Vegst
1970 PRINT
1990 Tavg=T(13)+Delt*.5
1996 Rhoeg=FNRhoeg(Tavg,Egrat)
2000 Nuueg=FNNueg(Tavg,Egrat)
2005 Mueg=Nuueg*Rhoeg
2010 Cpeg=FNCPeg(Tavg,Egrat)
2015 Keg=FNKeg(Tavg,Egrat)
2020 Preg=Cpeg*Mueg/Keg
2025 Mdot=FNFMcal(T(13),Pc(0))
2030 Veg=Mdot/(Rhoeg*Ax)
2035 Reeg=Veg*Di/Nuueg
2040 Res=4*Mdot/(PI*Mueg*(Di-4*Delta))
2045 Qdot=Mdot*Cpeg*Delt

```

```

2048!   ITERATE TO FIND INSIDE WALL TEMPERATURES
2049       Tm1=Tw1av
2050       Tm2=Tw1av
2051       Tm1=(Tm1+Tm2)/2.
2052       Cti=Qdot*LOG(Dtc/Di)/(2.*PI*L*Km)
2053       Tm2=Tw1av-Cti
2056       IF ABS(Tm2-Tm1)>.001 THEN GOTO 2051
2057       FOR I=1 TO 12
2058           T(I)=T(I)-Cti
2059           Twm=Twm+T(I)
2060       NEXT I
2061       Twm=Twm/12
2062       Nuuegw=FNNuegw(Twm,Egrat)
2063       Muegw=Nuuegw*Rhoeg
2064       Twm1=(T(12)+T(11)+T(10))/3
2065       Twm2=(T(9)+T(8)+T(7))/3
2066       Twm3=(T(6)+T(5)+T(4))/3
2067       Twm4=(T(3)+T(2)+T(1))/3
2068       Twm12=(T(12)+T(11)+T(10)+T(9)+T(8)+T(7))/6
2069       Twm123=(T(12)+T(11)+T(10)+T(9)+T(8)+T(7)+T(6)+T(5)+T(4))/9
2070       Tlm=(Tout-T(13))/LOG((Twm-T(13))/(Twm-Tout))
2071       Qloss=(Twm-44.15)/4.39 ! HEAT LOSS TO ATMOSPHERE
2072       IF Twm<45 THEN Qloss=0
2073       Qtape=Qtape-Qloss
2074       Qdpi=Qdot/Ai
2075       Alfa1=Qdpi/Tlm
2076!   FIN CORRECTION TO ACCOUNT FOR CONDUCTION TO ENDS OF TUBE
2077       Ff1=(Km*Perim*Anarea)^.5
2078       Alfa11=Alfa1
2079       Alfa12=Alfa1!
2080       Alaml=((Alfa12*Perim)/(Km*Anarea))^.5
2081       Ff3=Ff1*Alfa12^.5*(Twm-T(13))
2082       Ff4=Ff1*Alfa12^.5*(Twm-Tout)
2083       Func6=Ff3*FNTanh(Alaml*Ulen1)
2084       Func7=Ff4*FNTanh(Alaml*Ulen2)
2085       Func8=Alfa12*Ai*(Twm-Tavg)
2086       Funcx=Func6+Func7+Func8-Qdot
2087       Dfunc6=(.5*Func6/Alfa12)+2.*Ff3*Ulen1/(1.+FNCosh(2.*Alaml*Ulen1))
2088       Dfunc7=(.5*Func7/Alfa12)+2.*Ff4*Ulen2/(1.+FNCosh(2.*Alaml*Ulen2))
2089       Dfunc8=Ai*(Twm-Tavg)
2090       Dfuncx=Dfunc6+Dfunc7+Dfunc8
2091       Alfa11=Alfa12-Funcx/Dfuncx
2092       IF ABS(Alfa11-Alfa12)>.05 THEN GOTO 2079
2093       Alfa12=Alfa11
2095       Cpeg=(Mueg/Muegw)^.14
2096!   FIND TEMPERATURE INCREASE DUE TO UNHEATED LENGTHS
2097       Deltin=Func6/(Mdot*Cpeg)
2098       Deltout=Func7/(Mdot*Cpeg)
2099       Thlin=T(13)+Deltin
2100       Thlout=Tout-Deltout
2101       Delhl=(Thlout-Thlin)
2105       IF Itube=1 THEN
2106           Heatin=Lcu1*Delhl/(L+Lcu1+Lcuo) ! HEATED SMOOTH INLET SECTION FOR CU
/NI FIN TUBE
2107           Heatout=Lcuo*Delhl/(L+Lcu1+Lcuo) ! HEATED SMOOTH OUTLET SECTION FOR
CU/NI FIN TUBE
2109       Thlin=Thlin+Heatin
2110       Thlout=Thlout-Heatout
2111       Delhl=(Thlout-Thlin)
2114       END IF

```

```

2115 Qh1=Mdot*Cpeg*Delh1
2116 Qdph1=Qh1/A1
2117 Qdpxx=Func8/A1
2118 Tco1=Thlin+(Delh1/4)
2119 Tco2=Thlin+(Delh1/2)
2120 Tco3=Thlin+(3*Delh1/4)
2121 Ttc1=T(13)+(Ld(0)*O1*Delh1/L)
2122 Ttc2=T(13)+(Ld(1)*O1*Delh1/L)
2123 Ttc3=T(13)+(Ld(2)*O1*Delh1/L)
2124 Ttc4=T(13)+(Ld(3)*O1*Delh1/L)
2126 Tlm11=(Thlout-Thlin)/LOG((Twm-Thlin)/(Twm-Thlout)) ! ALL (1,2,3,4)
2127 Tlm1=(Tco1-Thlin)/LOG((Twm1-Thlin)/(Twm1-Tco1)) ! SECTION 1
2128 Tlm2=(Tco2-Tco1)/LOG((Twm2-Tco1)/(Twm2-Tco2)) ! SECTION 2
2129 Tlm3=(Tco3-Tco2)/LOG((Twm3-Tco2)/(Twm3-Tco3)) ! SECTION 3
2130 Tlm4=(Thlout-Tco3)/LOG((Twm4-Tco3)/(Twm4-Thlout)) ! SECTION 4
2131 Tlm12=(Tco2-Thlin)/LOG((Twm12-Thlin)/(Twm12-Tco2)) ! SECTION 1,2
2132 Tlm123=(Tco3-Thlin)/LOG((Twm123-Thlin)/(Twm123-Tco3)) ! SECTION 1,2,3
2133 Alp11=Qdph1/Tlm11
2134 Alp1=Qdph1/Tlm1
2135 Alp2=Qdph1/Tlm2
2136 Alp3=Qdph1/Tlm3
2137 Alp4=Qdph1/Tlm4
2138 Alloc1=Qdph1/(Twm1-Ttc1)
2139 Alloc2=Qdph1/(Twm2-Ttc2)
2140 Alloc3=Qdph1/(Twm3-Ttc3)
2141 Alloc4=Qdph1/(Twm4-Ttc4)
2143 Alp12=Qdph1/Tlm12
2144 Alp123=Qdph1/Tlm123
2145 Keg1=FNKeg((Tco1+Thlin)/2,Egrat)
2146 Keg2=FNKeg((Tco2+Tco1)/2,Egrat)
2147 Keg3=FNKeg((Tco3+Tco2)/2,Egrat)
2148 Keg4=FNKeg((Thlout+Tco3)/2,Egrat)
2149 Keg12=FNKeg((Tco2+Thlin)/2,Egrat)
2150 Keg123=FNKeg((Tco3+Thlin)/2,Egrat)
2151 Num11=Alp11*O1/Keg1
2152 Nu1=Alp1*O1/Keg1
2153 Nu2=Alp2*O1/Keg2
2154 Nu3=Alp3*O1/Keg3
2155 Nu4=Alp4*O1/Keg4
2156 Nuloc1=Alloc1*O1/Keg1
2157 Nuloc2=Alloc2*O1/Keg2
2158 Nuloc3=Alloc3*O1/Keg3
2159 Nuloc4=Alloc4*O1/Keg4
2161 Nu12=Alp12*O1/Keg12
2162 Nu123=Alp123*O1/Keg123
2163 ! LOCAL NUSSELT FROM SHAH/LONDON PAGE 128, EQN 240-242
2164 ! CALCULATE XSTAR FIRST FOR EACH THERMOCOUPLE LOCATION
2165 ! DEFINE COOLANT PECLET NUMBER
2166 Peeg=Preg*Reeg
2167 Xs(1)=Ldd(1)/Peeg ! FOR MEAN VALUES OF h
2168 Xs(2)=Ldd(2)/Peeg
2169 Xs(3)=Ldd(3)/Peeg
2170 Xs(4)=Ldd(4)/Peeg
2171 FOR I=1 TO 4
2172 Xstar(I)=Ld(I-1)/Peeg ! FOR LOCAL VALUES AT T/C POSITIONS
2173 Nux(I)=1.302*Xstar(I)^(-1/3)-.5
2175 ! DEVELOPING HYDRO AND THERMAL BOUNDARY LAYER (S/L P148, EQN. 258)
2176 Xx1=(1+((220/PI)*Xstar(I))^(10/9))^(3/5)
2177 Xx2=(1+(Preg/.0207)^(2/3))^(.5)
2178 Xx3=PI/(115.2*Xstar(I))

```

```

2179      Xx4=(1+(Xx3/(Xx2*Xx1))^(5/3))^(3/10)
2180      Xx5=(1+((220/PI)*Xstar(I))^(10/9))^(3/10)
2181      Nuss(I)=(Xx4*5.364*Xx5)-1
2188      IF Xstar(I)<.00005 THEN
2189          Nux(I)=1.302*Xstar(I)^(-1/3)-1
2190      END IF
2194      IF Xstar(I)>.0015 THEN
2195          Nux(I)=4.364+8.68*(1000*Xstar(I))^(.506)*EXP(-41*Xstar(I))
2196      END IF
2200      NEXT I
2202      IF Insert=0 THEN
2203          PRINT USING "3X," LOCAL NUSSELT VALUES""
2205          PRINT USING "3X," Exp. Nux(TLM) Exp. Nux(BULK) Pred. Nux(1)
            Pred. Nux(2) Xstar(tc)""
2206          PRINT
2207          PRINT USING "3X,""POS 1 "" ,5(MZ.3DE,SX)":Nu1,Nuloc1,Nux(1),Nuss(1),X
            star(1)
2208          PRINT USING "3X,""POS 2 "" ,5(MZ.3DE,SX)":Nu2,Nuloc2,Nux(2),Nuss(2),X
            star(2)
2209          PRINT USING "3X,""POS 3 "" ,5(MZ.3DE,SX)":Nu3,Nuloc3,Nux(3),Nuss(3),X
            star(3)
2210          PRINT USING "3X,""POS 4 "" ,5(MZ.3DE,SX)":Nu4,Nuloc4,Nux(4),Nuss(4),X
            star(4)
2211          PRINT
2215          ELSE
2216          PRINT USING "3X,""POSITION # = Exp. Nux (TLM) Exp. Nux (BULK)
            Xstar at tc pos.""
2217          PRINT
2218          PRINT USING "3X,""POSITION 1 (LOCAL) = "" ,3(MZ.3DE,SX)":Nu1,Nuloc1,X
            star(1)
2219          PRINT USING "3X,""POSITION 2 (LOCAL) = "" ,3(MZ.3DE,SX)":Nu2,Nuloc2,X
            star(2)
2220          PRINT USING "3X,""POSITION 3 (LOCAL) = "" ,3(MZ.3DE,SX)":Nu3,Nuloc3,X
            star(3)
2221          PRINT USING "3X,""POSITION 4 (LOCAL) = "" ,3(MZ.3DE,SX)":Nu4,Nuloc4,X
            star(4)
2222          END IF
2223          PRINT
2230          FOR I=1 TO 4
2232              IF Insert=0 THEN
2233                  Bb1=.0668*Reeg*Preg/Ldd(I)
2234                  Bb2=1+.04*(Reeg*Preg/Ldd(I))*.6666
2235                  Nueg(I)=3.66*(Bb1/Bb2)
2236              END IF
2237              IF Insert=1 OR Insert=4 THEN
2239                  Nueg(I)=Cia(Insert)*(1+5.484E-3*Preg*.7*(Res/Hod)^1.25)^.5
2240                  Nuoth=.383*Preg*.35*(Res/Hod)^.622
2241              END IF
2242              IF Insert=2 THEN
2243                  Nueg(I)=Cia(Insert)*(Reeg*.65)*Preg*.46
2244              END IF
2245              IF Insert=3 THEN
2246                  Nueg(I)=Cia(Insert)*(Reeg*.76)*Preg*.46
2247              END IF
2248              BEEP
2249          CALCULATED VALUE OF INSIDE HT. TRANSFER COEFF. FROM CORRELATIONS
2250          H1=Nueg(4)*Keg/Di
2251          MEAN NUSSELT NUMBER FROM SHAH/LONDON PAGE 128, EQN 245-246
2254          IF Xs(I)<.03 THEN
2255              Num(I)=1.953*Xs(I)^(-1/3)

```

```

2256      F_SE
2258      Num(I)=4.364+(.0722/Xs(I))
2259      END IF
2262      NEXT I
2263      PRINT USING "3X,""POSITION : =      Exp. mean Nu      Pred. mean Nu
      Xstar at section""
2264      PRINT
2266      PRINT USING "3X,""POSITION 1 (MEAN) =      ",3(MZ.3DE,SX)":Nu1,Num(1)
,Xs(1)
2267      PRINT USING "3X,""POSITION 12 (MEAN) =      ",3(MZ.3DE,SX)":Nu12,Num(2
),Xs(2)
2268      PRINT USING "3X,""POSITION 123 (MEAN) =      ",3(MZ.3DE,SX)":Nu123,Num(
3),Xs(3)
2269      PRINT USING "3X,""POSITION 1234 (MEAN) =      ",3(MZ.3DE,SX)":Numall,Num
(4),Xs(4)
2270      PRINT
2271      PRINT
2272      PRINT USING "10X,""Mass flow rate (kg/s) =      ",MZ.3DE":Mdot
2273      PRINT USING "10X,""Inside Tube Dia. (m) =      ",MZ.3DE":Dia(1tube)
2274      IF Insert=1 THEN PRINT USING "10X,""180 DEG OVER Dia. (HOD) =      ",
MZ.3DE":Hod
2275      PRINT USING "10X,""Inlet temperature (C) =      ",MZ.3DE":T(13)
2276      IF Insert=1 OR Insert=4 THEN
2277      PRINT USING "10X,""DELTA Tape Thickness =      ",MZ.3DE":Delta
2278      END IF
2279      PRINT USING "10X,""DELT temp Dif. (C) =      ",MZ.3DE":Delt
2280      PRINT USING "10X,""H. T. to coolant (W) =      ",MZ.3DE":Qdot
2281      PRINT USING "10X,""H. T. from heater tape (W) =      ",MZ.3DE":Qtape
2282      PRINT USING "10X,""Prandtl number =      ",MZ.3DE":Preg
2283      PRINT USING "10X,""Reynolds number =      ",MZ.3DE":Reeg
2284      IF Insert=1 OR Insert=4 THEN PRINT USING "10X,""Reynolds number H
&S S =      ",MZ.3DE":Res
2285      PRINT USING "10X,""H1 from correl. (W/m^2.K) =      ",MZ.3DE":H1
2286      PRINT USING "10X,""H1 from heat bal. (W/m^2.K) =      ",MZ.3DE":Alfai
2
2287      IF Insert=0 THEN PRINT USING "10X,""Nu for no insert (Hausen) =
",MZ.3DE":Nueg(4)
2288      IF Insert=1 OR Insert=4 THEN PRINT USING "10X,""Nu for twisted ta
pe (Bergles2)"",MZ.3DE":Nuoth
2289      IF Insert=1 OR Insert=4 THEN PRINT USING "10X,""Nu for twisted ta
pe (Bergles3)"",MZ.3DE":Nueg(4)
2290      IF Insert=2 THEN PRINT USING "10X,""Nu for large HeateX (Mazzone)
",MZ.3DE":Nueg(4)
2291      IF Insert=3 THEN PRINT USING "10X,""Nu for small HeateX (Mazzone)
",MZ.3DE":Nueg(4)
2292      IF Insert=0 THEN PRINT USING "10X,""Nu from Shah/London =      ",
MZ.3DE":Num(4)
2293      PRINT USING "10X,""Xstar for heated length =      ",MZ.3DE":Xs(4)
2294      PRINT USING "10X,""Experimental Nusselt no. =      ",MZ.3DE":Numall
2295      PRINT
2296      PRINT USING "3X,""Wall t/c 12,11,10 (pos. 1) (C) =      ",3(000.00,3X
)",T(12),T(11),T(10)
2297      PRINT USING "3X,""Wall t/c 9,8,7 (pos. 2) (C) =      ",3(000.00,3X
)",T(9),T(8),T(7)
2298      PRINT USING "3X,""Wall t/c 6,5,4 (pos. 3) (C) =      ",3(000.00,3X
)",T(6),T(5),T(4)
2299      PRINT USING "3X,""Wall t/c 3,2,1 (pos. 4) (C) =      ",3(000.00,3X
)",T(3),T(2),T(1)
2300      PRINT USING "3X,""Av. inside wall temp (C) =      ",MZ.3DE":Twm
2301      PRINT

```

```

2302      Nu(1)=Nu1
2303      Nu(2)=Nu12
2304      Nu(3)=Nu123
2305      Nu(4)=Nu11
2307      IF Insert=0 THEN
2308      FOR I=1 TO 4
2310      Xxx1(I)=LOG(Nu(I))
2311      Xxx2(I)=LOG(Xs(I))
2312      Xxx3(I)=LOG(Nueg(I))
2313      Xxx4(I)=LOG(Num(I))
2314      NEXT I
2315      PRINT USING "3X," "MEAN VALUES AT"          POS 1          POS 1
2      POS 123      POS 1234""
2317      PRINT USING "6X," "EXP. LOG(Nu)      = "" ,4(MZ.3DE,4X)":Xxx1(1),X
xx1(2),Xxx1(3),Xxx1(4)
2318      PRINT USING "6X," "COR. LOG(Nu) (H)      = "" ,4(MZ.3DE,4X)":Xxx3(1),X
xx3(2),Xxx3(3),Xxx3(4)
2319      PRINT USING "6X," "COR. LOG(Nu) (S/L) = "" ,4(MZ.3DE,4X)":Xxx4(1),X
xx4(2),Xxx4(3),Xxx4(4)
2320      PRINT USING "6X," "LOG(Xstar)      = "" ,4(MZ.3DE,4X)":Xxx2(1),X
xx2(2),Xxx2(3),Xxx2(4)
2321      END IF
2323      IF Insert=2 OR Insert=3 THEN
2324      FOR I=1 TO 4
2325      Xxx1(I)=LOG(Nu(I)/Preg*.46)
2326      Xxx2(I)=LOG(Reeg)
2327      Xxx3(I)=LOG(Nueg(I)/Preg*.46)
2328      NEXT I
2329      PRINT USING "3X," "MEAN VALUES AT"          POS 1          POS 1
2      POS 123      POS 1234""
2331      PRINT USING "6X," "EXP. LOG(Nu/Pr*.46) = "" ,4(MZ.3DE,4X)":Xxx1(1),
Xxx1(2),Xxx1(3),Xxx1(4)
2332      PRINT USING "6X," "COR. LOG(Nu/Pr*.46) = "" ,4(MZ.3DE,4X)":Xxx3(1),
Xxx3(2),Xxx3(3),Xxx3(4)
2334      PRINT USING "6X," "LOG(Re)      = "" ,4(MZ.3DE,4X)":Xxx2(1),
Xxx2(2),Xxx2(3),Xxx2(4)
2335      END IF
2336      IF Insert=1 OR Insert=4 THEN
2337      FOR I=1 TO 4
2338      Xxx1(I)=LOG(Nu(I)/Preg*.35)
2339      Xxx2(I)=LOG(Res/Hod)
2340      Xxx3(I)=LOG(Nuoth/Preg*.35)
2341      Xxx4(I)=LOG(Nu(I))
2342      Xxx5(I)=LOG(Preg*(Res/Hod)^1.78)
2343      Xxx6(I)=LOG(Nueg(I))
2344      NEXT I
2345      PRINT USING "3X," "MEAN VALUES AT"          POS 1          POS 1
2      POS 123      POS 1234""
2346      PRINT USING "6X," "EXP. LOG(Nu/Pr*.35) = "" ,4(MZ.3DE,4X)":Xxx1(1),
Xxx1(2),Xxx1(3),Xxx1(4)
2347      PRINT USING "6X," "COR. LOG(Nu/Pr*.35) = "" ,4(MZ.3DE,4X)":Xxx3(1),
Xxx3(2),Xxx3(3),Xxx3(4)
2348      PRINT USING "6X," "LOG(Res/y)      = "" ,4(MZ.3DE,4X)":Xxx2(1),
Xxx2(2),Xxx2(3),Xxx2(4)
2349      PRINT
2350      PRINT USING "6X," "EXP. LOG(Nu)      = "" ,4(MZ.3DE,4X)":Xxx4(1),
Xxx4(2),Xxx4(3),Xxx4(4)
2351      PRINT USING "6X," "COR. LOG(Nu)      = "" ,4(MZ.3DE,4X)":Xxx6(1),
Xxx6(2),Xxx6(3),Xxx6(4)
2352      PRINT USING "6X," "LOG(Pr(Res/y)^1.78) = "" ,4(MZ.3DE,4X)":Xxx5(1),

```

```

Xxx5(2),Xxx5(3),Xxx5(4)
2353     END IF
2354     IF Insert=0 AND Reeg>2300 THEN
2355         Nutu=.027*Reeg*.8*Preg*.3333*Ofeg
2356         PRINT USING "6X,"TURBULENT S/T CORRELATION = "",4(MZ.3DE,4X)":Nu
tu
2357         Xxx7=LOG(Nutu)
2358         PRINT USING "6X,"TURB. COR. LOG(Nu) = "",4(MZ.3DE,4X)":Xxx7
2359     END IF
2360     Okaccept=1
2361     BEEP
2362     INPUT "OK TO ACCEPT THIS SET (1=DEFAULT=YES, 0=NO)?",Okaccept
2363     IF Okaccept=1 THEN OUTPUT @File:Pc(*),Emf(*),Tp(*)
2364     IF Im=0 THEN
2365         Okrpt=1
2366         BEEP
2367         INPUT "WILL THERE BE ANOTHER RUN (1=YES=DEFAULT,0=NO)",Okcpt
2368         IF Okcpt=1 THEN 1701
2369     ELSE
2370         IF Jset<Nsets THEN 1701
2371     END IF
2372     ASSIGN @File TO *
2373     IF Iout=1 THEN ASSIGN @File TO *
2374     SUBEND
2375     DEF FNGrad(T)
2376     Grad=-3.877857E-5-2*4.7142857E-8*T
2377     RETURN Grad
2378     FNEND
2379     DEF FNKcu(T)
2380     OFHC COPPER 250 TO 300 K
2381     Tk=T+273.15
2382     K=434-.112*Tk
2383     RETURN K
2384     FNEND
2385     DEF FNNueg(Tc,Egr)
2386     RANGE OF VALIDITY: -20 TO 20 DEG C
2387     Tk=Tc+273.15
2388     Nu1=7.1196507E-3-Tk*(7.4863347E-5-Tk*(2.6294943E-7-Tk*3.0833329E-10))
2389     Nu2=4.9237638E-3-Tk*(4.9213912E-5-Tk*(1.6437534E-7-Tk*1.8333331E-10))
2395     Nu3=8.6586293E-3-Tk*(8.8837902E-5-Tk*(3.0495032E-7-Tk*3.4999996E-10))
2400     A2=(Nu3-2*Nu2+Nu1)/200
2405     A1=(Nu2-Nu1-940*A2)/10
2410     A0=Nu1-42*A1-1764*A2
2415     Nu=A0+Egr*(A1+Egr*A2)
2420     RETURN Nu
2425     FNEND
2430     DEF FNCpeg(Tc,Egr)
2435     RANGE OF VALIDITY 0 TO 20 DEG C
2440     Tk=Tc+273.15
2445     Cp1=1.6701550E+3+Tk*6.3
2450     Cp2=1.4748125E+3+Tk*6.25
2455     Cp3=9.5800500E+2+Tk*7.3
2460     A2=(Cp3-2*Cp2+Cp1)/200
2465     A1=(Cp2-Cp1-900*A2)/10
2470     A0=Cp1-40*A1-1600*A2
2475     Cp=A0+Egr*(A1+Egr*A2)
2480     RETURN Cp
2485     FNEND
2490     DEF FNRhoeg(T,Egr)
2495     Ro1=1.0607093E+3-T*(3.7031283E-1+T*4.0837183E-3)

```

```

2500 Ro2=1.0748272E+3-T*(4.4266195E-1+T*4.0939706E-3)
2505 Ro3=1.0885934E+3-T*(5.7355653E-1+T*6.1281405E-3)
2510 A2=(Ro3-2*Ro2+Ro1)/200
2515 A1=(Ro2-Ro1-900*A2)/10
2520 A0=Ro1-40*A1-1600*A2
2525 Ro=A0+Egr*(A1+Egr*A2)
2530 RETURN Ro
2535 FNEND
2540 DEF FNPreg(T,Egr)
2545 Pr=FNCpeg(T,Egr)*FNNueg(T,Egr)*FNRoeg(T,Egr)/FNKeg(T,Egr)
2550 RETURN Pr
2555 FNEND
2560 DEF FNKeg(Tc,Egr)
2565 ! RANGE OF VALIDITY: -20 TO 20 DEG C
2570 Tk=Tc+273.15
2575 K1=2.2824708E-1+Tk*(5.5989286E-4+Tk*3.5714286E-7)
2580 K2=2.5846616E-1+Tk*(2.3978571E-4+Tk*7.1428571E-7)
2585 K3=3.2138932E-1-Tk*(3.0042857E-4-Tk*1.4285714E-6)
2590 A2=(K3-2*K2+K1)/200
2595 A1=(K2-K1-900*A2)/10
2600 A0=K1-40*A1-1600*A2
2605 K=A0+Egr*(A1+Egr*A2)
2610 RETURN K
2615 FNEND
2620 DEF FNTanh(X)
2625 P=EXP(X)
2630 Q=1/P
2635 Tanh=(P-Q)/(P+Q)
2640 RETURN Tanh
2645 FNEND
2650 DEF FNTvsu(V)
2655 COM /Cc/ C(7)
2660 T=C(0)
2665 FOR I=1 TO 7
2670 T=T+C(I)*V*I
2675 NEXT I
2680 RETURN T
2685 FNEND
2690 DEF FNBeta(T)
2695 Rop=FNrho(T+.1)
2700 Rom=FNrho(T-.1)
2705 Beta=-2/(Rop+Rom)*(Rop-Rom)/.2
2710 RETURN Beta
2715 FNEND
2720 DEF FNPsat(Tc)
2725 ! 0 TO 80 deg F CURVE FIT OF Psat
2730 Tf=1.8*Tc+32
2735 Pa=5.945525+Tf*(.15352082+Tf*(1.4840963E-3+Tf*9.6150671E-6))
2740 Pg=Pa-14.7
2745 IF Pg>0 THEN ! +=PSIG, -=in Hg
2750 Psat=Pg
2755 ELSE
2760 Psat=Pg*29.92/14.7
2765 END IF
2770 RETURN Psat
2775 FNEND
2905 SUB Purge
2910 BEEP
2915 INPUT "ENTER FILE NAME TO BE DELETED",Files
2920 PURGE Files

```



```

2925 GOTO 2910
2930 SUBEND
2935 SUB Wilson
2940 COM /Wil1/ Doa(4),Dia(4),Kma(4),Iact,Droot(4),Ld(3)
2945 COM /Wil2/ Delta,Isat,Nsets,Hod,Cia(4),Alpaa(3)
2950 DIM Emf(17),T(17),Xa(100),Ya(100),Pc(4),Tp(4)
2955 BEEP
2960 INPUT "PLEASE RE-ENTER NAME OF FILE",File$
2965 ASSIGN @File TO File$
2970 INPUT "0=SMOOTH COPPER TUBE, 1=CUNI FIN, 2=KORODENSE, 3=FIN TITAN",Itube
2975 BEEP
2976 INPUT "0=NO INSERT, 1= TWISTED TAPE INSERT, 2=HITRAN1, 3=HITRAN2",Insert
2977 BEEP
2980 INPUT "GIVE A NAME FOR XY FILE",Xy$
2985 CREATE @DAT Xy$,20
2990 ASSIGN @Xy TO Xy$
2995 L=1.2192
3000 Do=Doa(Itube)
3005 Di=Dia(Itube)
3010 Km=Kma(Itube)
3015 Ax=PI*Di^2/4 ! Cross-sectional area
3020 Ao=PI*Do*L
3025 Rm=Do*LOG(Do/Di)/(2*Km)
3030 !
3035 ! Initial values
3040 Tf=Tsat
3045 Alpa=.655
3046 IF Insert=0 THEN
3050 Ci=1.0.
3051 END IF
3052 IF Insert=1 THEN
3053 Ci=5.172
3054 END IF
3055 IF Insert=2 THEN
3056 Ci=.226
3057 END IF
3058 IF Insert=3 THEN
3059 Ci=.063
3060 END IF
3062 G=9.81
3063 Ibeg=0
3065 Iend=0 !CHANGE TO 4, IF FIVE TUBES IN BUNDLE
3070 IF Iact/10 THEN
3075 Ibeg=Iact
3080 Iend=Iact
3085 END IF
3090 !
3095 FOR I=Ibeg TO Iend
3100 Sx=0
3105 Sy=0
3110 Sxs=0
3115 Sxy=0
3120 Jset=0
3125 ASSIGN @File TO File$
3130 ENTER @File:Dtg$,Itube,Egrat,Od1,Od2,Od3,Od4,Od5
3135 ENTER @File:Pc(*),Emf(*),Tp(*)
3140 FOR J=0 TO 17
3145 T(J)=FNTvsv(Emf(J))
3150 NEXT J
3155 Tvap=(T(0)+T(1)+T(2))/3

```

```

3160 Tliq=(T(3)+T(4))/2
3161 Tliq1=T(5)
3165 IF Isat=0 THEN
3170 Tsat=Tliq1
3175 ELSE
3180 Tsat=Tvap
3185 END IF
3190 Grad=FNGrad(T(I+6))
3191 Tout=(T(2*I+10)+T(2*I+11))/2
3195 Qdelt=Tout-T(I+6)
3200 Tavg=T(I+6)+Qdelt*.5
3201 IF I=Iend THEN
3202 Qdelt=T(10)-T(9)
3204 Tavg=(T(10)-T(9))/2
3205 END IF
3206
3210 Water/Ethylene Glycol Mixture Properties
3215 Rhoeg=FNRhoeg(Tavg,Egrat)
3220 Nueg=FNNueg(Tavg,Egrat)
3225 Mueg=Nueg*Rhoeg
3230 Cpeg=FNCPeg(Tavg,Egrat)
3235 Keg=FNKeg(Tavg,Egrat)
3240 Preg=Cpeg*Mueg/Keg
3245
3250 Mdot=FNFmcal(I,T(I+6),Pc(I))
3255 Veg=Mdot/(Rhoeg*Ax)
3260 Reeg=Veg*Di/Nueg
3265 Res=4*Mdot/(Mueg*(Pi*Di-4*Qdelt))
3270 Qdot=Mdot*Cpeg*Qdelt
3275 Qdp=Qdot/Ao
3280 Lntd=Qdelt/LOG((Tsat-T(I+6))/(Tsat-T(I+6)-Qdelt))
3285 Uo=Qdp/Lntd
3286 IF Insert=0 THEN
3287 Bb1=.0668*(Di/L)*Reeg*Preg
3288 Bb2=1+.04*((Di/L)*Reeg*Preg)^.6666
3289 Omega=3.66*(Bb1/Bb2)
3290 END IF
3291 IF Insert=1 THEN
3293 Omega=(1+5.484E-3*Preg^.7*(Res/Hod)^1.25)^.5
3294 END IF
3295 IF Insert=2 THEN
3296 Omega=(Reeg^.65)*(Preg^.46)
3297 END IF
3298 IF Insert=3 THEN
3299 Omega=(Reeg^.76)*(Preg^.46)
3300 END IF
3302
3303 R-114/R113 Properties
3305 Hfg=FNHfg(Tsat)
3310 Kf=FNK(Tf)
3315 RhoF=FNRRho(Tf)
3320 Muf=FNMu(Tf)
3325
3330 F=(Kf^3*RhoF^2*G*Hfg/(Muf*Qo*Qdp))^33333
3335 Ho=Alpa*F
3340 Two=Tsat-Qdp/Ho
3345 Tf=Tsat/3+2*Two/3
3350 Y=(1/Uo-Rm)*F
3355 X=Qo*F/(Keg*Omega)
3360 PRINT "OMEGA=";Omega;"F=";F;"X=";X;"Y=";Y

```

```

3365      Xa(Jset)=X      INEFFICIENT (MODIFY LATER)
3370      Ya(Jset)=Y
3375      Sx=Sx+X
3380      Sy=Sy+Y
3385      Sxs=Sxs+X*X
3390      Sxy=Sxy+X*Y
3395      Jset=Jset+1
3400      IF Jset<Nsets THEN 3135
3405      ASSIGN @File TO *
3410      Slope=(Nsets*Sxy-Sx*Sy)/(Nsets*Sxs-Sx^2)
3415      Intcpt=(Sy-Slope*Sx)/Nsets
3420      Cic=1/Slope
3425      Alpac=1/Intcpt
3430      Cerr=ABS((Ci-Cic)/Cic)
3435      Aerr=ABS((Alpac-Alpa)/Alpac)
3440      IF Cerr>.001 OR Aerr>.001 THEN
3445          Alpa=(Alpa+Alpac)*.5
3450          Ci=(Ci+Cic)*.5
3455      PRINT "CIC=";Cic;"ALPA=";Alpa
3460      GOTO 3100
3465      END IF
3470      BEEP
3475      BEEP
3480      PRINTER IS 1
3485      PRINT "CIC=";Cic;"ALPA=";Alpa
3490      Cia(Insert)=Cic
3495      Alpa(I)=Alpac
3500      PRINTER IS 701
3505      FOR J=0 TO Nsets-1
3510          OUTPUT @Xy:Xa(J),Ya(J)
3515      NEXT J
3520      PRINTER IS 1
3525      NEXT I
3530      ASSIGN @Xy TO *
3535      SUBEND
8270      DEF FNFmc1(T,Pc)
8280          Mdot15=.0019*Pc-.0098
8290          Mdot0=.00206*Pc-.00414
8300          Mdot24=.00225*Pc-.00329
8310      IF T<0 THEN
8311          Mdt=((T+15)*(Mdot0-Mdot15)/15)+Mdot15
8320      ELSE
8470          Mdt=(T*(Mdot24-Mdot0)/24)+Mdot0
8471      END IF
8480      RETURN Mdt
8490      FNEND
8500      DEF FNCosh(X)
8510          P=EXP(X)
8520          Q=EXP(-X)
8530          Cosh=.5*(P+Q)
8540      RETURN Cosh
8550      FNEND

```

LIST OF REFERENCES

1. *Montreal Protocol on Substances that Deplete the Ozone Layer, Final Act*, Montreal, Canada, United Nations Environment Program (UNEP), September 1987.
2. Federal Register, *Protection of Stratospheric Ozone; Final Rule*, 40 CFR Part 82, Vol. 53, No. 156, pp. 30566-30602, Washington, D.C., U.S. Environmental Protection Agency, August 12, 1988.
3. *Montreal Protocol on Substances that Deplete the Ozone Layer, Amendments and Adjustments*, London, England, United Nations Environment Program (UNEP), June 1990.
4. Zebrowski, D.S., *Condensation Heat Transfer Measurements of Refrigerants on Externally Enhanced Surfaces*, M.S. Thesis, Naval Postgraduate School, Monterey, California, September 1987.
5. Mabrey, B.D., *Condensation of Refrigerants on Small Tube Bundles*, M.S. Thesis, Naval Postgraduate School, Monterey, California, December 1988.
6. Mazzone, R.W., *Enhanced Condensation of R-113 on a Small Bundle of Horizontal Tubes*, Master's Thesis, Naval Postgraduate School, Monterey, California, December 1991.
7. Graetz, L., "Über die Wärmeleitungsfähigkeit von Flüssigkeiten (On the Thermal Conductivity of Liquids), Part 1," *Ann. Phys. Chem.*, 18, 79-94 (1883); "Part 2," *Ann. Phys. Chem.*, 25, 337-357 (1885).
8. Nusselt, W., "Die Abhängigkeit der Wärmeübergangszahl von der Rohrlänge (The Dependence of the Heat-transfer Coefficient on the Tube Length)," *VDI Z*, 54, 1154-1158 (1910).
9. Shah, R.K., and London, A.L., *Laminar Flow Forced Convection in Ducts*, Academic Press, New York, 1978.
10. Incropera, F.P., and DeWitt, D.P., *Introduction to Heat Transfer*, 2nd Edition, John Wiley and Sons, New York, pp. 127-133, 1990.
11. Kays, W., and Crawford, M.E., *Convective Heat and Mass Transfer*, 2nd Edition, McGraw Hill Book Company, New York, 1980.

12. Schlichting, H., *Boundary Layer Theory*, 7th Edition, McGraw-Hill Book Company, New York, 1987.
13. Churchill, S.W., and Ozoe, H., "Correlations for Laminar Forced Convection with Uniform Heating in Flow Over a Plate and in Developing and Fully Developed Flow in a Tube," *J. Heat Transfer*, 95, 78-84, 1973.
14. Bergles, A.E., and Joshi, S.D., *Augmentation Techniques for Low Reynolds Number In-Tube Flow*, *Low Reynolds Number Flow Heat Exchanges*, ed. by Kakac, S., Shah, R.K., and Bergles, A.E., Hemisphere Publishing Company, pp. 695-720, 1983.
15. Hong, S.W. and Bergles, A.E., "Augmentation of Laminar Flow Heat Transfer in Tubes by Means of Twisted Tape Insert," *J. Heat Transfer*, vol. 98, no. 2, pp. 251-256, 1976.
16. Date, A.W., and Singham, J.R., *Numerical Prediction of Friction and Heat Transfer Characteristics of Fully-Developed Laminar Flow in Tube Containing Twisted Tape*, ASME Paper No. 72-HT-17, 1972.
17. Saha, S.K., Gatinoe, U.N., and Date, A.W., *Heat Transfer and Pressure Drop Characteristics of Laminar Flow in a Circular Tube Fitted with Regularly Spaced Twisted Tape Elements*, *Experimental Heat Transfer, Fluid Mechanics and Thermodynamics*, ed. by Shah, R.K., Ganic, E.N., and Yang, K.T., Elsevier Science Publishing Company, pp. 511-518, 1988.
18. Marner, W.J., and Bergles, A.E., "Augmentation of Tubeside Laminar Flow Heat Transfer by Means of Twisted-Tape Inserts, Static-Mixer Inserts and Internally Finned Tubes," *Heat Transfer 1978*, Proceedings of the Sixth International Heat Transfer Conference, vol. 2, pp. 583-588, Hemisphere Publishing Corp., Washington, D.C., 1978.
19. Gough, M.J., Rodgers, J.V., and Russel, G.M.B., "The Development of a Practical Answer to the Improvement of Tubeside Heat Transfer," *12th HTFS Res. Symposium*, University of Warwick, United Kingdom, pp. 123-134, 1982.
20. Oliver, D.R., and Aldington, R.W.J., "Heat Transfer Enhancement in Round Tubes using Wire Matrix Turbulators: Newtonian and Non-Newtonian Liquids," *Chem. Eng. Res. Des.*, vol. 66, pp. 555-565, 1988.
21. Wolverine Technical Bulletin No. 4020, *Wolverine Korodense Tube*, Wolverine Tube Company, Decatur, Alabama, 1982.

22. Cragoe, C.S., *Properties of Ethylene Glycol and its Aqueous Solutions*, Cooperative Research Council, New York, Unpublished.
23. Gallant, R.W., *Ethylene Glycols, Physical Properties of Hydrocarbons*, Gulf Publishing Co., Houston, Texas, Chapter 13, pp. 109-123, 1968.
24. Kline, S.J., and McClintock, F.A., "Describing Uncertainties in Single Sample Experiments," *Mechanical Engineering*, vol. 78, pp. 3-8, 1953.

INITIAL DISTRIBUTION LIST

	No. Copies
1. Defense Technical Information Center Cameron Station Alexandria, Virginia 22304-6145	2
2. Library, Code 52 Naval Postgraduate School Monterey, California 93943-5000	2
3. Professor Paul J. Marto, Code ME/Mx Department of Mechanical Engineering Naval Postgraduate School Monterey, California 93943-5000	2
4. Professor Stephen B. Memory, Code ME/Mr Department of Mechanical Engineering Naval Postgraduate School Monterey, California 93943-5000	1
5. Department Chairman, Code ME Department of Mechanical Engineering Naval Postgraduate School Monterey, California 93943-5000	1
6. Naval Engineering Curricular Office, Code 34 Department of Mechanical Engineering Naval Postgraduate School Monterey, California 93943-5000	1
7. Mr. R. Helmick, Code 2722 Annapolis Detachment, CD Naval Surface Warfare Center Annapolis, Maryland 21402-5067	1

- | | | |
|-----|--|---|
| 8. | Mr. Bruce G. Unkel
NAVSEA (CODE 56Y15)
Department of the Navy
Washington, D.C. 20362-5101 | 1 |
| 9. | LCDR Joseph D. Guido
5846-D Mission Ctr. Rd.
San Diego, California 92123 | 1 |
| 10. | Dr. William Guido
9 Sophomore Lane
Stoney Brook, New York 11790 | 1 |
| 11. | Mr. William Guido
440 Park Blvd.
Massapequa Pk., New York 11762 | 1 |
| 12. | Mr. William Melvin
CMR 451, Box 25
Shape Education Center
APO, AE 09708 | 1 |